ESTIMATION OF ACCELERATOR NEUTRINO FLUX

Paras Koundal

Registration Number - MS14083

A dissertation submitted for the partial fulfillment
of BS-MS dual degree in Science

Under the guidance of

Dr. Satyajit Jena

April 2019

Indian Institute of Science Education and Research Mohali

Sector - 81, SAS Nagar, Mohali 140306, Punjab, India

Dedicated to my parents and sister.

Certificate of Examination

This is to certify that the dissertation titled **"Estimation of Accelerator Neutrino Flux"** submitted by **Paras Koundal** (Reg. No. MS14083) for the partial fulfillment of BS-MS dual degree programme of the Institute, has been examined by the thesis committee duly appointed by the Institute. The committee finds the work done by the candidate satisfactory and recommends that the report be accepted.

Dr. Kinjalk Lochan Dr. Anosh Joseph Dr. Satyajit Jena
(Supervisor)

Dated: 26.04.2019

Declaration

The work presented in this dissertation has been carried out by me under the guidance of Dr. Satyajit Jena at the Indian Institute of Science Education and Research Mohali.

This work has not been submitted in part or in full for a degree, a diploma, or a fellowship to any other university or institute. Whenever contributions of others are involved, every effort is made to indicate this clearly, with due acknowledgment of collaborative research and discussions. This thesis is a bonafide record of original work done by me and all sources listed within have been detailed in the bibliography.

Paras Koundal
(Candidate)

Dated: April 26, 2019

In my capacity as the supervisor of the candidate's project work, I certify that the above statements by the candidate are true to the best of my knowledge.

Dr. Satyajit Jena
(Supervisor)

Acknowledgement

First and foremost, I would like to thank my supervisor, Dr. Satyajit Jena, for his motivation, guidance and invaluable criticism of my work without which this thesis would have never been possible. The discussions that I had with him has enhanced my capabilities as a researcher. I also thank Dr. Kinjalk Lochan and Dr. Anosh Joseph for their valuable insights.

I also thank my family for their constant emotional support throughout my degree. I also thank Sampsa Vihonen (University of Jyvaskyla, Finland), who helped me understand the GLoBES Simulation Software and helped resolve my doubts regarding the analyses with GLoBES through a series of Facebook chats and emails. I would also like to thank Jean-Eric Campagne (University of Paris-Sud, France) for providing me useful information regarding long baseline neutrino experiments at various stages of this work. I also thank my colleagues here at the IISER Mohali, India for contributing to the friendly environment which has made my time here so enjoyable. Thanks especially to my friends and office-mates Rishabh Singh, Ravneet Singh Bedi, Nilotpal Kakati, Vassu Doomra, Ojaswi Gupta, Akhil Bhardwaj, Rohit Gupta and Kriti Kamal Gupta, for the good company and chat, both work and non-work related, inside and outside the office. I would also like to thank Nishat Fiza and Dr. Kirandeep for proofreading this document and providing useful inputs. Finally, I would also like to thank Prof. Sanjib Kumar Agarwalla (Institute of Physics, Bhubaneswar, India) who first guided me to the interesting field of Neutrino Physics during a summer internship.

Paras Koundal

MS14083

IISER Mohali

List of Figures

2.1 Zenith Angle distribution of the observed number of electron and muon type events.[F+98] 11

4.1 Schematic Diagram: Conventional Neutrino Beams [Str19]. 24
4.2 Schematic of the focussing principle of the secondary particles [NP16]. 30
4.3 PREM Density Profiles for various baselines. 32
4.4 Earth's radial density map according to PREM [McC19]. 32
4.5 Location of the SPL on the CERN site [Fre17]. 33
4.6 Total Neutrino Flux at Near detector - **CERN** for **Plus** Horn focussing. 34
4.7 **Total Anti-Neutrino Flux** at Near detector - **CERN** for **Plus** Horn focussing. . 34
4.8 **Total Neutrino Flux** at Near detector - **CERN** for **Minus** Horn focussing. . . . 35
4.9 **Total Anti-Neutrino Flux** at Near detector - **CERN** for **Minus** Horn focussing. 35
4.10 **Total Neutrino Flux** at Near detector - **Fermilab** for **Plus** Horn focussing. . . 36
4.11 **Total Anti-Neutrino Flux** at Near detector - **Fermilab** for **Plus** Horn focussing. 37
4.12 **Total Neutrino Flux** at Near detector - **Fermilab** for **Minus** Horn focussing. . 37
4.13 **Total Anti-Neutrino Flux** at Near detector - **Fermilab** for **Minus** Horn focussing. 38
4.14 Schematic Diagram: J-PARC Neutrino Facility [JP19]. 38
4.15 **Total Neutrino Flux** at Near detector - **J-PARC** for **Plus** Horn focussing. . . . 39
4.16 **Total Anti-Neutrino Flux** at Near detector - **J-PARC** for **Plus** Horn focussing. 40
4.17 **Total Neutrino Flux** at Near detector - **J-PARC** for **Minus** Horn focussing. . . 40
4.18 **Total Anti-Neutrino Flux** at Near detector - **J-PARC** for **Minus** Horn focussing. 41

5.1 Schematic of INO to be established at Bodi West Hills near Theni, Tamil Nadu, India [STIE15]. 43
5.2 Matter Density Profile for neutrino propagating from CERN-SPL to INO. . . . 44

5.3 **Total Neutrino Flux** at INO from CERN for **Plus** Horn Focusing. 44
5.4 **Total Anti-Neutrino Flux** at INO for **Plus** Horn Focusing. 45
5.5 **Total Neutrino Flux** at INO from CERN for **Minus** Horn Focusing. 45
5.6 **Total Anti-Neutrino Flux** at INO from CERN for **Minus** Horn Focusing. . . . 46
5.7 **Neutrino** Transition Probability Values for CERN to INO Baseline. 47
5.8 **Anti-Neutrino** Transition Probability Values for CERN to INO Baseline. . . . 47
5.9 Matter Density Profile for neutrino propagating from Fermilab-NOvA to INO. . 48
5.10 **Total Neutrino Flux** at INO from Fermilab for **Plus** Horn Focusing. 48
5.11 **Total Anti-Neutrino Flux** at INO from Fermilab for **Plus** Horn Focusing. . . . 49
5.12 **Total Neutrino Flux** at INO from Fermilab for **Minus** Horn Focusing. 49
5.13 **Total Anti-Neutrino Flux** at INO from Fermilab for **Minus** Horn Focusing. . . 50
5.14 **Neutrino** Transition Probability Values for Fermilab to INO Baseline. 51
5.15 **Anti-Neutrino** Transition Probability Values for Fermilab to INO Baseline. . . 51
5.16 Matter Density Profile for neutrino propagating from J-PARC to INO. 52
5.17 **Total Neutrino Flux** at INO from J-PARC for **Plus** Horn Focusing. 52
5.18 **Total Anti-Neutrino Flux** at INO from J-PARC for **Plus** Horn Focusing. . . . 53
5.19 **Total Neutrino Flux** at INO from J-PARC for **Minus** Horn Focusing. 53
5.20 **Total Anti-Neutrino Flux** at INO from J-PARC for **Minus** Horn Focusing. . . 54
5.21 **Neutrino** Transition Probability Values for J-PARC to INO Baseline 55
5.22 **Anti-Neutrino** Transition Probability Values for J-PARC to INO Baseline . . . 55

6.1 Location of Detector (Blue Dot) in IISER Mohali, India Campus. 57
6.2 Matter Density Profile for neutrino propagating from CERN-SPL to EHEP Lab, IISER Mohali. 58
6.3 **Total Neutrino Flux** at EHEP Lab, IISER Mohali from CERN for **Plus** Horn Focusing. 58
6.4 **Total Anti-Neutrino Flux** at EHEP Lab, IISER Mohali from CERN for **Plus** Horn Focusing. 59
6.5 **Total Neutrino Flux** at EHEP Lab, IISER Mohali from CERN for **Minus** Horn Focusing. 59
6.6 **Total Anti-Neutrino Flux** at EHEP Lab, IISER Mohali from CERN for **Minus** Horn Focusing. 60

6.7 **Neutrino** Transition Probability Values for CERN to EHEP Lab, IISER Mohali Baseline. 61
6.8 **Anti-Neutrino** Transition Probability Values for CERN to EHEP Lab, IISER Mohali Baseline. 61
6.9 Matter Density Profile for neutrino propagating from Fermilab to EHEP Lab, IISER Mohali, India 62
6.10 **Total Neutrino Flux** at EHEP Lab, IISER Mohali from Fermilab for **Plus** Horn Focusing. 62
6.11 **Total Anti-Neutrino Flux** at EHEP Lab, IISER Mohali from Fermilab for **Plus** Horn Focusing. 63
6.12 **Total Neutrino Flux** at EHEP Lab, IISER Mohali from Fermilab for **Minus** Horn Focusing. 63
6.13 **Total Anti-Neutrino Flux** at EHEP Lab, IISER Mohali from Fermilab for **Minus** Horn Focusing. 64
6.14 **Neutrino** Transition Probability Values for Fermilab to EHEP Lab, IISER Mohali Baseline 65
6.15 **Anti-Neutrino** Transition Probability Values for Fermilab to EHEP Lab, IISER Mohali Baseline. 65
6.16 Matter Density Profile for neutrino propagating from J-PARC to EHEP Lab, IISER Mohali. 66
6.17 **Total Neutrino Flux** at EHEP Lab, IISER Mohali from J-PARC for **Plus** Horn Focusing. 66
6.18 **Total Anti-Neutrino Flux** at EHEP Lab, IISER Mohali from J-PARC for **Plus** Horn Focusing. 67
6.19 **Total Neutrino Flux** at EHEP Lab, IISER Mohali from J-PARC for **Minus** Horn Focusing. 67
6.20 **Total Anti-Neutrino Flux** at EHEP Lab, IISER Mohali from J-PARC for **Minus** Horn Focusing. 68
6.21 **Neutrino** Transition Probability Values for J-PARC to EHEP Lab, IISER Mohali Baseline. 69
6.22 **Anti-Neutrino** Transition Probability Values for J-PARC to EHEP Lab, IISER Mohali Baseline. 69

A.1 Zenith Angle distribution of observed number of events in sub-MeV and multi-GeV range for electron and muon like events [F+98] 79

Contents

Acknowledgement **i**

List of Figures **iii**

Abstract **xiii**

1 Introduction **1**

1.1 Detecting the Poltergeist 2

1.2 Motivation 2

1.3 Early anomalies in Neutrino Physics 3

1.3.1 Solar Neutrino Problem 3

1.4 Atmospheric Neutrino Problem 4

1.4.1 Double Ratio 5

2 Neutrino Oscillation (In Vacuum) **7**

2.1 General Derivation 7

2.2 2-Flavor Neutrino Oscillation 9

2.2.1 Parameters 10

2.2.2 2-Flavor Neutrino Oscillation: Interpretation of Atmospheric Neutrino Problem 11

2.2.3 2-Flavor Neutrino Oscillation: Interpretation of Solar Neutrino Problem 12

2.3 3-Flavor Neutrino Oscillation 13

2.3.1 Probability Expressions for Three-Flavor Neutrino Oscillation 14

3 Neutrino Oscillation (In Matter) 17

3.1 General Derivation . . . 17

3.2 Two-Flavor Oscillations . . . 19

3.3 Three-Flavor Oscillations . . . 20

3.3.1 With OMSD Approximation . . . 21

3.3.2 Without OMSD approximation . . . 22

4 Neutrinos from Accelerators 23

4.1 Neutrino Beams . . . 24

4.2 Flux Calculation Methodology . . . 25

4.3 Source-Detector Setup . . . 26

4.3.1 Extrapolating Beam Flux . . . 28

4.4 Two-Detector Setup . . . 28

4.4.1 Extrapolating Beam Flux . . . 29

4.5 Horn focussing . . . 30

4.6 Simulating Experiments - GLoBES Software Package . . . 31

4.7 Density Distribution . . . 32

4.8 Flux at Near Detector . . . 33

4.8.1 Near Detector: CERN . . . 33

4.8.2 NOvA - Fermilab . . . 36

4.8.3 J-PARC . . . 38

5 INO: India-based Neutrino Observatory 43

5.1 Source: CERN . . . 44

5.1.1 Plus Focussing . . . 44

5.1.2 Minus Focussing . . . 45

5.1.3 Oscillation Probabilities . . . 46

5.2 Source: Fermilab . . . 48

5.2.1 Plus Focussing . . . 48

5.2.2 Minus Focussing . . . 49

5.2.3 Oscillation Probabilities . . . 50

5.3 Source: J-PARC . . . 52

5.3.1 Plus Focussing . . . 52

5.3.2 Minus Focussing . . . 53
5.3.3 Oscillation Probabilities . . . 54

6 EHEP Lab, IISER Mohali **57**
6.1 Source: CERN . . . 58
6.1.1 Plus Focussing . . . 58
6.1.2 Minus Focussing . . . 59
6.1.3 Oscillation Probabilities . . . 60
6.2 Source: Fermilab . . . 62
6.2.1 Plus Focussing . . . 62
6.2.2 Minus Focussing . . . 63
6.2.3 Oscillation Probabilities . . . 64
6.3 Source: J-PARC . . . 66
6.3.1 Plus Focussing . . . 66
6.3.2 Minus Focussing . . . 67
6.3.3 Oscillation Probabilities . . . 68

7 Conclusions **71**

A Solar and Atmospheric Neutrino Problem **75**
A.1 Solar Neutrino Problem: . . . 75
A.1.1 Homestake Experiment: . . . 75
A.1.2 Super Kamiokande Experiment: . . . 76
A.1.3 SAGE and GALLEX: . . . 76
A.1.4 Sudbury Neutrino Observatory (SNO): . . . 77
A.2 Atmospheric Neutrino Problem . . . 78
A.2.1 Super-Kamiokande(SK) Observations . . . 78

B Standard Derivation of Neutrino Oscillations **81**

C General Survival and Transition Probability Expressions **83**
C.1 Expression for Survival Probability, $\alpha = \beta$ . . . 83
C.2 Expression for Transition Probability, $\alpha \neq \beta$ . . . 85

D Few Survival and Transition Probability Expressions **87**

D.1 ν_e-ν_e Channel 87

D.2 ν_e-ν_μ Channel 88

E Matter Modified Neutrino Oscillation **91**

E.1 Two Flavor Case 91

E.2 Three Flavor Case 92

E.2.1 OMSD approximation 94

E.2.2 Without OMSD approximation 96

Bibliography **99**

Cosmic Gall

Neutrinos, they are very small.
They have no charge and have no mass
And do not interact at all.
The earth is just a silly ball
To them, through which they simply pass,
Like dustmaids down a drafty hall
Or photons through a sheet of glass.
They snub the most exquisite gas,
Ignore the most substantial wall,
Cold-shoulder steel and sounding brass,
Insult the stallion in his stall,
And, scorning barriers of class,
Infiltrate you and me! Like tall
And painless guillotines, they fall
Down through our heads into the grass.
At night, they enter at Nepal
And pierce the lover and his lass
From underneath the bed - you call
It wonderful; I call it crass.

- John Updike

Abstract

"A billion neutrinos go swimming in heavy water: one gets wet."

- Michael Kamakana

Neutrino Physics over decades has proved crucial in improving our understanding of the Standard Model of Particle Physics and has moreover opened ways to probe Beyond Standard Model Physics too. The discovery of the process of conversion of neutrino from one flavor to other during propagation, called as Neutrino Oscillation has demonstrated that neutrinos have a non-zero mass (a major correction needed in Updike's poem). It has also made us possible to ask if neutrinos may hold the key to many other great questions of physics such as why is the Universe dominated by matter (over anti-matter). Neutrino data collection from various sources has already provided us with some insights into these mechanisms. However, all these suffer from a significant drawback of no control over the source. This limits the number as well as the sensitivity of the parameters we want to measure. Accelerator facilities come to rescue here. Due to greater control over the source, we can produce neutrinos of all flavors as well as control other parameters like intensity, propagation direction, etc. It is also essential to understand the flux because of its direct dependence in every neutrino-nucleus cross-section measurement, estimation of oscillation parameters [A$^+$16] etc.. This thesis details the neutrino flux estimation at any detector location on earth considering three accelerator neutrino sources, namely: CERN, Fermilab, and J-PARC. This provides the benefit of accessing three different baselines for a single detector experiment. Presence of three different baselines not only offer a way to cross-check results but also provide an opportunity to access different sensitivity regions to probe different parameters. This thesis focusses on flux estimation at two detector locations, namely: Indian Neutrino Observatory and EHEP (Experimental High Energy Physics) Lab, IISER Mohali, India. The thesis starts with an introduction to neutrinos in Chapter 1 and then goes on to describe Neutrino Oscillation in vacuum and matter in Chapter 2 and Chapter 3 respectively. Chapter 4 discusses about the neutrinos produced at accelerators and methodology used to estimate flux at detectors. Finally, Chapter 5, 6 and 7 present the results obtained and conclusions drawn.

Chapter 1

Introduction

> Neutrinos ... win the minimalist contest: zero charge, zero radius, and very possibly zero mass.
>
> Leon M. Lederman

A neutrino (ν) is a fermion with zero charge and half-integer spin. Neutrinos are unique since they have very distinct properties from other particles. Their mass is several orders less than other fermions. They travel with ultra-relativistic speeds, don't feel strong interactions and interact via weak interactions.

W. Pauli in 1930, was the first one to propose the existence of neutrinos [Rei96] to justify the issue of obtaining a continuous energy spectrum in β-decay of atomic nuclei. He initially called this particle as "neutron". Pauli was very speculative of his proposal and did not publish his results until 1934. However, till this time E. Fermi had already developed the theory of β-decay process. Fermi later renamed the particles to **" Neutrino (Little neutral one)"** (as a wordplay on neutrone, the Italian name of the neutron) to distinguish it from neutron (as we know today), discovered by J. Chadwick in 1932.

Neutrinos with a CMB (Cosmic Microwave Background) density of around 300 per cm^3 hold the second place for their abundance in the universe, with photons being the most abundant [Kik09]. Thus to comprehend the universe, the study of neutrinos is critical.' They also interact very weakly; hence they can travel long distances to provide us information about the dynamics of distant stars. Also, in the last few decades, it has been confirmed by multiple experiments that neutrinos have nonzero mass. This inference has been based on the discovery of

the phenomenon called **Neutrino Oscillation** - neutrinos changing flavors during propagation.

1.1 Detecting the Poltergeist

Due to their very weakly interacting property, neutrinos remained elusive for around 20 years, since they were first proposed. The Reines-Cowan experiment, titled as **Project Poltergeist** [RC97], was the first experiment to detect neutrinos.The detection was carried in 1956 at Savannah River Reactor. For his discovery, Reines was later awarded the Nobel Prize. They used the Inverse β decay process as their detection process, given by:

$$p + \bar{\nu}_e \rightarrow n + e^+$$

These were called as "electron-type neutrinos" or "electron-flavored neutrinos".
Later, two other flavors on neutrinos were detected. Muon Neutrinos (ν_μ) were detected in 1962 by L. Lederman, M. Schwarz and J. Stienberger (later awarded Nobel Prize) [DGG$^+$62]; and in 2000, DONUT Collaboration discovered the tau flavored neutrino (ν_τ) [K$^+$01]. The word "flavor" is just to signify the correspondence between their corresponding charged Lepton partner. Electron Neutrinos are produced or detected with their corresponding charged Lepton, i.e. electron and similarly for two other flavors of Neutrinos.

1.2 Motivation

Motivation for a Physicist

- Neutrinos can provide us with a huge amount of information about the universe by acting as alternative astrophysical tracers since photons can be trapped by interstellar dust.
- Due to their weakly interacting property, they can travel long distances to tell us about distant star dynamics.
- Probing different phenomenon related to Neutrinos can help put constraints on "Beyond Standard Model" physics.

Motivation for Public

- Nuclear reactors undergo a lot of decay processes which release a large flux of neutrinos. We can remotely monitor these neutrinos from nuclear reactors which can help in nuclear non-proliferation [Cri11].

- Similar to reactors earth also undergoes a lot of decay processes releasing neutrinos, called as **Geo-neutrinos**. Geo-neutrinos could provide us important seismological data [Kot79] which can detect early disturbances produced by earthquakes. These can also help us to detect Mineral and Oil deposits deep in the earth.
- **Medical Use:** The RPC (resistive plate chambers) detectors used for detection of neutrinos can detect cancer early and prove to be a much cheaper facility if developed on commercial scale [B$^+$06].

1.3 Early anomalies in Neutrino Physics

1.3.1 Solar Neutrino Problem

Sun besides releasing its energy as heat and light, also spends around (2-3)% of its energy as neutrinos. Detecting solar neutrinos is important since the weakly interacting neutrinos generated near the core of the sun can retain most of the information and tell us about its internal dynamics.

Standard Solar Model given by John Bahcall and his collaborators [Bah99] [BBP98], gives an excellent estimate of the number of neutrinos produced by the sun. Over the years, through various refinements in the Solar Model, we have great information and accuracy of the spectrum of solar neutrinos incident on earth [Bel04]. The *pp*-chain releases the largest flux of neutrinos with E$<$0.411MeV. However, the early experiments performed to calculate solar neutrino flux gave surprising results. **Ray Davis's Homestake experiment(1965)** [DHH68] and **Super Kamiokande Experiment(1985)** [You97] observed about 50%-60% deficit than the expected neutrino flux. Later other experiments like **SAGE** [Gav01] and **GALLEX** [H$^+$96] were able to make better measurements of the solar neutrino flux but still observed a deficit in the neutrino flux. After the unexpected neutrino flux measurements measured by various experiments, questions were raised whether the model we are using, i.e., "Standard Solar Model" to estimate neutrino flux is correct or not. Helioseismology results turned the decision in favor of "Standard Solar Model." The results were matching with the expectations to better than 99.5%. So it was concluded that there was still some problem with the measurement process only.

It was realized that the previous experiments were exclusively sensitive to electron neutrinos only. We might be getting other flavors, but the experiment was unable to those flavors. **Sud-**

bury Neutrino Observatory (SNO) [Kle02] was used to resolve this problem. SNO confirmed that the total expected solar neutrino flux on earth is the sum of neutrino fluxes of all three types of neutrinos, i.e., electron-neutrino, muon-neutrino, tau-neutrino. However, through the solar model, it is known that the Sun only produces electron type of neutrinos. Hence, it was concluded that while their propagation from the sun to earth **neutrinos must be changing from one flavor to another**. Multiple theories attempted to explain this flavor change process. **Neutrino Oscillation** was one such theory. For details refer to **Appendix A**.

1.4 Atmospheric Neutrino Problem

The atmosphere is constantly bombarded by cosmic rays. When cosmic rays (mostly composed of protons and helium nuclei) hit air nuclei in the atmosphere they produce secondary particles like pions, kaons, etc.. Atmospheric neutrinos Stem from the decay of these charged pions and subsequently muons. Neutrinos in the atmosphere are predominantly produced in two flavors (ν_e, ν_μ).The decay chain is:

$$\pi^\pm \to \mu^\pm + \nu_\mu(\bar{\nu_\mu})$$
$$\mu^\pm \to e^\pm + \bar{\nu_\mu}(\nu_\mu) + \nu_e(\bar{\nu_e})$$

The energy spectrum for atmospheric neutrinos varies from few GeV to around 10^4 GeV. The inputs to estimate the atmospheric neutrino flux are mostly [DV99]: **a).** The energy spectrum of cosmic rays. **b).** The energy spectrum of muons produced through the decay of secondary particles like pions and kaons. **c).** Modeling of the interaction of cosmic rays and secondary particles with air nuclei. **d).** Modeling of geomagnetic effect on the flux of cosmic rays. **e).** Modeling of the longitudinal development of extensive air showers produced by cosmic rays.
The flux of ν_e and ν_μ depends on the flux of muons produced in the decay of pi/K in the atmosphere. Hence the uncertainties on the flux of each of them are highly correlated. Therefore, even if uncertainties on the absolute flux are high, the ratio of ν-induced muon to electron events, for a given detector configuration, can be estimated more accurately. We have:

$$R_{theory}(E) = \frac{N_\mu^{exp}(E)}{N_e^{exp}(E)}$$

where $N_\mu^{exp}(E)$ and $N_e^{exp}(E)$ are the expected number of muons and electrons respectively. Here E is the energy of the charged lepton produced in the interaction. The ratio R_{theory} is expected to be around two at low energies.

Experiment	Type of Experiment	R
Super-Kamiokande	Water Cerenkov	0.675± 0.085
Soudan 2	Iron Tracking Calorimeter	0.69± 0.13
IMB	Water Cerenkov	0.54± 0.12
Kamiokande	Water Cerenkov	0.60± 0.07

Table 1.1: Measurements of the double ratio for various atmospheric neutrino experiments.

1.4.1 Double Ratio

The spectrum of low energy $\nu-$induced muons and electrons has been measured experimentally by various experiments (Soudan 2, MACRO and Super-Kamiokande) and compared with predictions. The ratio is defined as:

$$R_{obs}(E) = \frac{N_{\mu}^{obs}(E)}{N_{e}^{obs}(E)}$$

The ratio of observed and theoretical values of the above parameter is called the Double Ratio and is given by:

$$R = \frac{R_{obs}(E)}{R_{theory}(E)} \tag{1.1}$$

Theoretically, this ratio is expected to be unity. But various experiments (***Table 1.1***) showed that R varies significantly from unity.

This observation was referred to as the **Atmospheric Neutrino Anomaly**. Super-Kamiokande was able to measure the direction of the incoming neutrinos in addition to R-value. This detector in addition to confirming anomaly with high statistics also gave evidence of **Neutrino Oscillation**.

Chapter 2

Neutrino Oscillation (In Vacuum)

First proposed by Bruno Pontecorvo in 1957 [Pon57], experiments with neutrinos from various sources(solar, atmospheric, reactor and accelerator) have very well established that *neutrinos produced and identified in a specific flavor (at the source) has a nonzero probability of changing their flavor during propagation* leading to detection in a different flavor state later. This phenomenon is referred to as **Neutrino Oscillation**. The likelihood of flavor transition has its dependence on the neutrino energy and the propagation distance, i.e., the distance between the source and the detector. Neutrino Oscillation was able to resolve the solar (and atmospheric) neutrino problem and explain their deficits. It is also vital to study neutrino oscillation since till date it is the only method to observe the physical effects of nonzero neutrino masses. Further, it also tells that neutrino mass eigenstates are different from neutrino flavor eigenstates.
As discussed in the previous chapter, the measurement done by SNO of solar neutrinos can be characterized by neutrino flavor changes [Win10]. Also, the observation of atmospheric neutrinos by the Super-Kamiokande experiment further offered evidence in support for neutrino oscillations as the leading flavor change mechanism. Both the solar and atmospheric neutrino flavor changes can be portrayed as sub-segments of the general three-flavor oscillation case, explained by different sets of oscillation parameters.

2.1 General Derivation

If neutrinos have masses, the weak eigenstates, ν_α, produced in a weak interaction are, in general, linear combinations of the mass eigenstates ν_i [GGM08]. For three neutrino flavors, it is described by a 3*3 unitary mixing matrix paramterised by 3 mixing angle and 1 (or 3)

physical phases.[T$^+$18] Deriving expression for a general case:

$$|\nu_\alpha\rangle = \sum_{i=1}^{n} U^*_{\alpha k}|\nu_k\rangle \tag{2.1}$$

where U is unitary matrix, α corresponds to flavor states and k is for mass eigenstates.These are states at the source (i.e. x=0, t=0).

Apply the propagation operator to the mass eigenstates [$|\nu_k(x,t)\rangle = e^{-\imath\phi_k}|\nu_k(0,0)\rangle$, where $\phi_k = E_k t - p_k x$]. Also invert the mixing matrix to mass eigenstates as superposition of flavor states.[$|\nu_k\rangle = \sum_\gamma U_{\gamma k}|\nu_\gamma\rangle$]. Hence we can write:

$$|\nu_\alpha(x,t)\rangle = \sum_\gamma \sum_k U^*_{\alpha k} U_{\gamma k} e^{-\imath\phi_k}|\nu_k(x,t)\rangle \tag{2.2}$$

The probability of getting flavor β at (x,t) if α is generated at the source is given by the square of the amplitude.

$$P_{\nu_\alpha(0,0)\to\nu_\beta(x,t)} = |\langle\nu_\alpha(0,0)|\nu_\beta(x,t)\rangle|^2 \tag{2.3}$$

$$P_{\nu_\alpha\to\nu_\beta} = |\sum_k U^*_{\alpha k} U_{\beta k} e^{-\imath\phi_k}|^2 \tag{2.4}$$

This formula can be expanded to get:

$$P_{\nu_\alpha\to\nu_\beta} = \sum_{k,j} U^*_{\alpha k} U_{\beta k} U_{\alpha j} U^*_{\beta j} exp[-\imath(\phi_k - \phi_j)] \tag{2.5}$$

We can now consider an approximation that neutrinos are ultra-relativistic and hence for any realistic energy(E), the rest mass (i.e. mass eigenvalue (m_i)) is very small in comparison to E. Hence

$$p_i = \sqrt{E_i^2 - m_i^2} = E_i\sqrt{1 - \frac{m_i^2}{E_i^2}} \approx E_i\left(1 - \frac{m_i^2}{2E_i^2}\right)$$

Use the above approximation for the ϕ_i and consider the neutrinos to be of same energy. Also since neutrinos are ultra-relativistic we can replace t(c=1) by x (or L = Distance between source and detector).

$$P_{\nu_\alpha\to\nu_\beta} = \sum_{k,j} U^*_{\alpha k} U_{\beta k} U_{\alpha j} U^*_{\beta j} exp\left[-\imath\frac{\Delta m^2_{kj} L}{2E}\right] \tag{2.6}$$

where $\Delta m^2_{kj} = m^2_k - m^2_j$.

Using the identity:

$$|z_1 + z_2 + z_3 + ...|^2 = \sum_k |z_k|^2 + 2Re\sum_{k>j} z_k z_j^*$$

Hence

$$P_{\nu_\alpha \to \nu_\beta} = \sum_k |U_{\alpha k}|^2 |U_{\beta k}|^2 + 2Re \sum_{k>j} U^*_{\alpha k} U_{\beta k} U_{\alpha j} U^*_{\beta j} exp\left[-2\pi\imath \frac{L}{L^{Osc.}_{kj}}\right] \tag{2.7}$$

where $L^{Osc.}_{kj} = OscillationLength = \frac{4\pi E}{\Delta m^2_{kj}}$ is the distance at which phase generated by Δm^2_{kj} becomes 2π. It is interesting to note that the above formula consists of a constant part (independent of L) and other which shows oscillation. So even if the second part somehow goes to zero, we can still observe some value of $P_{\alpha\beta}$ $(= P_{\nu_\alpha \to \nu_\beta})$.

We can also write the above formula in different form using the following identity (obtained by squaring the condition on matrix elements of a unitary matrix) :

$$\sum_k |U_{\alpha k}|^2 |U_{\beta k}|^2 = \delta_{\alpha\beta} - 2Re \sum_{k>j} U^*_{\alpha k} U_{\beta k} U_{\alpha j} U^*_{\beta j}$$

Hence **(detailed derivation given in Appendix B)**

$$P_{\alpha\beta} = \delta_{\alpha\beta} - 4 * \sum_{k>j} Re[U^*_{\alpha k} U_{\beta k} U_{\alpha j} U^*_{\beta j}] * \sin^2\left(\frac{\Delta m^2_{kj} L}{4E}\right) + 2 * \sum_{k>j} Im[U^*_{\alpha k} U_{\beta k} U_{\alpha j} U^*_{\beta j}] * \sin\left(\frac{\Delta m^2_{kj} L}{2E}\right) \tag{2.8}$$

When $\alpha = \beta$ its called the **"Survival Probability"** and when $\alpha \neq \beta$ its called the **"Transition Probability"**.

Survival Probability is measured by "**Disappearance Channel**" i.e. we are measuring fraction of neutrinos of original flavor left. On the other hand, transition Probability is measured by "**Appearance Channel**" i.e. we are measuring fraction of neutrinos of new flavor.

2.2 2-Flavor Neutrino Oscillation

To simplify things, let's initially suppose two flavor states. Analysis done here will be of great use to understand 3-flavor neutrino oscillations. However, for precise measurements three-flavor analysis is essential. Two flavor oscillation is described by one mixing angle (θ) and one mass difference. The flavor states and mass states are related to each other by a unitary matrix (U), which can be written as:

$$U = \begin{pmatrix} U_{\alpha 1} & U_{\alpha 2} \\ U_{\beta 1} & U_{\beta 2} \end{pmatrix} = \begin{pmatrix} cos(\theta) & sin(\theta) \\ -sin(\theta) & cos(\theta) \end{pmatrix}$$

Hence

$$\begin{pmatrix} \nu_\alpha \\ \nu_\beta \end{pmatrix} = \begin{pmatrix} cos(\theta) & sin(\theta) \\ -sin(\theta) & cos(\theta) \end{pmatrix} \begin{pmatrix} \nu_1 \\ \nu_2 \end{pmatrix}$$

The transition probability now can be obtained by using **Equation (2.8)**

$$P_{\alpha\beta} = sin^2(2\theta) sin^2(\frac{\Delta m^2 L}{4E})$$
$$P_{\alpha\beta} = sin^2(2\theta) sin^2(1.27 \frac{\Delta m^2(\mathbf{eV^2}) L(\mathbf{km})}{E(\mathbf{GeV})}) \tag{2.9}$$

where the second relation is obtained by re-introducing $\hbar$ and c:

$$\frac{\Delta m^2 L}{4E} = \frac{\Delta m^2 c^4 L}{4E\hbar c} = 1.27 \frac{\Delta m^2(\mathbf{eV^2}) L(\mathbf{km})}{E(\mathbf{GeV})} = 1.27 \frac{\Delta m^2(\mathbf{eV^2}) L(\mathbf{m})}{E(\mathbf{MeV})} \tag{2.10}$$

The corresponding survival probability is given by:

$$P_{\alpha\alpha} = 1 - P_{\alpha\beta} \tag{2.11}$$

Since θ is a physical parameter, it is the amplitude determining part of $P_{\alpha\beta}$ **(Equation (2.9))**. On the other hand Δm^2 is the frequency determining part.

2.2.1 Parameters

- **Mixing Angle,** θ

  It determines how different are flavor states from mass states. If $\theta = 0$, it can be easily seen from mixing matrix form that flavor states are identical to mass states. This is the **no mixing** case. If $\theta = \frac{\pi}{4}$, it's the **maximal mixing** situation.

- **Mass-squared difference,** Δm^2

  (Equation (2.9)) clearly tells us that if we are getting a non-zero transition probability

(for some neutrino mixing) in a measurement, then the mass eigenvalues should be **non-zero and non-degenerate** i.e. ***at-least one of the neutrinos must have a non-zero mass*** for oscillation to happen. Also $P_{\alpha\beta}$ is invariant under $\Delta m^2 \to -\Delta m^2$. Hence we can't tell whether m_1 is heavier or lighter than m_2.

- **Baseline to Energy Ratio, L/E**

  This is the only parameter under control of experimentalists. L is the distance between source and detector, and E is the energy of the neutrino.Experimentally if we want to experimentally check a value of Δm^2, then we try to build the experiment to be maximally sensitive to the oscillation probability. Hence the argument of sin should be integral multiple of $\pi/2$ i.e.

$$1.27\Delta m^2 \frac{L}{E} = (2n+1)\frac{\pi}{2}$$
$$\implies \frac{L}{E} = \frac{\pi}{2.54\Delta m^2}$$

2.2.2 2-Flavor Neutrino Oscillation: Interpretation of Atmospheric Neutrino Problem

Due to isotropic distribution, we expect observed number of neutrino events to be symmetric about horizon i.e. $cos(\theta = \ zenith\ angle) = 0$ (i.e. number of upward going neutrinos $\approx$ number of downward going neutrinos).There is consistency between observed and expected results in case of electron-like events. However in case of muon type, a distinct asymmetry is observed around the horizon ($cos(\theta) = 0$) [F$^+$98].The deficit of muon neutrinos is more prevalent for upward going neutrinos (which have larger pathlengths). This pattern can be consistently reconstructed considering $\nu_\mu \leftrightarrow \nu_\tau$ oscillation.

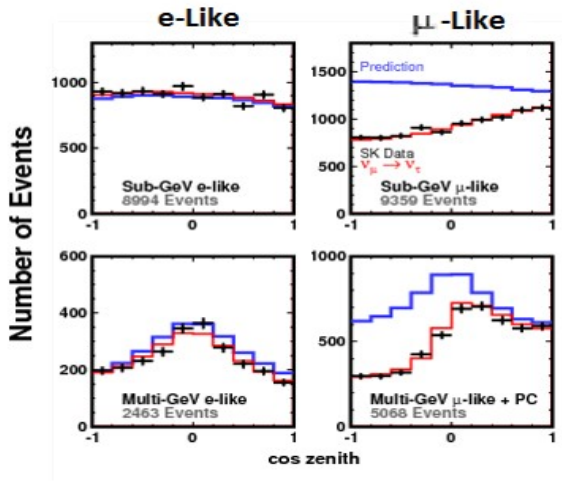

Figure 2.1: Zenith Angle distribution of the observed number of electron and muon type events.[F$^+$98]

Multi-GeV neutrinos, which have longer path-length are depleted more by the oscillations. As the path-length reduces (cos(θ) increases), i.e., for neutrinos coming from the upper hemi-

sphere, the depletion becomes less pronounced. Because of smaller energy for the sub-GeV μ-like neutrino events, the oscillation lengths are smaller. This causes sizable depletion due to oscillations to neutrinos even coming from the upper hemisphere. For up-going sub-GeV neutrinos the oscillation length is much shorter than the path-length, and they experience averaged oscillations.

2.2.2.1 Mathematical Analysis

We can easily estimate the extent of oscillation for different cases by using predetermined values of the different variables in the formula. A rough analysis for multi-GeV events is done below:

- **For Small L/E (Coming directly from Atmosphere)**
  - $P_{\mu\tau} = sin^2(2\theta_{atm})sin^2(0.00127) \leq 1.6 * 10^{-6} \longrightarrow$ We should only see a very slight shift for neutrinos traveling through atmosphere only. $\Longrightarrow$ Confirmed through the plot.
- **For Large L/E (Crossing Earth Surface)**
  - $P_{\mu\tau} = sin^2(2\theta_{atm})sin^2(16.61) \leq .51 \longrightarrow$ We should see around 50 % depletion in expected flux. $\Longrightarrow$ Confirmed through the plot.

It can be clearly seen that neutrino oscillation provides a great way to interpret the experimental results.
After proper analysis the best fit values were found to be:

$$\mathbf{\Delta m^2_{atm} = 2.5 * 10^{-3} eV^2, sin^2(2\theta_{atm}) = 1.0} \; i.e. \; \theta_{\mathbf{atm}} \approx 45^\circ$$

2.2.3 2-Flavor Neutrino Oscillation: Interpretation of Solar Neutrino Problem

Since various models approximately knew most of the solar parameters, it was possible to confirm them using a neutrino source on the earth and to observe the depletion of the flux after the neutrinos travel a known distance. Reactors produce ν_e having energies of the order of few MeV. The oscillation parameters can be measured and tested by placing a neutrino detector at a distance most sensitive to that measurement.

KamLAND detector, the average baseline of $\approx$ 180km, carried out detailed analysis (also using Solar Neutrino Data) in $e-e$ survival channel and found out the best-fit values to be:

$$\mathbf{\Delta m^2_{sol} = 7.5 * 10^{-5} eV^2, \sin^2(2\theta_{sol}) \approx .31} i.e. \mathbf{\theta_{sol}} \approx 34^\circ$$

The above results have been reconfirmed time and again, by various experiments and by various channels, suggesting that the model we have proposed to describe flavor mixing i.e. **Neutrino Oscillation** model is robust.

2.3 3-Flavor Neutrino Oscillation

By dividing the general three-flavor case into sub-sectors, we can easily analyze Solar and atmospheric neutrinos. However, to build a consistent picture of neutrino mixing, we have to develop a framework for the mixing of all three neutrino species,ν_e, ν_μ, ν_τ. Writing the flavor states as the superposition of mass states:

$$|\nu_\alpha\rangle = \sum_{i=1}^{n} U^*_{\alpha k} |\nu_k\rangle \tag{2.12}$$

where $\alpha = e, \mu, \tau$ and $i = 1, 2, 3$

In the case of three flavors, the mixing matrix(U) can be parametrized with three mixing angles and one CP violating phase (two additional Majorana phases do not influence the flavor evolution). The most commonly used parametrization has the form:

$$U_{PMNS} = \begin{pmatrix} 1 & 0 & 0 \\ 0 & c_{23} & s_{23} \\ 0 & -s_{23} & c_{23} \end{pmatrix} \begin{pmatrix} c_{13} & 0 & s_{13}e^{-\iota\delta_{CP}} \\ 0 & 1 & 0 \\ -s_{13}e^{\iota\delta_{CP}} & 0 & c_{13} \end{pmatrix} \begin{pmatrix} c_{12} & s_{12} & 0 \\ -s_{12} & c_{12} & 0 \\ 0 & 0 & 1 \end{pmatrix}$$

$$U_{PMNS} = \begin{pmatrix} c_{12}c_{13} & s_{12}c_{13} & s_{13}e^{-\iota\delta_{CP}} \\ -s_{12}c_{23} - c_{12}s_{13}s_{23}e^{\iota\delta_{CP}} & c_{12}c_{23} - s_{12}s_{13}s_{23}e^{\iota\delta_{CP}} & c_{13}s_{23} \\ s_{12}s_{23} - c_{12}s_{13}c_{23}e^{\iota\delta_{CP}} & -c_{12}s_{23} - s_{12}s_{13}c_{23}e^{\iota\delta_{CP}} & c_{13}c_{23} \end{pmatrix}$$

where $c_{ij} = cos(\theta_{ij})$, $s_{ij} = sin(\theta_{ij})$ and θ_{ij} are the mixing angles.

The probability that a neutrino flavor state ν_α ,generated at the source, is observed in another

flavor state ν_β, at the detector, is give by:

$$P_{\nu_\alpha \to \nu_\beta} = \delta_{\alpha\beta} - 4 * \sum_{k>j} Re[U^*_{\alpha k} U_{\beta k} U_{\alpha j} U^*_{\beta j}] * \sin^2(\frac{\Delta m^2_{kj} L}{4E}) + 2 * \sum_{k>j} Im[U^*_{\alpha k} U_{\beta k} U_{\alpha j} U^*_{\beta j}](\sin(\frac{\Delta m^2_{kj} L}{2E})) \quad (2.13)$$

It can be easily seen from the above equation that the neutrino oscillation probabilities depend on the neutrino energy, **E**, the source-detector distance **L**, on the elements of **U** and, $\Delta m^2_{ij} = m^2_i - m^2_j, i \neq j$,(for relativistic neutrinos). In the case of 3-neutrino mixing there are only two independent neutrino mass squared differences, say $\Delta m^2_{21} \neq 0$ and $\Delta m^2_{31} \neq 0$.The splitting given by $\Delta m^2_{21} = \Delta m^2_\odot > 0$ is identified as the mass splitting responsible for solar neutrino oscillations.On the other hand $|\Delta m^2_{31}| \approx |\Delta m^2_{21}| = |\Delta m^2_A| >> m^2_{21}$ is responsible for the dominant oscillation, atmospheric neutrino oscillation. "$\theta_{12} = \theta_\odot$ and $\theta_{23} = \theta_A$" are the **solar and atmospheric neutrino mixing angles**, respectively. The angle "θ_{13}" is the called **"CHOOZ mixing angle"**.It connects the solar sector with the atmospheric sector.

2.3.1 Probability Expressions for Three-Flavor Neutrino Oscillation

The Survival and Transition Probability expression in case of three flavor neutrino oscillation is given by (derived in **Appendix C**):

$$P_{\alpha\alpha} = 1 - 4|U_{\alpha 2}|^2(1-|U_{\alpha 2}|^2) sin^2\left(\frac{\nabla_{21}}{2}\right) - 4|U_{\alpha 3}|^2(1-|U_{\alpha 3}|^2) sin^2\left(\frac{\nabla_{31}}{2}\right) + 2|U_{\alpha 2}|^2|U_{\alpha 3}|^2\left[4 sin^2\left(\frac{\nabla_{21}}{2}\right) sin^2\left(\frac{\nabla_{31}}{2}\right) + sin(\nabla_{31}) sin(\nabla_{21})\right]$$

$$P_{\alpha\beta} = 4|U_{\alpha 2}|^2|U_{\beta 2}|^2 sin^2\left(\frac{\nabla_{21}}{2}\right) + 4|U_{\alpha 3}|^2|U_{\beta 3}|^2 sin^2\left(\frac{\nabla_{31}}{2}\right) + 2Re[U^*_{\alpha 3} U_{\beta 3} U_{\alpha 2} U^*_{\beta 2}]\left(4 sin^2\left(\frac{\nabla_{21}}{2}\right) sin^2\left(\frac{\nabla_{31}}{2}\right) + sin(\nabla_{31}) sin(\nabla_{21})\right) - 4J_{(\alpha\beta)}\left(4 sin^2(\nabla_{31}) sin^2\left(\frac{\nabla_{21}}{2}\right) - sin(\nabla_{21}) sin\left(\frac{\nabla_{31}}{2}\right)\right)$$

where $\nabla_{ij} = \frac{\Delta m^2_{ij} L}{2E}$ and $J_{(\alpha\beta)}$ is called the Jarlskog Invariant:

$$\begin{aligned} J_{\alpha\beta} = -J_{\beta\alpha} &= Im[U^*_{\alpha 1} U_{\beta 1} U_{\alpha 2} U^*_{\beta 2}] = Im[U^*_{\alpha 2} U_{\beta 2} U_{\alpha 3} U^*_{\beta 3}] = Im[U^*_{\alpha 3} U_{\beta 3} U_{\alpha 1} U^*_{\beta 1}] \\ &= -Im[U^*_{\alpha 2} U_{\beta 2} U_{\alpha 1} U^*_{\beta 1}] = -Im[U^*_{\alpha 1} U_{\beta 1} U_{\alpha 3} U^*_{\beta 3}] = -Im[U^*_{\alpha 3} U_{\beta 3} U_{\alpha 2} U^*_{\beta 2}] \end{aligned} \quad (2.14)$$

Using the standard parametrization i.e. U_{PMNS}, we have:

$$J_{\mu e} = -J_{e\mu} = J_{e\tau} = J_{\tau\mu} = -J_{\mu\tau} = \hat{J} sin(\delta_{CP})$$

with

$$\hat{J} = s_{12}c_{12}s_{13}c_{13}^2 s_{23}c_{23}$$

Chapter 3

Neutrino Oscillation (In Matter)

The works of Wolfenstein [Wol78], Mikheyev and Smirnov [Smi03] were able to tell that the presence of matter can significantly affect the propagation of neutrinos. In the presence of matter, the electron neutrino experiences an additional potential in comparison to muon and the tau neutrino. Electron neutrino in addition to experiencing neutral current scattering (experienced by all three neutrino flavors) also undergoes elastic charged-current scattering. This is mainly because of the presence of an abundance of electrons in matter, and in general, absence of muons and tau-particles.

3.1 General Derivation

The time-evolution of a neutrino mass eigenstate is given by Schrodinger equation:

$$\imath\hbar\frac{\partial}{\partial t}|\nu\rangle_{mass} = H|\nu\rangle_{mass} \tag{3.1}$$

where H is the hamiltonian in the mass eigenbasis. The hamiltonian in flavor eigenbasis can be obtained by calculating the time-evolution of the inner product, as:

$$\psi_{\alpha\beta} = \langle\nu_\beta|\nu_\alpha(t)\rangle$$

$$\imath\hbar\frac{\partial}{\partial t}\psi_{\alpha\beta} = \langle\nu_\beta|\imath\hbar\frac{\partial}{\partial t}\nu_\alpha(t)\rangle$$

Using the completeness relation for neutrino eigenstates we get:

$$\begin{aligned} \imath\hbar\frac{\partial}{\partial t}\psi_{\alpha\beta} &= \sum_{jk\gamma}\langle\nu_\beta|\nu_j\rangle\langle\nu_j|\imath\hbar\frac{\partial}{\partial t}|\nu_k\rangle\langle\nu_k|\nu_\gamma\rangle\langle\nu_\gamma|\nu_\alpha(t)\rangle \\ &= U_{\beta j}E_k\delta_{jk}U^*_{\gamma k}\psi_{\alpha\gamma} \\ &= U_{\beta k}E_k(U^\dagger)_{k\gamma}\psi_{\alpha\gamma} \end{aligned} \tag{3.2}$$

It is evident from above equation that the hamiltonian for flavor neutrinos will be given by:

$$H^{flav} = UHU^\dagger \tag{3.3}$$

In the presence of matter, the Schrodinger equation will be given by:

$$\imath\hbar\frac{\partial}{\partial t}|\nu\rangle_{flav} = \widetilde{H}|\nu\rangle_{flav} \tag{3.4}$$

where $\widetilde{H} = H^{flav} + V$ is the total hamiltonian. Here V is the potential the neutrino experiences due to the presence of matter. $V = V_{CC} + V_{NC}$, where V_{CC} is the potential energy due to charged current scattering and V_{NC} is the potential energy due to neutral current scattering. These can be related to the number density of the matter by

$$V_{CC} = \sqrt{2}G_F N_e \tag{3.5}$$

$$V_{NC} = -\sqrt{2}G_F\frac{N_n}{2} \tag{3.6}$$

where N_e and N_n are the number density due to electron and neutron respectively.
Let the relation between the flavor eigenbasis and the matter-modified mass eigenbasis $|\nu\rangle^m$, in which the total hamiltonian $\widetilde{H}$ is diagonal, be given by a mixing matrix U_m parameterized by matter-modified mixing angle θ^m:

$$|\nu\rangle_{flav} = U_m(\theta^m)|\nu\rangle^m \tag{3.7}$$

Assuming U_m and V to be time-independent; Equation 3.4 can be re-written as

$$\begin{aligned} \imath\hbar\frac{\partial}{\partial t}U_m|\nu\rangle^m &= \widetilde{H}U_m|\nu\rangle^m \\ \imath\hbar\frac{\partial}{\partial t}|\nu\rangle^m &= U_m^\dagger\widetilde{H}U_m|\nu\rangle^m \\ \imath\hbar\frac{\partial}{\partial t}|\nu\rangle^m &= H^m|\nu\rangle^m \end{aligned} \tag{3.8}$$

where

$$H^m = U_m^\dagger [U H U^\dagger + V] U_m \tag{3.9}$$

.

Hence we need to find the diagonal matter-modified hamiltonian in the matter modified-mass eigenbasis $|\nu\rangle^m$.This can then be used to find the matter-modified mixing angle θ^m and the matter-modified squared-mass difference Δ^m [MP16].

3.2 Two-Flavor Oscillations

The hamiltonian in vacuum mass basis is given by:

$$H = \frac{1}{2E} \begin{bmatrix} m_1^2 & 0 \\ 0 & m_2^2 \end{bmatrix} \tag{3.10}$$

We can modify the above hamiltonian [Pra13] to express it as a sum of a matrix consisting of squared-mass differences and a matrix proportional to identity:

$$H = \frac{1}{2E} \begin{bmatrix} \frac{m_1^2 - m_2^2}{2} & 0 \\ 0 & \frac{-m_1^2 + m_2^2}{2} \end{bmatrix} + \frac{1}{2E} \begin{bmatrix} \frac{m_1^2 + m_2^2}{2} & 0 \\ 0 & \frac{m_1^2 + m_2^2}{2} \end{bmatrix} \tag{3.11}$$

The term proportional to identity will only lead to an overall phase and hence can be ignored for all observational purposes. So,

$$H = \frac{1}{4E} \begin{bmatrix} -\Delta & 0 \\ 0 & \Delta \end{bmatrix} \tag{3.12}$$

here $\Delta = m_2^2 - m_1^2$.

Using the relation from equation 3.9 we obtain the matter-modified hamiltonian (details in **Appendix E**), whose diagonal elements are given as:

$$(H^m)_{1,1} = -(H^m)_{2,2} = \frac{1}{4E}[(A - \Delta\cos 2\theta)\cos 2\theta_m - (\Delta \sin 2\theta)\sin 2\theta_m] \tag{3.13}$$

and the off-diagonal elements are:

$$(H^m)_{1,2} = (H^m)_{2,1} = \frac{1}{4E}[(\Delta \sin 2\theta)\cos 2\theta_m + (A - \Delta\cos 2\theta)\sin 2\theta_m] \tag{3.14}$$

where $A = 2EV_{CC}$ (V_{CC} is the potential energy due to charged current scattering and can be obtained from charge number density of matter.)

The matrix H^m can be expressed as:

$$\frac{1}{4E}\begin{bmatrix} -\Delta^m & 0 \\ 0 & \Delta^m \end{bmatrix} \tag{3.15}$$

where $\Delta^m = (m_2^2)_{mat} - (m_1^2)_{mat}$ is the squared-mass difference in the matter-modified mass eigenbasis.

Comparing the diagonal and off-diagonal elements with the form given in equation 3.15, we get:

$$\theta_m = \frac{1}{2}\tan^{-1}\left(\frac{\Delta\sin 2\theta}{\Delta\cos 2\theta - A}\right) \tag{3.16}$$

and

$$\Delta^m = \sqrt{(\Delta\cos 2\theta - A)^2 + (\Delta\sin 2\theta)} \tag{3.17}$$

Thus, in the presence of matter, the two-flavor oscillation probabilities can be obtained by substituting θ_m and Δ_m for the mixing angle and the squared-mass difference respectively in **Equation 2.12**(in natural units)

$$P_{ee}^m = 1 - \sin^2 2\theta_m \sin^2\left(1.27\tfrac{\Delta^m L}{E}\right) \tag{3.18}$$

$$P_{e\mu}^m = \sin^2 2\theta_m \sin^2\left(1.27\tfrac{\Delta^m L}{E}\right) \tag{3.19}$$

3.3 Three-Flavor Oscillations

For three-flavor case, the hamiltonian in vacuum mass basis is given by:

$$H = \frac{1}{2E}\begin{bmatrix} m_1^2 & 0 & 0 \\ 0 & m_2^2 & 0 \\ 0 & 0 & m_3^2 \end{bmatrix} \tag{3.20}$$

Writing the hamiltonian in flavor eigenbasis will be:

$$H^{flav} = UHU^{\dagger} \tag{3.21}$$

$$= \frac{1}{2E} U \begin{bmatrix} m_1^2 & 0 & 0 \\ 0 & m_2^2 & 0 \\ 0 & 0 & m_3^2 \end{bmatrix} U^{\dagger} \tag{3.22}$$

$$= \frac{1}{2E} U \begin{bmatrix} 0 & 0 & 0 \\ 0 & \Delta_{21} & 0 \\ 0 & 0 & \Delta_{31} \end{bmatrix} U^{\dagger} \qquad = \frac{1}{2E}(UM^2U^{\dagger}) \tag{3.23}$$

3.3.1 With OMSD Approximation

We will now be deriving the expression for matter-modified mixing angles and squared-mass differences, considering three neutrino flavors [AJL$^+$04]. As derived and explained multiple times before, neutrino oscillation has sensitivity to squared mass-differences only and not to the neutrino mass eigenvalues. However, for the three mass eigenvalues for a three-flavor oscillation case, only two are independent squared-mass differences.

Data from experiments have shown that the parameter $\alpha = \frac{\Delta_{21}}{\Delta_{31}}$ is roughly 0.03. This can be exploited to derive approximate results, by considering $\Delta_{21} = 0$ **[OMSD (One Mass Scale Dominant) Approximation]**. Later results with Δ_{21} non-zero can also be derived.

To obtain the matter-modified squared-mass differences and the mixing angles, we repeat similar steps (details in **Appendix E**) as done for matter-modified two flavor case. We get the matter-modified squared-mass differences as:

$$\Delta_{31}^m = \sqrt{(\Delta_{31} cos2\theta_{13} - A)^2 + (\Delta_{31} sin2\theta_{13})^2} \tag{3.24}$$

$$\Delta_{21}^m = \frac{1}{2}(\Delta_{31}^m - \Delta_{31} - A) \tag{3.25}$$

$$\Delta_{23}^m = \frac{1}{2}(-\Delta_{31}^m - \Delta_{31} - A) \tag{3.26}$$

and matter-modified mixing angle is given by:

$$\theta_{13}^m = \frac{1}{2}\tan^{-1}\left(\frac{\Delta_{31} sin2\theta_{13}}{\Delta_{31} cos2\theta_{13} - A}\right) \tag{3.27}$$

Hence few probability expressions can be given as (in natural units):

$$P_{ee} = 1 - \sin^2 2\theta^m_{13} \sin^2 \left[\frac{1.27(\Delta^m_{31})L}{E}\right] \tag{3.28}$$

$$\begin{aligned} P_{\mu\mu} = 1 &- \cos^2 2\theta^m_{13} sin^2 2\theta_{23} \sin^2 \left[\frac{1.27(\Delta_{31} + A + \Delta^m_{31})L}{2E}\right] \\ &- \sin^2 2\theta^m_{13} sin^2 2\theta_{23} \sin^2 \left[\frac{1.27(\Delta_{31} + A - \Delta^m_{31})L}{2E}\right] \\ &- \sin^4 \theta_{23} \sin^2 2\theta_{13} \sin^2 \left[\frac{1.27\Delta^m_{31}L}{E}\right] \end{aligned} \tag{3.29}$$

$$P_{\mu e} = \sin^2 \theta_{13} \sin^2 \theta_{23} \sin^2 \left[\frac{1.27\Delta^m_{31}L}{E}\right] \quad \textit{and so on..} \tag{3.30}$$

3.3.2 Without OMSD approximation

Sometimes for certain L and E values, the phase in the leading term can diminish the leading term to the extent at which α cannot be ignored. Also, in the **OMSD approximation**, the δ_{CP}-dependence is lost from the probability expressions. It is, therefore, necessary to include a non-zero Δ_{21} in the calculations.For details please refer to **Appendix E**.

Chapter 4

Neutrinos from Accelerators

High Energy Physics has revolutionized the way we look at the universe. Neutrino Physics has taken a central role in it for quite some time. Observing neutrinos from various sources has helped measure multiple parameters which have not only helped us understand neutrino physics in more detail but has also opened paths to probe beyond Standard Model Physics. It bridges many disciplines of physics which complement each other. However, recent experiments on neutrinos from the sun have shown that the flux of solar neutrinos reaching the earth is not sufficient to probe all the parameters[Ric00][Spu18]. Experiments also reveal that muon-type neutrinos produced in the atmosphere seem to be depleted while passing through the earth compared to that incident on detectors directly from above[Suz06]. This puts a limit on the number as well as the precision of parameters we can measure. Neutrino beams from accelerators have been proved to be of the great rescue here. They have not only helped us understand the phenomenon that governs neutrino but has also helped in unifying weak-nuclear force and electromagnetic force[Kop07]. Accelerator-based experiments have led to important discoveries like the neutral currents at the CERN PS to the determination of the number of neutrinos at LEP [D^+18].

Accelerator neutrino experiments can be classified by the length of its baseline, which is a major factor in determining its sensitivity to various parameters like Δm^2. Accordingly:

- **Long Base Line (LBL)** accelerator neutrino experiments can probe still unknown parameters since matter effects become significant: L$>$ 100 km.
- **Short Base Line (SBL)** accelerator neutrino experiments that are devoted to the search of additional neutrinos beyond the 3*3 scenario: L$\approx$ 1km.

Here, I will only discuss the Long Base Line (LBL) accelerator neutrino experiments. These kinds of experiments generally have a two detector setup, where neutrinos generated by the accelerator are first measured before oscillation in a near detector and then again, after oscillation in a far detector. This technique has a major advantage that a very intense beam can be operated at the optimal L/E value. Several LBL experiments like K2K [A$^+$05] and T2K [A$^+$11] in Japan, MINOS [M$^+$06] in USA and OPERA [G$^+$00] in Italy, not only implement this technique but have also helped improve the precision of oscillation parameters measured by previous experiments.

4.1 Neutrino Beams

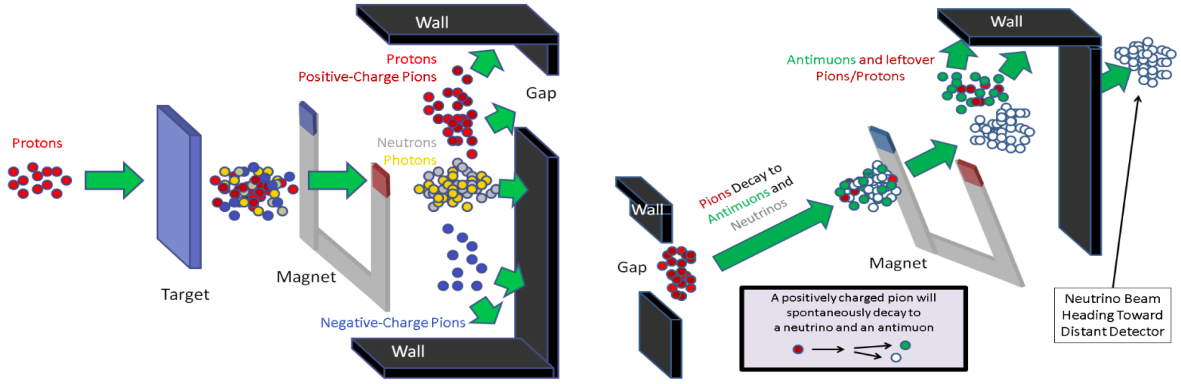

Figure 4.1: Schematic Diagram: Conventional Neutrino Beams [Str19].

First proposed by M. Schwartz [Sch60] and Pontecorvo; and first tested out by Lederman, Schwartz, Steinberger, and collaborators [DGG$^+$62], conventional neutrino beams are generated impinging a high-energy beam of protons produced by an accelerator upon a nuclear target (as shown in **Figure 4.1**). After the protons hit the thin slab of material, the atomic nuclei form a beam of particles like protons and neutrons with a beam of other secondaries like pion and kaons. The beam is then allowed to pass through a magnetic field, which bends and deviates the charged particles from their original path. The direction of bending is determined by the electric charge of the particle, whereas its energy decides the bending amount. This is used as a filter, and positive(negative) charged pions (in a fixed energy range) are allowed to propagate further — the pions decay into an anti-muon(muon) and a muon-neutrino(muon anti-neutrino). The beam now has muons, with a few as-yet-undecayed pions and stray protons left over, and neutrinos. Again with the use of magnetic field all charged particles are focused out and stopped, and an almost pure neutrino beam is produced. Similar processes are carried out to create other

flavors of neutrinos. By controlling the parameters, we can restrict the beam direction. The neutrino sources which are considered for the present work are the **CERN Facility**, the **Fermilab Facility** and the **J-PARC Facility**. The detector location that I will be explicitly using are **INO (Indian Neutrino Observatory)** and **EHEP-Lab IISER Mohali, India**. However, the setup developed by me allows to enter any detector location on earth and calculate the final number of events from CERN, Fermilab, and J-PARC. The significant advantage of longer-baselines over shorter baselines is the presence of probability peak at higher energies, which in turn improves cross-sections [CLP13]. Long baselines because of enhanced matter-effects are also able to probe problems of mass-hierarchy.

4.2 Flux Calculation Methodology

To calculate the final number of events, I have used a simplistic computation method that gives the number of neutrinos for given energy (spectrum) and transition channel. In spite of its simplistic form, for practical purposes, it provides a sufficiently good estimate. The underlying formula for the calculation is

$$N^{exp}_{\nu_\beta}(E) = \varepsilon(E)\sigma(E)P_{\nu_\alpha\to\nu_\beta}(E,L,\theta,\Delta m^2)\Phi_{\nu_\beta}(E,L) \tag{4.1}$$

Here: E,L = *Energy and baseline* ; $\theta,\Delta m^2$ = *Mixing angle and squared − mass − eigenvalues difference.* ; $N^{exp}_{\nu_x}(E)$ = *Number of neutrinos detected in* β *− flavor at the far detector* ; ε = *Detection Efficiency of the far detector* ; σ = *Interaction Cross − Section at the far detector* ; $P_{\nu_\alpha\to\nu_\beta}$ = *Neutrino − Oscillation Probability* ; Φ_{ν_β} = *Total interpolated incident flux at far detector.*

Out of the factors, as mentioned above, detection-efficiency and cross-section are obtained by detector calibration. In my case because of no established detector or detection information, I have considered the values of both these parameters as unity. However, for detailed and accurate analysis the detector information has to be considered to get the full-picture (The number of neutrinos collected by a given detector depends on the cross-section, detector mass, and neutrino flux incident on the detector. Hence both large detectors and high neutrino flux are needed to observe these particles.). The Neutrino-oscillation probability factor has been considered in

length before, and transition probability relation for matter case is considered in GLoBES for the simulation. The total flux at the far detector is obtained by extrapolating flux from **source** or from **near detector**. Both cases are discussed in detail later. However, for simulation, only two-detector setup was considered.

Most of the neutrino experiments are focussed on measuring oscillation parameters. Hence once a measurement is performed, the observed event distribution $N^{obs}(E)$ is compared to $N^{exp}(E)$ to extract the parameters that best match the observations. Usually, the uncertainties in the calculation of the predicted flux and neutrino interaction cross-sections are large. The deviations in the predicted flux are mainly due to the difficulty in accurate modeling of the hadronic interactions responsible for generating mesons (hadron production) that produce the neutrino beam. Whereas the uncertainties in the neutrino interaction cross-sections is due to the absence of available cross-section measurements and the large experimental errors associated with them [Gal12]. Two detector setup provides the opportunity to measure hadron production in a dedicated experiment, a significant advantage over source-detector configuration.

4.3 Source-Detector Setup

To know the unoscillated flux at the far detector, we can proceed step-wise by first obtaining the flux produced at the source in the lab frame and then interpolating it to the far detector. Later neutrino-oscillation physics can be added to it to get the total oscillated flux at the detector. Let's consider neutrinos in **centre of mass (C.O.M.)** frame have energy E^* and three-momentum $\vec{p^*} = (p_x^*, p_y^*, p_z^*)$. Also, since neutrinos are ultra-relativistic with their negligible mass in comparison to their energy we can write [Orm09]:

$$E^* = |\vec{p}^*| \; and \;\; p_x^* = E^* sin\theta^* cos\phi, \;\; p_y^* = E^* sin\theta^* sin\phi, \;\; p_z = E^* cos\theta^*$$

Without loss of generality we can take $\phi = 0^\circ$ and consider boost to be in $\theta = 0^\circ$ direction. The four-momentum in lab can be obtained from:

$$\begin{bmatrix} E \\ Esin\theta \\ 0 \\ Ecos\theta \end{bmatrix} = \begin{bmatrix} \gamma & 0 & 0 & \beta\gamma \\ 0 & 1 & 0 & 0 \\ 0 & 0 & 1 & 0 \\ \beta\gamma & 0 & 0 & 0 \end{bmatrix} \begin{bmatrix} E^* \\ E^* sin\theta^* \\ 0 \\ E^* cos\theta^* \end{bmatrix} \tag{4.2}$$

Therefore, energy in lab-frame is $=\gamma E^*(1+\beta cos\theta^*)$

However, this is still in terms of rest-frame angle and so needs to be transformed:

$$\frac{dE}{dcos\theta} = \frac{dE}{dcos\theta^*}\frac{dcos\theta^*}{dcos\theta} = \gamma E^* \frac{dcos\theta^*}{dcos\theta} \tag{4.3}$$

Using results of Lorentz transformation we can write

$$\begin{aligned} cos\theta &= \frac{\gamma E^*(\beta + cos\theta^*)}{\sqrt{(\gamma E^*(\beta + cos\theta^*))^2 + (E^* sin\theta^*)}} \\ &= \frac{\beta + cos\theta^*}{1+\beta cos\theta^*} \end{aligned} \tag{4.4}$$

Inverting this we get

$$\cos\theta^* = \frac{-\beta + cos\theta}{1-\beta cos\theta} \tag{4.5}$$

$$\Rightarrow \frac{dcos\theta^*}{dcos\theta} = [\gamma^2(1-\beta cos\theta)^2]^{-1} \tag{4.6}$$

From equation 4.3, the exact angle in lab frame is given by

$$E(\theta) = \frac{E^*}{\gamma}\frac{1}{1-\beta cos\theta} \tag{4.7}$$

In large γ and small θ approximation ($\beta \approx 1 - \frac{1}{2\gamma^2}$ *and* $cos\theta \approx 1 - \frac{\theta^2}{2}$),we get

$$E(\theta) = \frac{2\gamma E^*}{1+\gamma^2\theta^2} \tag{4.8}$$

We require neutrino spectrum which takes the form

$$\Phi(E_\nu) = \frac{dN}{dE_\nu dcos\theta} \tag{4.9}$$

However, boosting from centre of mass frame to lab-frame is equivalent to following transformations(as derived earlier):

$$E_\nu \longrightarrow E_\nu\gamma(1-\beta\cos\theta) \tag{4.10}$$

$$dE_\nu \longrightarrow \gamma(1-\beta\cos\theta)dE_\nu \tag{4.11}$$

Using the expected flux form and the transformations, it is clear that the lab spectrum is related to C.O.M. spectrum via [BLM04]

$$\Phi_{Lab}(E_\nu,\theta) = \frac{\Phi_{C.O.M.}(E_\nu\gamma[1-\beta\cos\theta])}{\gamma[1-\beta\cos\theta]} \tag{4.12}$$

4.3.1 Extrapolating Beam Flux

The differential width of β-decay, neglecting small Coulomb corrections is given by [ARS05] [ACR07]

$$\frac{d^2\Gamma^*}{d\Omega^* dE_\nu^*} = \frac{1}{4\pi}\frac{ln2}{m_e^5 f t_{1/2}}(E_0 - E_\nu^*)E_\nu^{*2}\sqrt{(E_0 - E_\nu^*)^2 - m_e^2} \tag{4.13}$$

where m_e is the electron mass and E_ν^* is the neutrino energy C.O.M.-frame. E_0 is the electron end-point energy, $t_{1/2}$ is the half life of the decaying ion in its C.O.M. frame and

$$f(y_e) = \frac{1}{60y_e^5}\left\{\sqrt{1-y_e^2}(2-9y_e^2-8y_e^4) + 15y_e^4 log\left[\frac{y_e}{1-\sqrt{1-y_e^2}}\right]\right\} \tag{4.14}$$

where $y_e = m_e/E_0$.

However the flux N is related to Γ by the radioactive decay law

$$\frac{d^2N}{dE_\nu dt} = g\gamma\tau\frac{d\Gamma}{dE_\nu} \tag{4.15}$$

where g is the number of injected ions per unit time, and τ is the lifetime of that ion in its rest frame.

We can now replace $d\Omega$ by $\frac{dA}{L^2}$ where dA is the small area of the detector and L is the baseline length. Therefore using equation relating flux in lab-frame to C.O.M. frame, equation 4.13 and equation 4.15, the number of neutrinos within the energy range E_ν to $E_\nu + dE_\nu$ hitting unit area of the detector located at a distance L aligned with the straight sections of the storage ring in time dt is given by:

$$\left.\frac{d^3N}{dAdE_\nu^* dt}\right|_{lab} = \frac{1}{4\pi L^2}\frac{ln2}{m_e^5 f t_{1/2}}\frac{g\tau}{\gamma(1-\beta\cos\theta)}(E_0 - E_\nu^*)E_\nu^{*2}\sqrt{(E_0 - E_\nu^*)^2 - m_e^2} \tag{4.16}$$

where $E_\nu^* = \gamma E_\nu(1-\beta\cos\theta)$.

4.4 Two-Detector Setup

Pioneered at CERN and Fermilab, it is a unique technique to estimate flux at the detector location [Min08]. A **near detector or ND** is placed close to the neutrino production site which directly measures the neutrinos from the beam over a span of energies. Whereas the other one, the **far detector or FD**, is placed at a distance where the oscillation probability is closer to

unity and is at a much greater distance than the near detector. It quantifies the energy range of neutrinos which have traveled through matter or vacuum (causing oscillation), for quite a while. The deviation between the two energy spectra is then used to infer phenomenon like **neutrino-oscillation** or measure relevant physical parameters. The utilization of an extra near detector diminishes the need to calculate beam spectrum which incredibly improves the investigation's sensitivity. It can also measure the interaction cross-sections with the same neutrino beam to constrain the cross-section uncertainties. The two-detector setup is favored for this work over source-detector configuration because of greater control and availability of data.

4.4.1 Extrapolating Beam Flux

The difference in distance between the near and far detector, causes a change in observed beam spectrum of the two detectors. This difference is prevalent even in the absence of neutrino oscillation. The prediction can be estimated by [Kop07] :

$$\Phi_{far} = R_{FN}\Phi_{Near} \tag{4.17}$$

When the beam is viewed as an extended source rather than a point source, we need to consider the factor of pion lifetime (in the decay length) in the extrapolation factor and the factor is given by [Kop07]

$$R_{FN} = \frac{\int_{z\approx 0}^{L} \frac{e^{-\frac{0.43 m_\pi z}{E_\nu c\tau}}}{(Z_F - z)^2} dz}{\int_{z\approx 0}^{L} \frac{e^{-\frac{0.43 m_\pi z}{E_\nu c\tau}}}{(Z_N - z)^2} dz} \tag{4.18}$$

where the integral is over the length **L** of the decay tunnel and the substitution.
However, GLoBES only allows us to simulate point sources(z=0). In that case the above extrapolation factor reduces to

$$R_{FN} = \frac{Z_{near}^2}{Z_{far}^2} \tag{4.19}$$

which is just the ratio of solid angles subtended by the two detectors. Hence if we know flux at the near detector, we can easily calculate the unoscillated flux at the far detector. To obtain the full picture other factor like transition probability, efficiency etc. can be incorporated.

4.5 Horn focussing

To study the properties of neutrinos at neutrino detectors, we have to guarantee that we have enough number of neutrinos at the detector. It can be achieved by neutrino horns, delivering a concentrated beam of neutrinos at the source itself. These were created at CERN by Simon van der Meer in 1961, a Nobel Prize-winning physicist.

Neutrino beam at accelerators is produced from a shower of short-lived particles, made when protons are going near the speed of light hammer into a target. However, this shower is not a clean, focused beam. Magnetic horns act the hero here. After the protons hammer into the target creating pions and kaons - the short-lived charged particles that decay into neutrinos - the magnetic horns focus them promptly by utilizing the magnetic field. The focusing must be done promptly before they decay into neutrinos. This is because, in contrast to the pions and kaons, neutrinos don't interact with magnetic fields. That implies we can't focus them directly. Thus concentrating pions and kaons at first will create a focused neutrino beam.

Few requirements that need to be imposed for neutrino horns are[Caz04] [Nez75]:

- Good focussing effectiveness
- High operational dependability
- Minimize failures because of radiation
- Modular design
- Simultaneous horn activity and subsystem testing

The principle of focussing secondary particles created in the target using two coaxial horns is illustrated as :

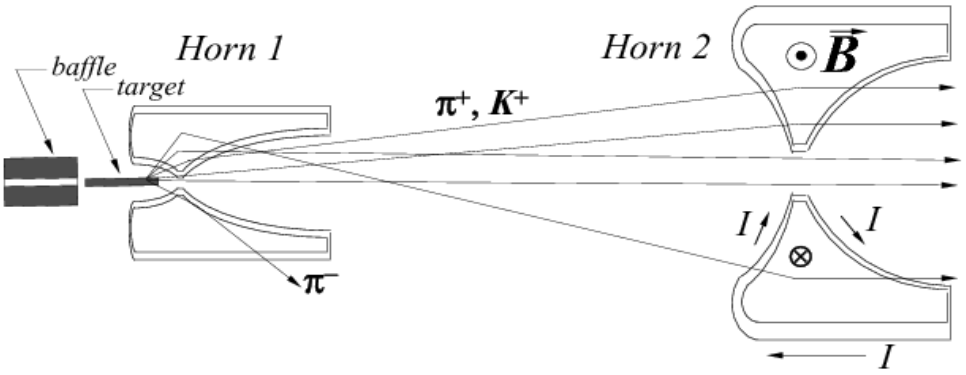

Figure 4.2: Schematic of the focussing principle of the secondary particles [NP16].

As depicted **Figure 4.2**, the first horn is placed close to the target. It is unable to sufficiently

deviate the more energetic particles, while the less energetic particles deviate too much. The second horn is placed to correct this effect (also the reason why it is called reflector). It is set sufficiently farther (less than decay length of pions and kaons) and is larger in diameter than the first horn, to increase its acceptance. If the particles have small deviation angles, they need not be focused much. The end of the inner driver is cylindrical, allowing the particles already focused by the horn to stay in the line of the beam. The reflector thus makes it possible to obtain a broadband energy beam. For most of the cases, a tube filled with helium at atmospheric pressure is placed between the horn and the reflector to minimize energy losses. The same goes for the distance between reflector output from the decay tunnel input. For this text, when positive-charged pions and kaons are focused it's called **Plus-focussing** and **Minus-focussing** if it's negative-charged pions and kaons [Kop07].

4.6 Simulating Experiments - GLoBES Software Package

To perform simulations for this work, I am using **GLoBES (General Long Baseline Experiment Simulator)**. GLoBES [HLS$^+$05] is an open-source software package for the simulation of long baseline neutrino oscillation experiments, currently maintained by **Patrick Huber, Joachim Kopp, Manfred Lindner, and Walter Winter**. With the use of several built-in algorithms, it computes final event rates that take into account neutrino propagation and energy-dependent efficiencies.

The major features of GLoBES which eases experiment simulations are:

- **AEDL (Abstract Experiment Definition Language)** which forms the backbone of GLoBES, gives a simple method to characterize test setups. It is the part of GLoBES where all the relevant information regarding the source (the accelerator for our case), baseline and detector is specified. Using the parameters defined in the AEDL file GLoBES software calculates the final number of events.
- We can easily include priors if we want to include arbitrary external physical information.
- It also allows us to incorporate correlations and degeneracies which might exist in the oscillation parameter space.
- To treat arbitrary systematical errors, it provides beneficial advanced routines.
- It likewise has predefined setups accessible for some investigations: Neutrino factories, Beta Beams, Superbeams, Reactors, different detector technologies.

4.7 Density Distribution

GLoBES provide the flexibility to use three different methods to define the matter density profile for our experiment. We can insert an **average matter density** or insert a manually defined **density map** or **PREM (Preliminary Reference Earth Mode)** profile [DA81]. For my study, I have used the **PREM profile**, which simulates the matter density by approximating the Earth to a series of layers. It provides a fairly accurate representation of density profile and moreover considers important parameters like elastic properties, pressure, density, attenuation, and gravity, as a function of planetary radius which is essential for an accurate representation [Vih14]. By comparing the two graphs given below (**Figure 4.3** and **Figure 4.4**), it can be easily seen that for baselines less than 6000 km the propagation of neutrinos mainly occurs in the crust layer of the earth. For baselines between 6000km-10000km the propagation occurs in Crust as well as Mantle and for baselines above 10000km, the propagation occurs within Earth Core in addition to Crust and Mantle.

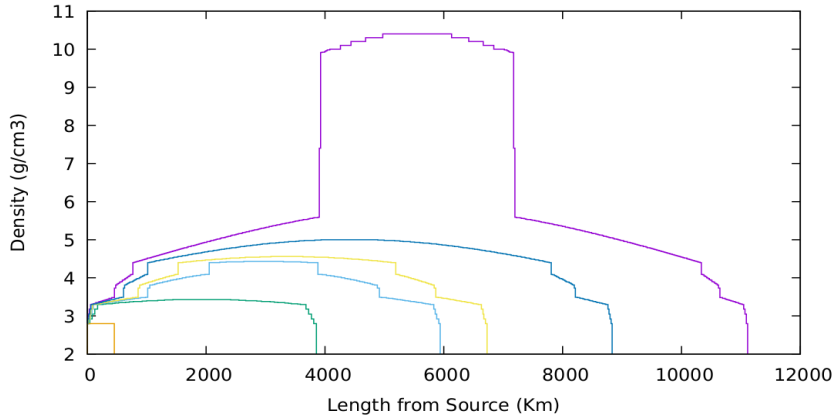

Figure 4.3: PREM Density Profiles for various baselines.

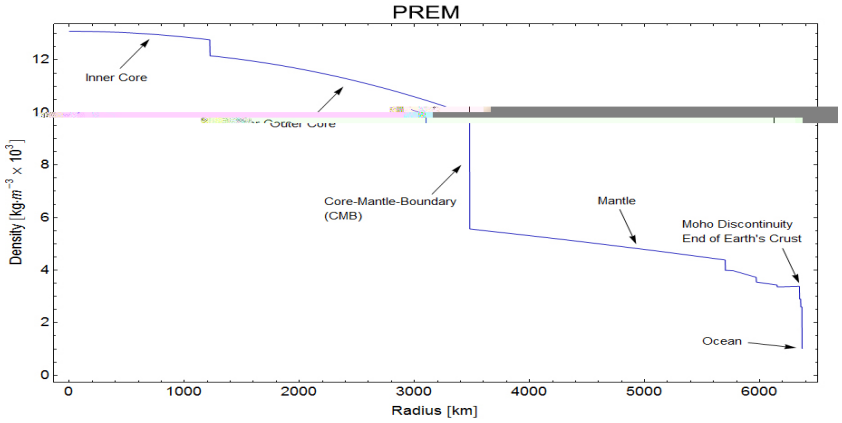

Figure 4.4: Earth's radial density map according to PREM [McC19].

4.8 Flux at Near Detector

The primary task of the near detector is to characterize the flux of the un-oscillated neutrino beam. It is crucial to the precision studies of neutrino oscillations as well as for other neutrino experiments. In addition to the estimation of neutrino flux by the evaluation of neutrino-electron scattering process[TW09], near detector is additionally utilized for the investigation of neutrino beam properties required for the flux to be extrapolated to the far detector, and estimation of charm production cross-sections(charm production in the far detector is one of the principal backgrounds to the oscillation signal) [B$^+$14]. It can likewise test new physics, for instance by detecting τ leptons, which are particularly sensitive probes of nonstandard interactions with matter. Additionally, ν_τ is also vital in the search for sterile neutrinos. Neutrino beam fluxes can be estimated by the information of neutrino-electron association cross sections[Oku82].

4.8.1 Near Detector: CERN

Figure 4.5: Location of the SPL on the CERN site [Fre17].

CERN's accelerator complex consists of various sections which successively accelerate particles to increasingly higher energies. Utilizing a simple container of hydrogen gas as a proton source, an electric field is used to strip hydrogen molecules of their electrons to yield protons. These protons are then allowed to pass through the **LINAC (Linear Accelerator)**, which accelerates them to an energy of 50 MeV. After initial acceleration, the beam is infused into the **Proton Synchrotron Booster (PSB)** followed by the **Proton Synchrotron (PS)**; where they are accelerated to an energy of 1.4 GeV and 25 GeV respectively. Finally, the protons are accelerated by **Super Proton Synchrotron (SPS)** to a final energy of 450 GeV. These highly

energetic protons are used to hit a target to finally produce neutrino beams.In this text, I have used data from **Superconducting Proton Linac (SPL)** [CMMS06] [CC06] [Mez03] which is used as driver for neutrinos [GG06]. The neutrino flux at the near detector for CERN-SPL for different focusing is given below.

4.8.1.1 Plus Focussing

Neutrino → Legends: ElecNeuFlux = Electron Neutrino Flux, MuonNeuFlux = Muon Neutrino Flux, TauNeuFlux = Tau Neutrino Flux (Negligible in number).

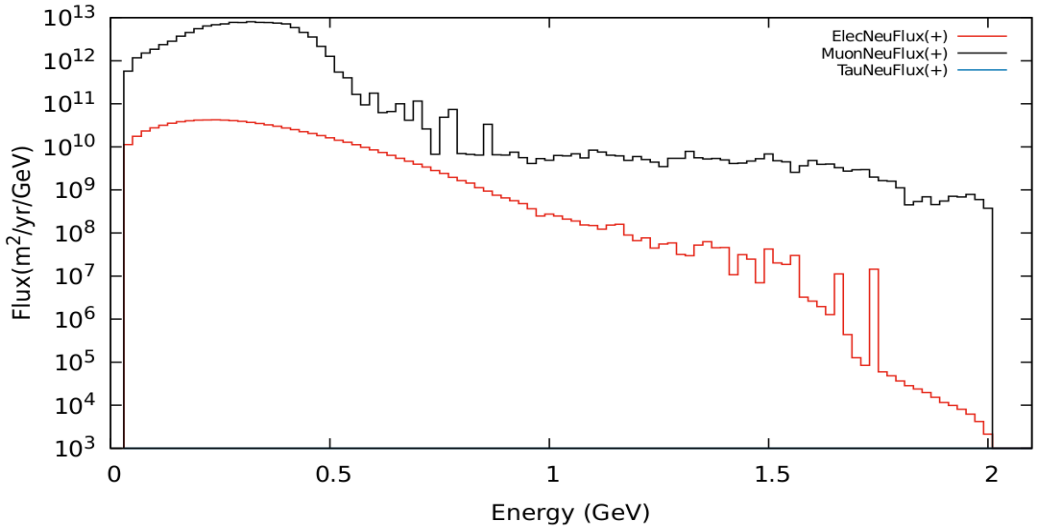

Figure 4.6: Total Neutrino Flux at Near detector - **CERN** for **Plus** Horn focussing.

Anti-neutrino → Legends: ElecNeuBarFlux = Electron Anti-neutrino Flux, MuonNeuBarFlux = Muon Anti-neutrino Flux, TauNeuBarFlux = Tau Anti-neutrino Flux (Negligible in number).

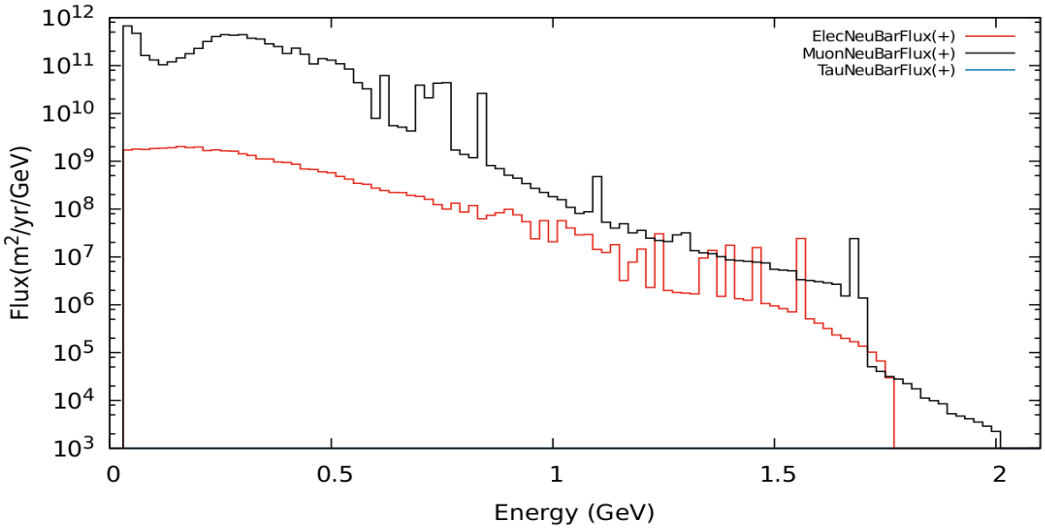

Figure 4.7: Total Anti-Neutrino Flux at Near detector - **CERN** for **Plus** Horn focussing.

4.8.1.2 Minus Focussing

Neutrino → Legends: ElecNeuFlux = Electron Neutrino Flux, MuonNeuFlux = Muon Neutrino Flux, TauNeuFlux = Tau Neutrino Flux (Negligible in number).

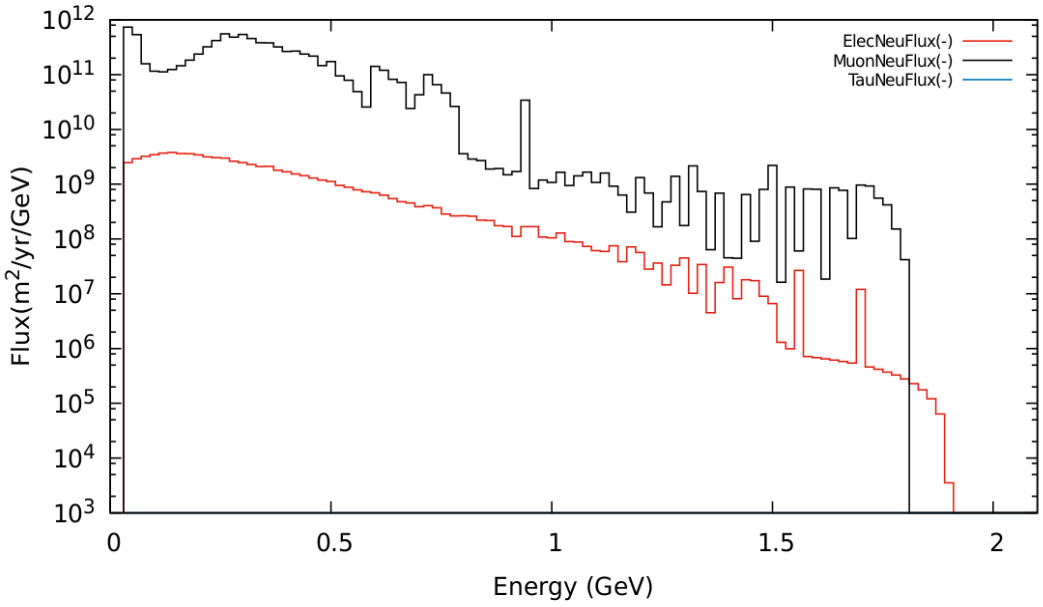

Figure 4.8: Total Neutrino Flux at Near detector - **CERN** for **Minus** Horn focussing.

Anti-neutrino → Legends: ElecNeuBarFlux = Electron Anti-neutrino Flux, MuonNeuBarFlux = Muon Anti-neutrino Flux, TauNeuBarFlux = Tau Anti-neutrino Flux (Negligible in number).

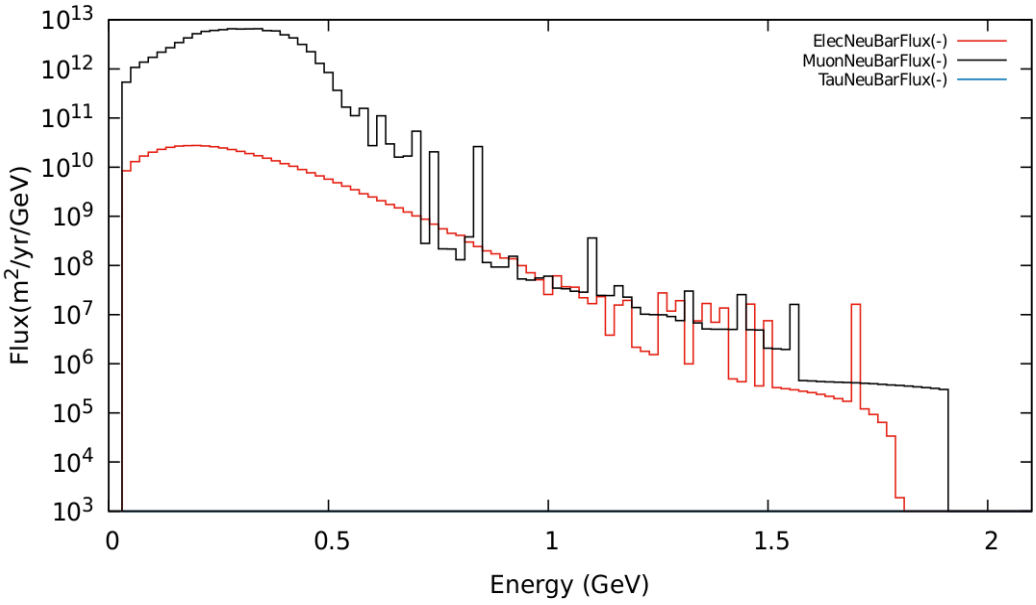

Figure 4.9: Total Anti-Neutrino Flux at Near detector - **CERN** for **Minus** Horn focussing.

4.8.2 NOvA - Fermilab

Fermilab current neutrino project is composed of three parts: the **Deep Underground Neutrino Experiment (DUNE)**, the **Long-Baseline Neutrino Facility (LBNF)** and the **Proton Improvement Plan II (PIP-II)**. The **DUNE** facility consists of massive neutrino detectors that capture neutrinos and analyze the data. **LBNF** provides the infrastructure that houses and cools the DUNE detectors and also delivers the neutrino beam from Fermilab. **PIP-II**, coupled to the existing Fermilab particle accelerator complex, provides the powerful stream of protons that create the neutrinos. Much similar to other facilities protons from PIP-II, hit the target, ultimately decaying into neutrinos that stream first through the near detector, then through the earth and finally through the far detector.

In this text, I have dealt with data from NOνA (NuMI Off-Axis ν_e Appearance) Near Detector [A$^+$04] [YW04] [Mes] [PY02] , which is designed to identify neutrinos in Fermilab's NuMI (Neutrinos at the Main Injector) beam. NOνA utilizes two detectors - the NOνA near detector (ND) and the NOνA far detector (FD). The neutrino flux at the near detector for NOvA - Fermilab for different focusing is given below.

4.8.2.1 Plus Focussing

Neutrino $\rightarrow$ Legends: ElecNeuFlux = Electron Neutrino Flux, MuonNeuFlux = Muon Neutrino Flux, TauNeuFlux = Tau Neutrino Flux (Negligible in number).

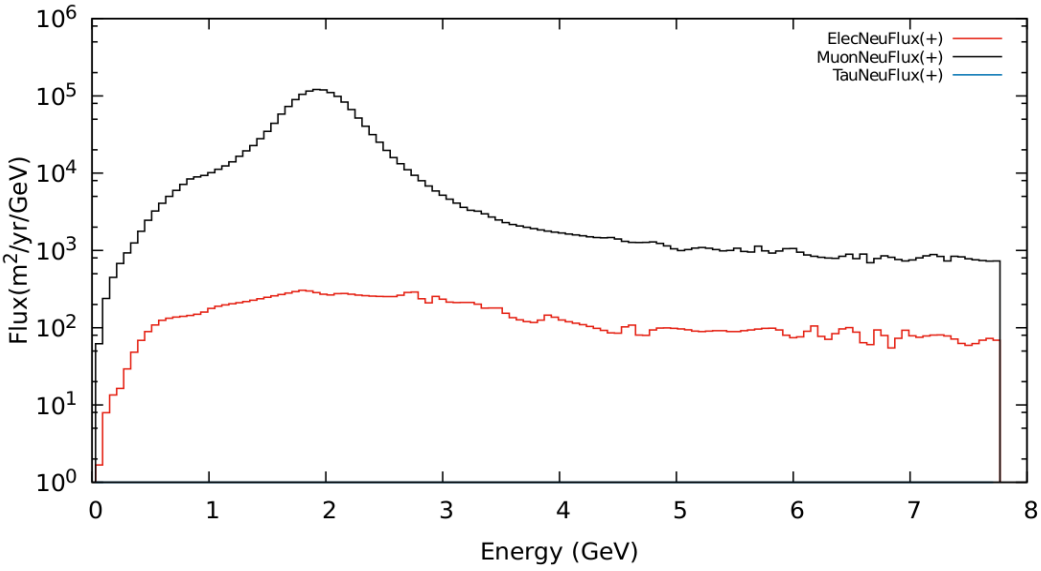

Figure 4.10: Total Neutrino Flux at Near detector - **Fermilab** for **Plus** Horn focussing.

Anti-neutrino → Legends: ElecNeuBarFlux = Electron Anti-neutrino Flux, MuonNeuBarFlux = Muon Anti-neutrino Flux, TauNeuBarFlux = Tau Anti-neutrino Flux (Negligible in number).

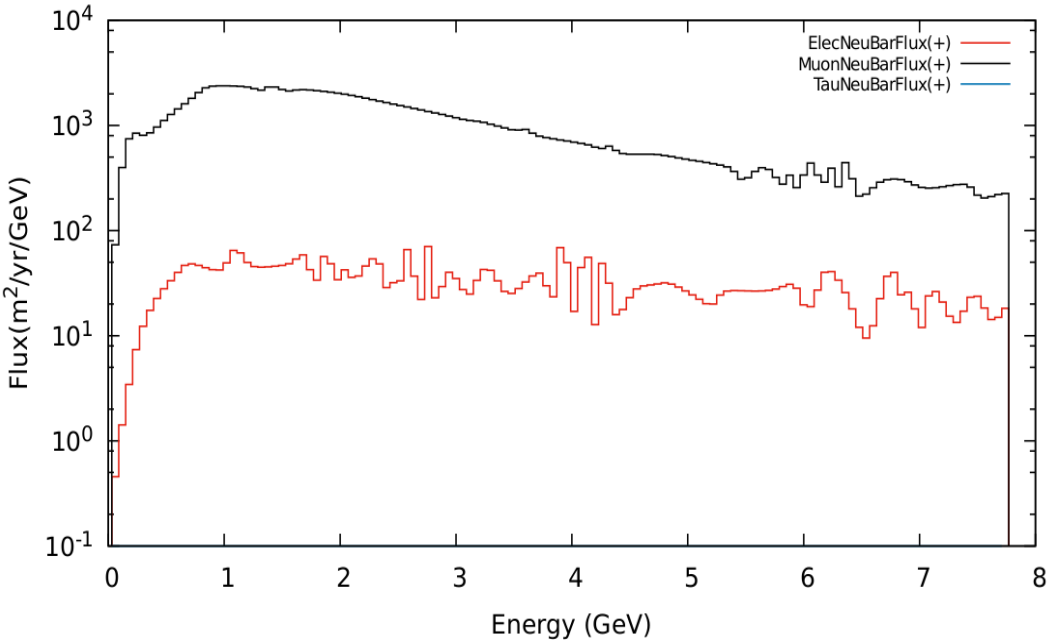

Figure 4.11: Total Anti-Neutrino Flux at Near detector - **Fermilab** for **Plus** Horn focussing.

4.8.2.2 Minus Focussing

Neutrino → Legends: ElecNeuFlux = Electron Neutrino Flux, MuonNeuFlux = Muon Neutrino Flux, TauNeuFlux = Tau Neutrino Flux (Negligible in number).

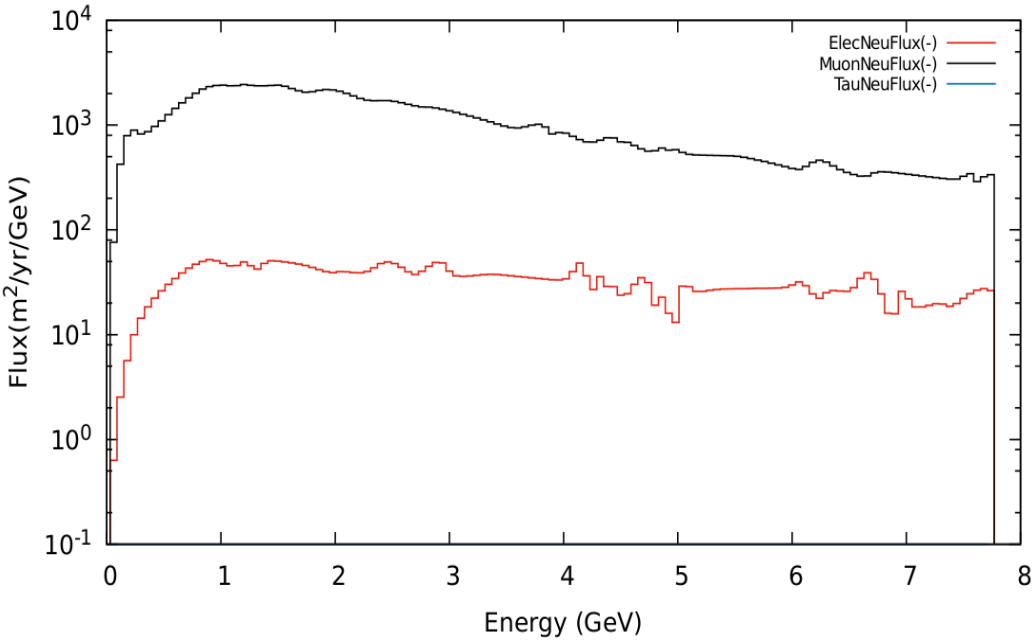

Figure 4.12: Total Neutrino Flux at Near detector - **Fermilab** for **Minus** Horn focussing.

Anti-neutrino → Legends: ElecNeuBarFlux = Electron Anti-neutrino Flux, MuonNeuBarFlux = Muon Anti-neutrino Flux, TauNeuBarFlux = Tau Anti-neutrino Flux (Negligible in number).

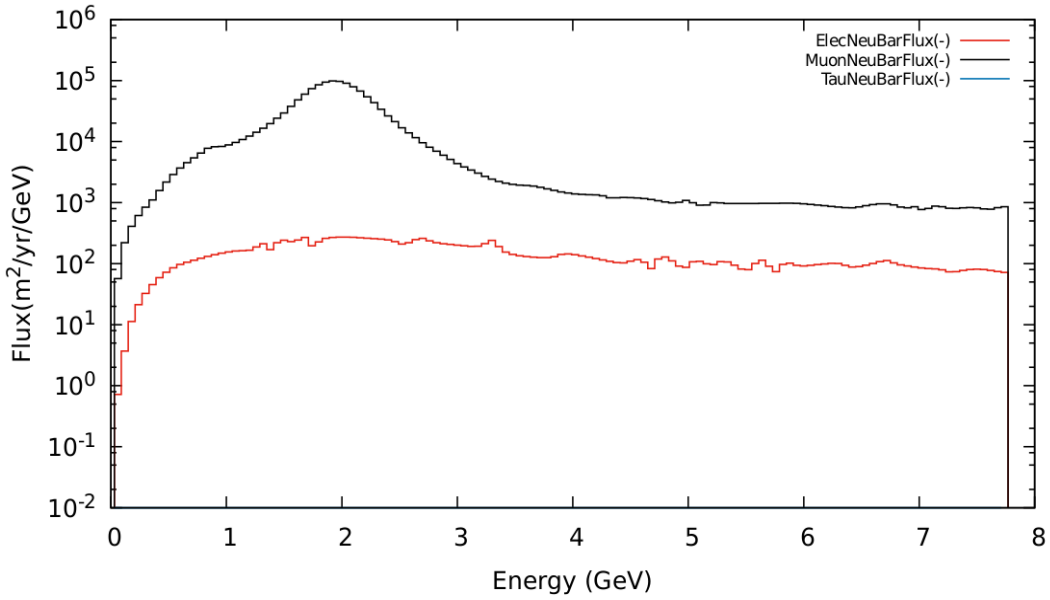

Figure 4.13: Total Anti-Neutrino Flux at Near detector - **Fermilab** for **Minus** Horn focussing.

4.8.3 J-PARC

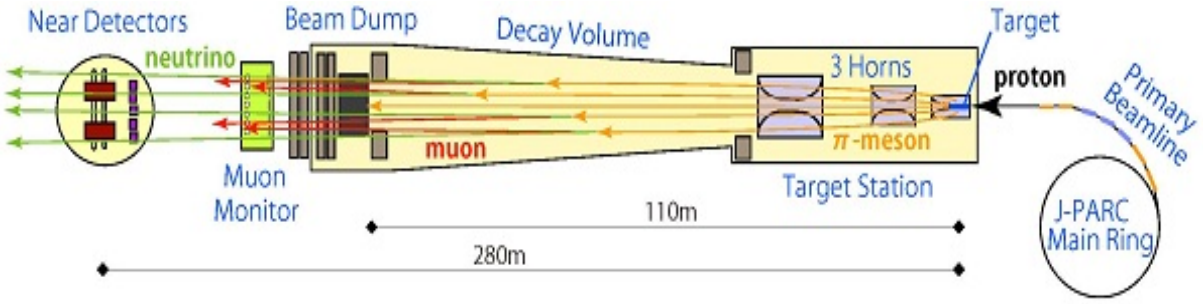

Figure 4.14: Schematic Diagram: J-PARC Neutrino Facility [JP19].

The **J-PARC** complex, comprise of a **Linear Accelerator (LINAC)**, a **Rapid Cycle Synchrotron (RCS)** and a **Main Ring Synchrotron (MR)**. The proton beams discharged by the MR are coordinated through the **primary beam line** by the assistance of multiple normal-conducting / super-conducting magnets and are then sent to the **target station**. At the target station, the protons slam into the target made out of graphite bars and produce various daughter particles. Among these particles, the positive charged π-mesons (parents of muon neutrinos), are focused with the assistance of **magnetic horns** in the forward direction. These are then

permitted to decay into muon and muon neutrino, in a 100m long **decay volume**. Every one of the neutrinos (and a little number of muons) escape from the facility, while all the other particles, for example, the rest of the protons and undecayed π-mesons are absorbed by a **beam dump**. The **Near Detector (ND280)** approximately 280m downstream of the target is then used to characterize the beam profile, its purity, and energy distribution of the muon-type neutrinos. For my investigation, I have used data from Near Detector(ND280) [HLSW09] [Fec06] [Kat08] [CMMS06] [Mes] [PY02] .

4.8.3.1 Plus Focussing

Neutrino $\rightarrow$ Legends: ElecNeuFlux = Electron Neutrino Flux, MuonNeuFlux = Muon Neutrino Flux, TauNeuFlux = Tau Neutrino Flux (Negligible in number).

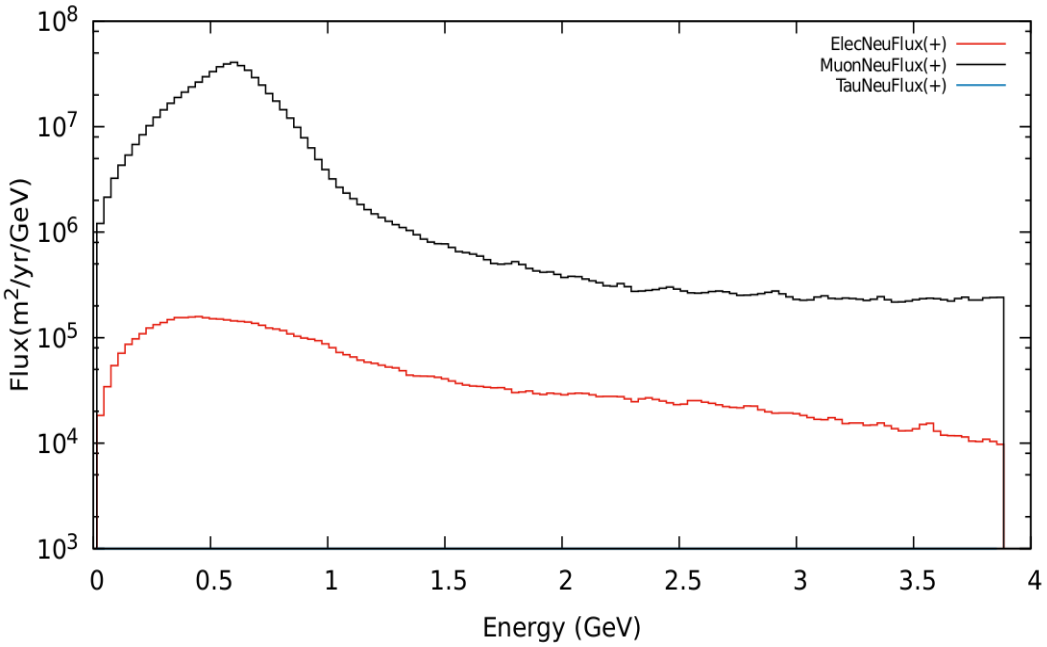

Figure 4.15: Total Neutrino Flux at Near detector - **J-PARC** for **Plus** Horn focussing.

Anti-neutrino → Legends: ElecNeuBarFlux = Electron Anti-neutrino Flux, MuonNeuBarFlux = Muon Anti-neutrino Flux, TauNeuBarFlux = Tau Anti-neutrino Flux (Negligible in number).

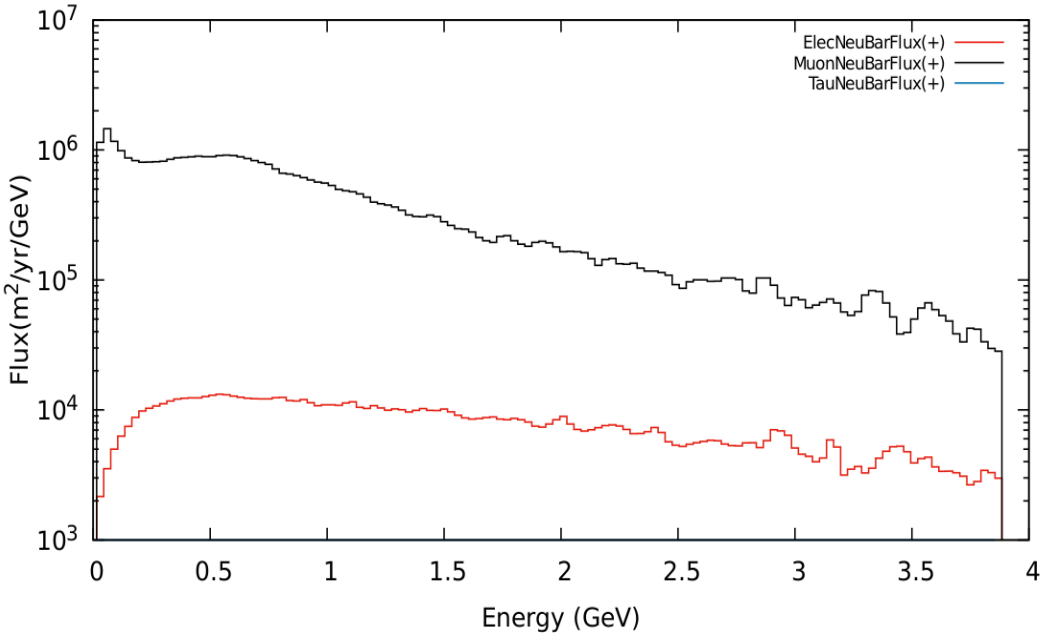

Figure 4.16: Total Anti-Neutrino Flux at Near detector - **J-PARC** for **Plus** Horn focussing.

4.8.3.2 Minus Focussing

Neutrino → Legends: ElecNeuFlux = Electron Neutrino Flux, MuonNeuFlux = Muon Neutrino Flux, TauNeuFlux = Tau Neutrino Flux (Negligible in number).

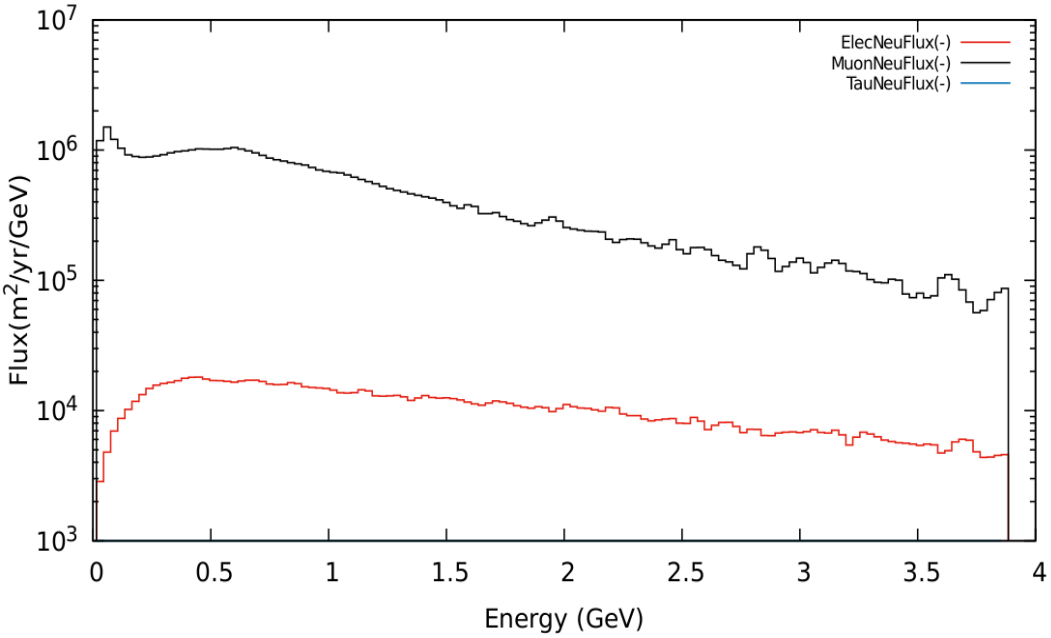

Figure 4.17: Total Neutrino Flux at Near detector - **J-PARC** for **Minus** Horn focussing.

Anti-neutrino → Legends: ElecNeuBarFlux = Electron Anti-neutrino Flux, MuonNeuBarFlux = Muon Anti-neutrino Flux, TauNeuBarFlux = Tau Anti-neutrino Flux (Negligible in number).

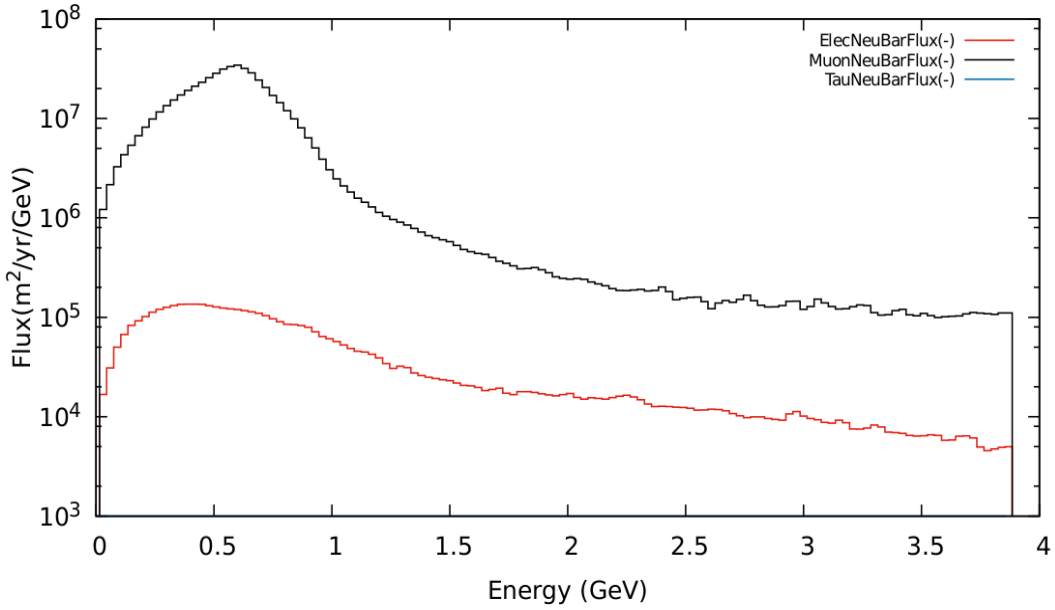

Figure 4.18: Total Anti-Neutrino Flux at Near detector - **J-PARC** for **Minus** Horn focussing.

Chapter 5

INO: India-based Neutrino Observatory

The India-based Neutrino Observatory (INO) [Gos17] is a proposed underground research center whose primary objective is to contemplate the properties and interactions of neutrinos. There is worldwide enthusiasm for the field of Neutrino Physics because of its implications for a several different and associated areas such as particle physics, energy production mechanisms in the Sun, cosmology and the origin of the Universe, and other stars, etc. During the initial run of INO it's focus is on making precise estimations parameters associated with atmospheric neutrino oscillations. Solving the mass-hierarchy problem of neutrino physics is one such possibility. INO's geographical location is additionally advantageous as there is no other detector closer to the equator, whereas INO presents the option to set up a detector at nearly 8° latitude. A detector at such a location allows neutrino astronomy searches to cover the entire celestial sky, investigation of solar-neutrinos propagating through Earth's core and lastly neutrino tomography of the Earth [DPRS19].

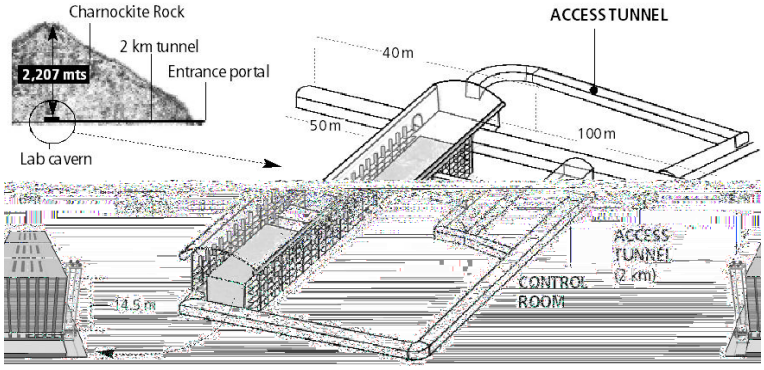

Figure 5.1: Schematic of INO to be established at Bodi West Hills near Theni, Tamil Nadu, India [STIE15].

5.1 Source: CERN

Using GLoBES the neutrino flux was calculated for all flavors at INO site, for Plus and Minus Horn Focussing. The baseline length from CERN Near Detector to INO site detector is 7302.89 Km, with density profile for the propagation length given by

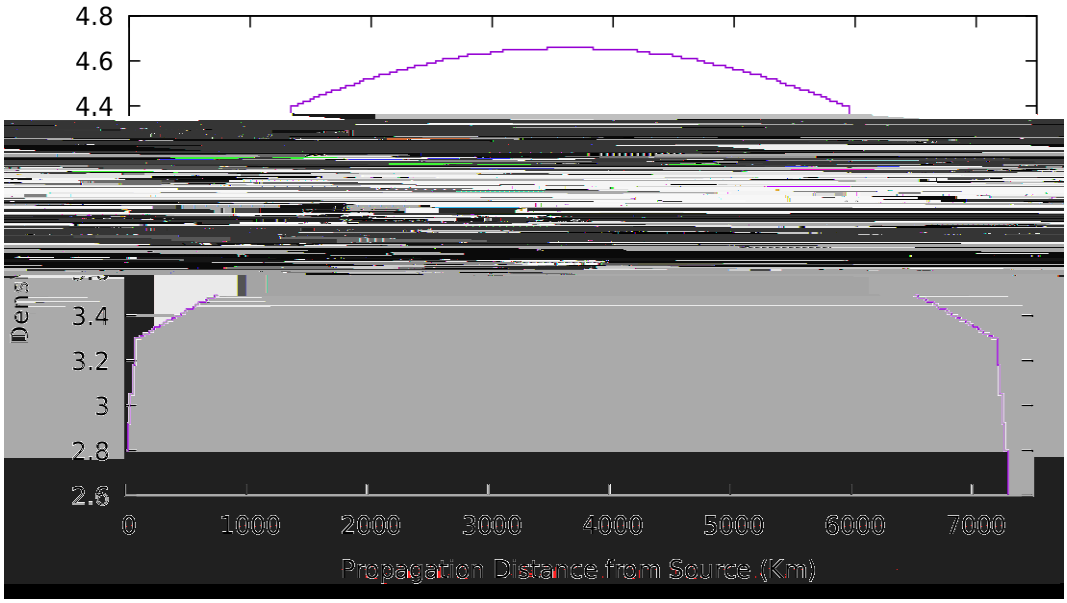

Figure 5.2: Matter Density Profile for neutrino propagating from CERN-SPL to INO.

5.1.1 Plus Focussing

Neutrino → Legends: ElecNeuFlux = Electron Neutrino Flux, MuonNeuFlux = Muon Neutrino Flux, TauNeuFlux = Tau Neutrino Flux.

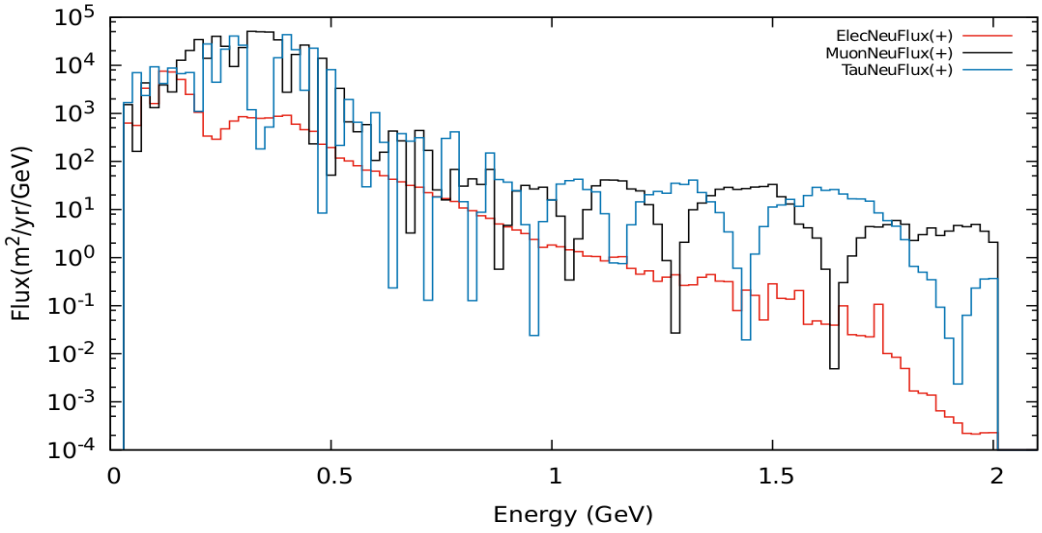

Figure 5.3: Total Neutrino Flux at INO from CERN for **Plus** Horn Focusing.

Anti-neutrino → Legends: ElecNeuBarFlux = Electron Anti-neutrino Flux, MuonNeuBarFlux = Muon Anti-neutrino Flux, TauNeuBarFlux = Tau Anti-neutrino Flux.

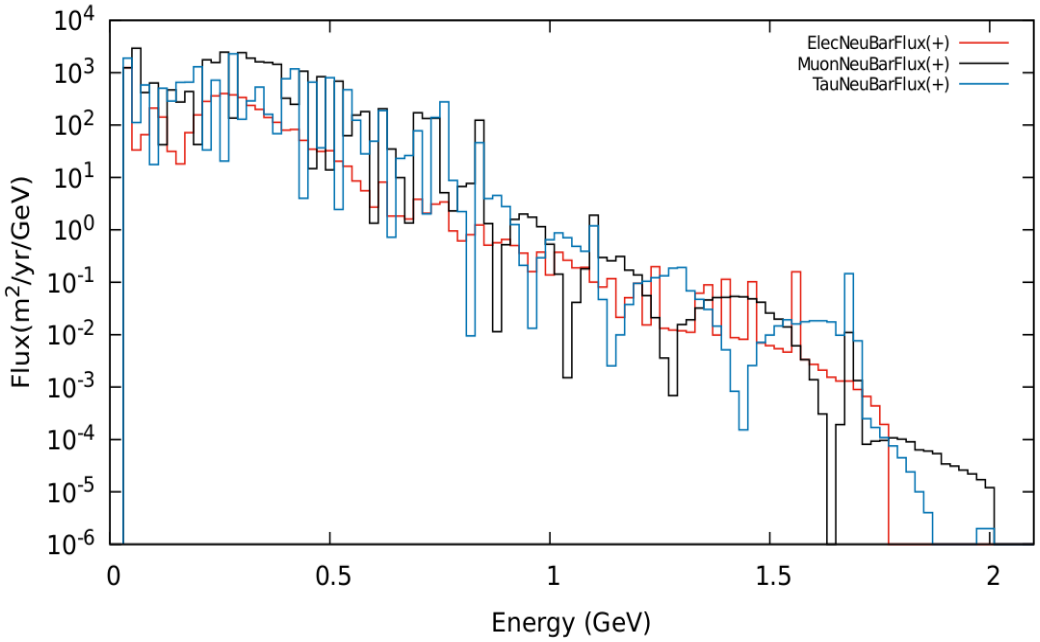

Figure 5.4: Total Anti-Neutrino Flux at INO for **Plus** Horn Focusing.

5.1.2 Minus Focussing

Neutrino → Legends: ElecNeuFlux = Electron Neutrino Flux, MuonNeuFlux = Muon Neutrino Flux, TauNeuFlux = Tau Neutrino Flux.

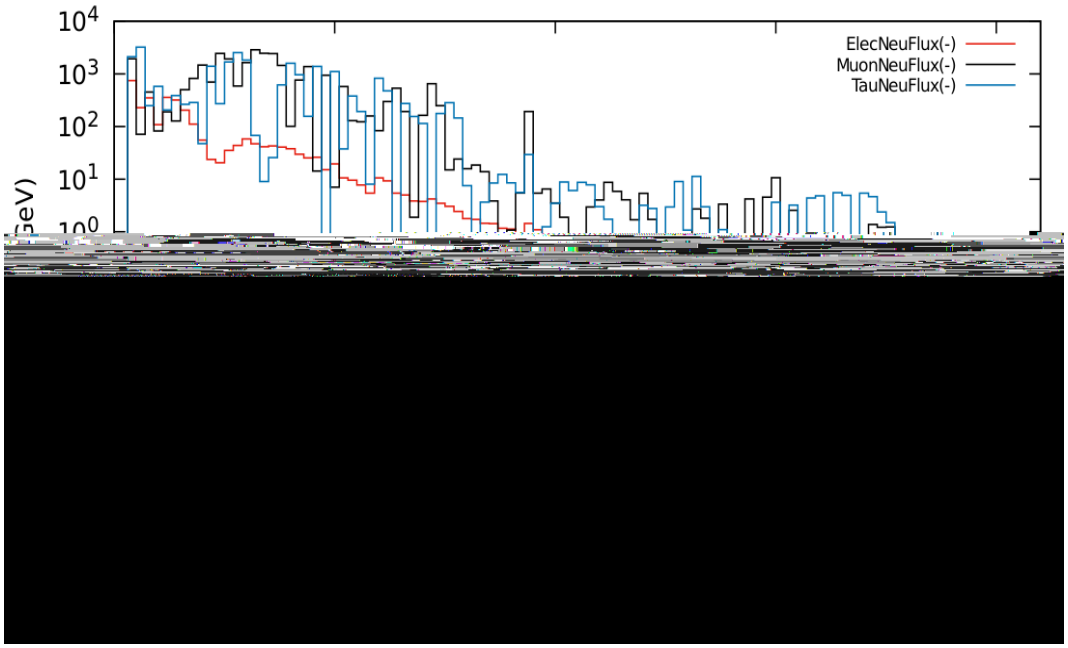

Figure 5.5: Total Neutrino Flux at INO from CERN for **Minus** Horn Focusing.

Anti-neutrino → Legends: ElecNeuBarFlux = Electron Anti-neutrino Flux, MuonNeuBarFlux = Muon Anti-neutrino Flux, TauNeuBarFlux = Tau Anti-neutrino Flux.

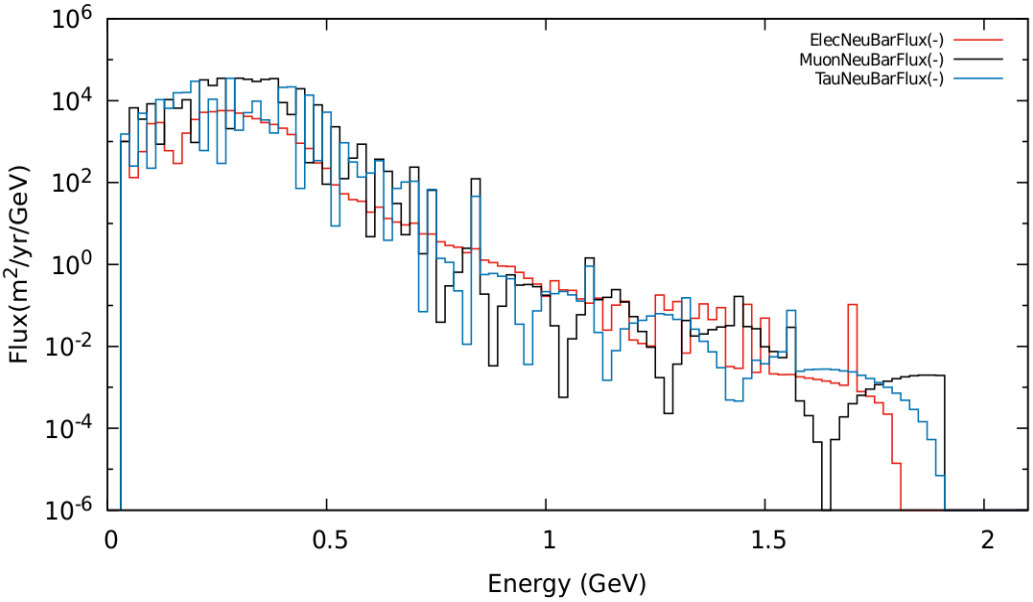

Figure 5.6: Total Anti-Neutrino Flux at INO from CERN for **Minus** Horn Focusing.

5.1.3 Oscillation Probabilities

Different Oscillations probabilities for neutrinos and anti-neutrinos propagating from CERN to INO site, India.

Legends:

- **Neutrino:** $P\alpha\beta \rightarrow \alpha = Initial\ Flavor$ and $\beta = Final\ Flavor$; e = Electron Neutrino , m = Muon Neutrino ,t = Tau Neutrino

- **Anti-neutrino:** $Pbar\alpha\beta \rightarrow \alpha = Initial\ Flavor$ and $\beta = Final\ Flavor$; e = Electron Neutrino , m = Muon Neutrino ,t = Tau Neutrino

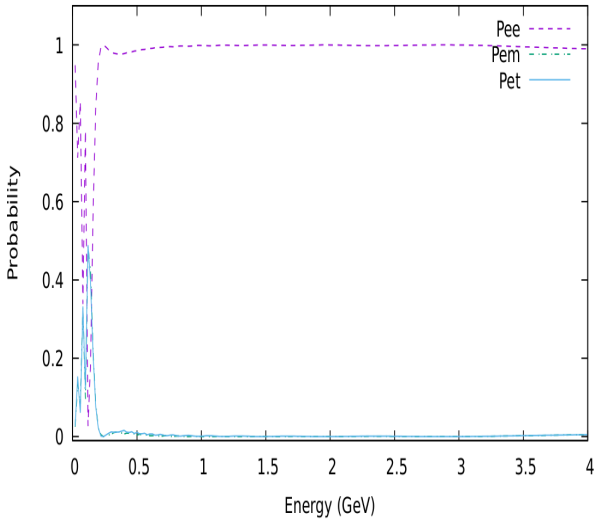

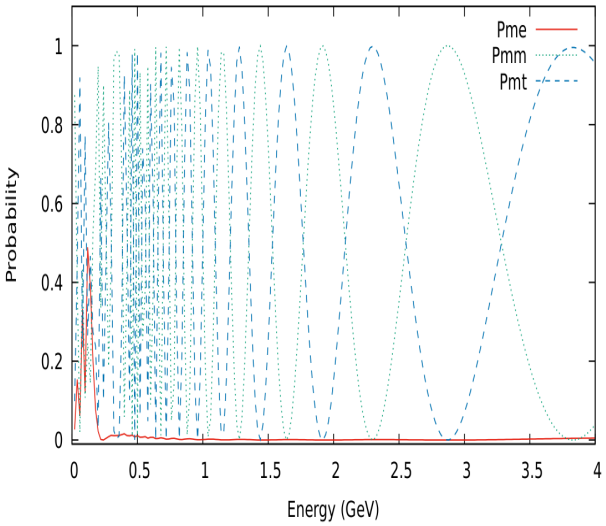

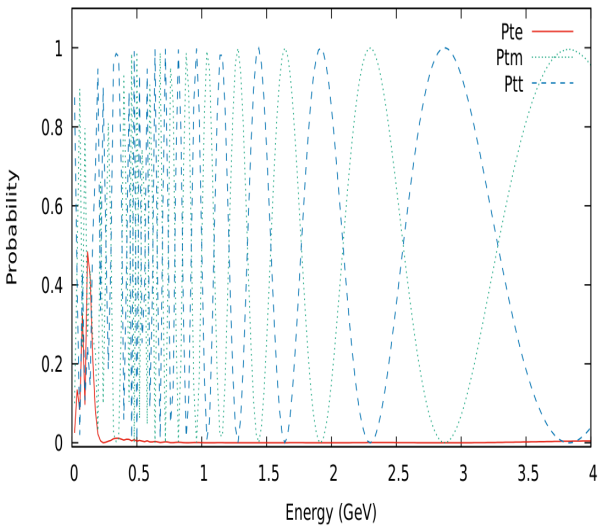

Figure 5.7: Neutrino Transition Probability Values for CERN to INO Baseline.

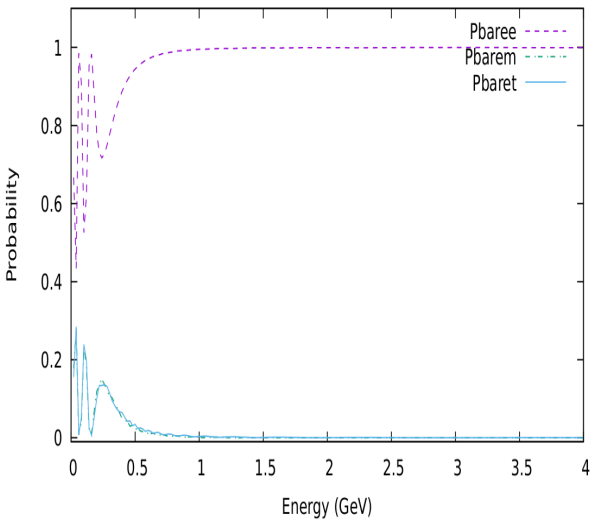

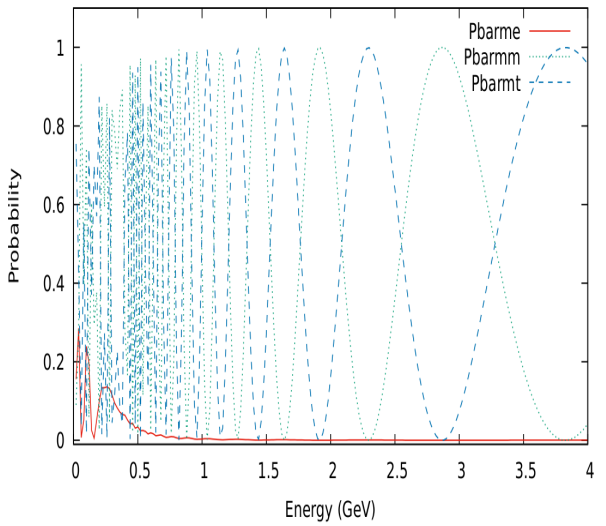

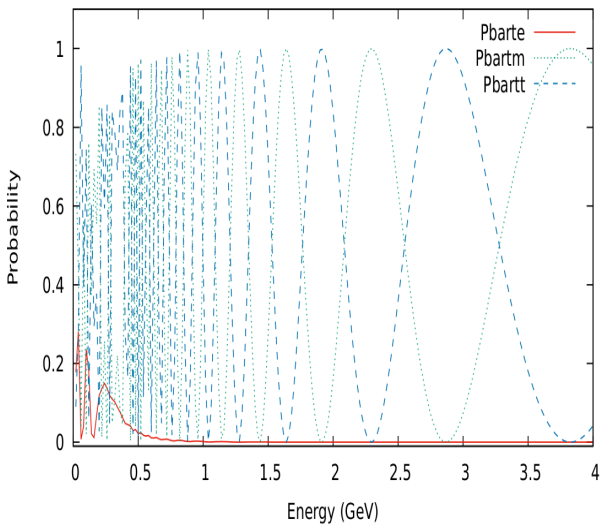

Figure 5.8: Anti-Neutrino Transition Probability Values for CERN to INO Baseline.

5.2 Source: Fermilab

Similar to previous case, using GLoBES the neutrino flux was calculated for all flavors at INO site, for Plus and Minus Horn Focussing, propagating from Fermilab Near detector. The baseline length is 11392.51 Km, with density profile for the propagation length given by

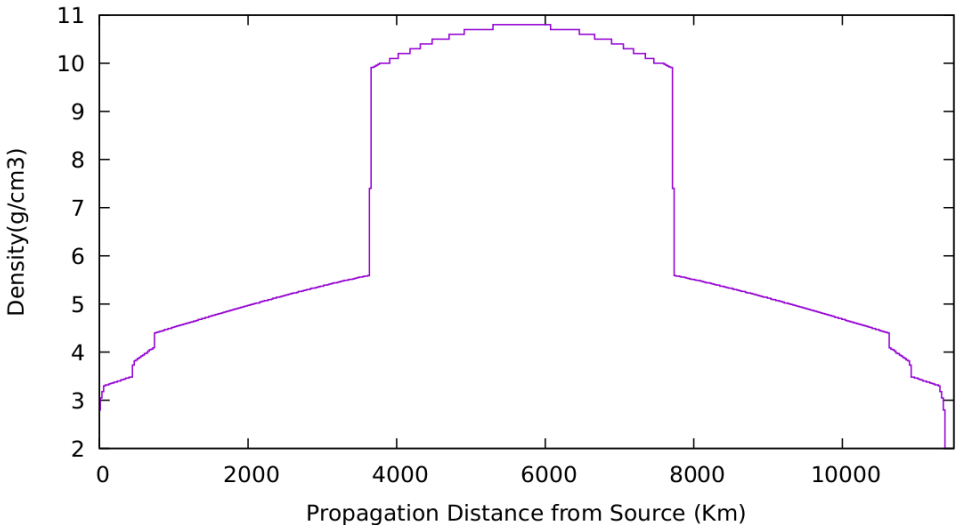

Figure 5.9: Matter Density Profile for neutrino propagating from Fermilab-NOvA to INO.

5.2.1 Plus Focussing

Neutrino → Legends: ElecNeuFlux = Electron Neutrino Flux, MuonNeuFlux = Muon Neutrino Flux, TauNeuFlux = Tau Neutrino Flux.

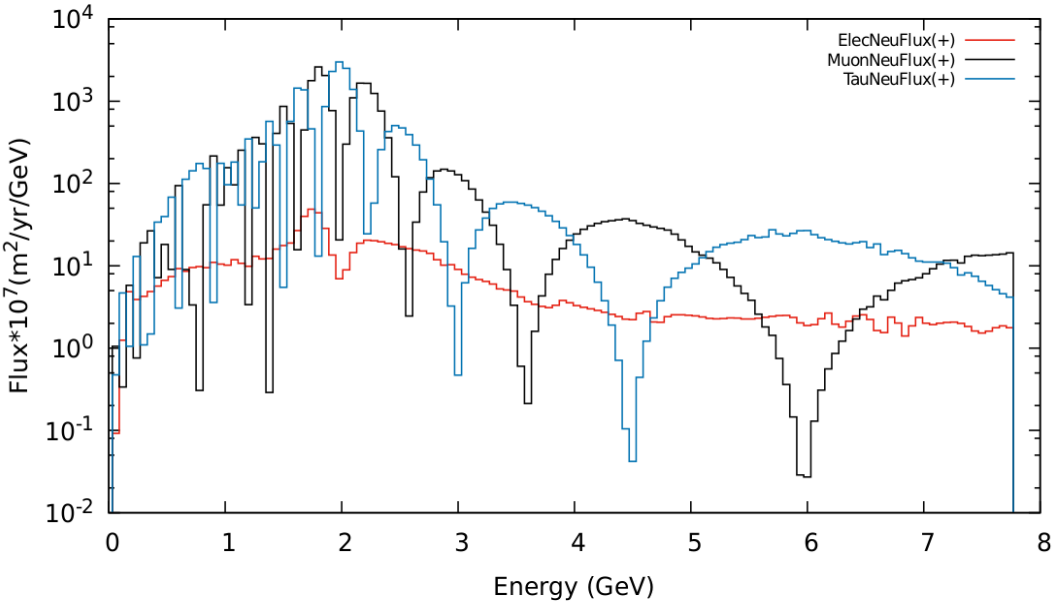

Figure 5.10: Total Neutrino Flux at INO from Fermilab for **Plus** Horn Focusing.

Anti-neutrino → Legends: ElecNeuBarFlux = Electron Anti-neutrino Flux, MuonNeuBarFlux = Muon Anti-neutrino Flux, TauNeuBarFlux = Tau Anti-neutrino Flux.

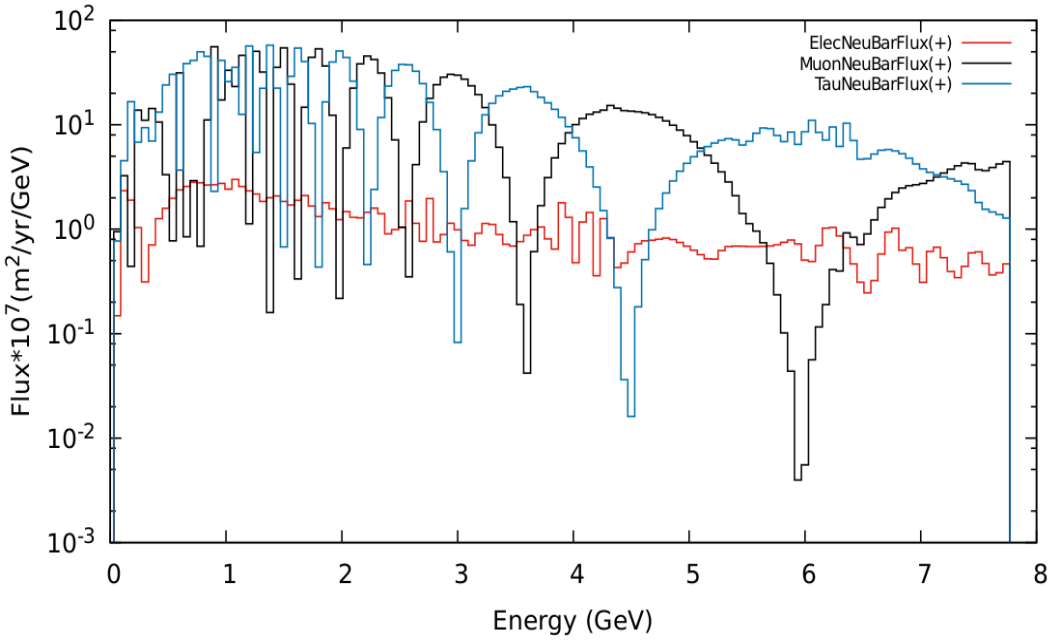

Figure 5.11: Total Anti-Neutrino Flux at INO from Fermilab for **Plus** Horn Focusing.

5.2.2 Minus Focussing

Neutrino → Legends: ElecNeuFlux = Electron Neutrino Flux, MuonNeuFlux = Muon Neutrino Flux, TauNeuFlux = Tau Neutrino Flux.

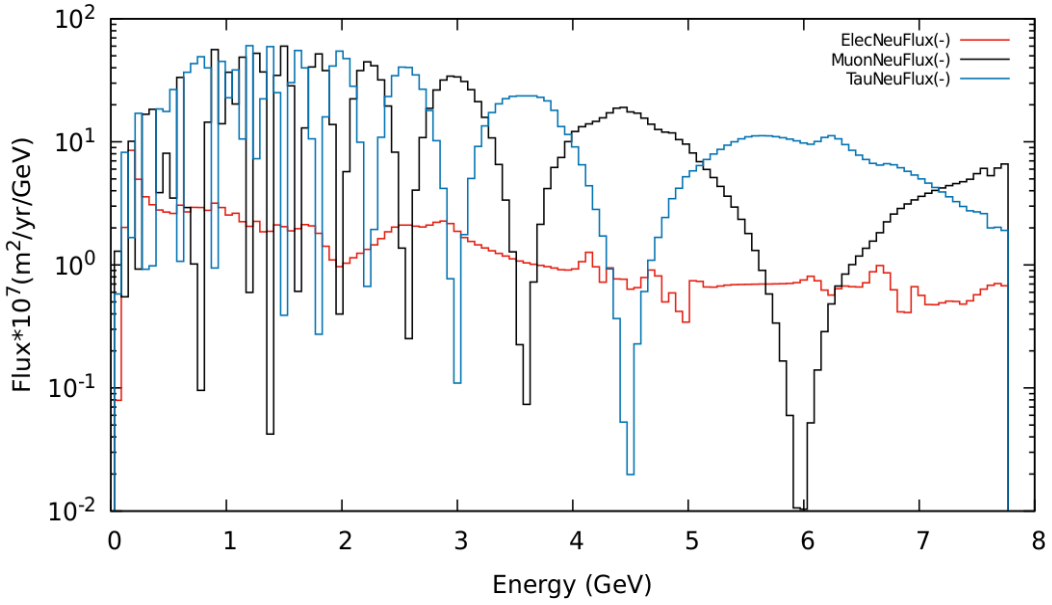

Figure 5.12: Total Neutrino Flux at INO from Fermilab for **Minus** Horn Focusing.

Anti-neutrino → Legends: ElecNeuBarFlux = Electron Anti-neutrino Flux, MuonNeuBarFlux = Muon Anti-neutrino Flux, TauNeuBarFlux = Tau Anti-neutrino Flux.

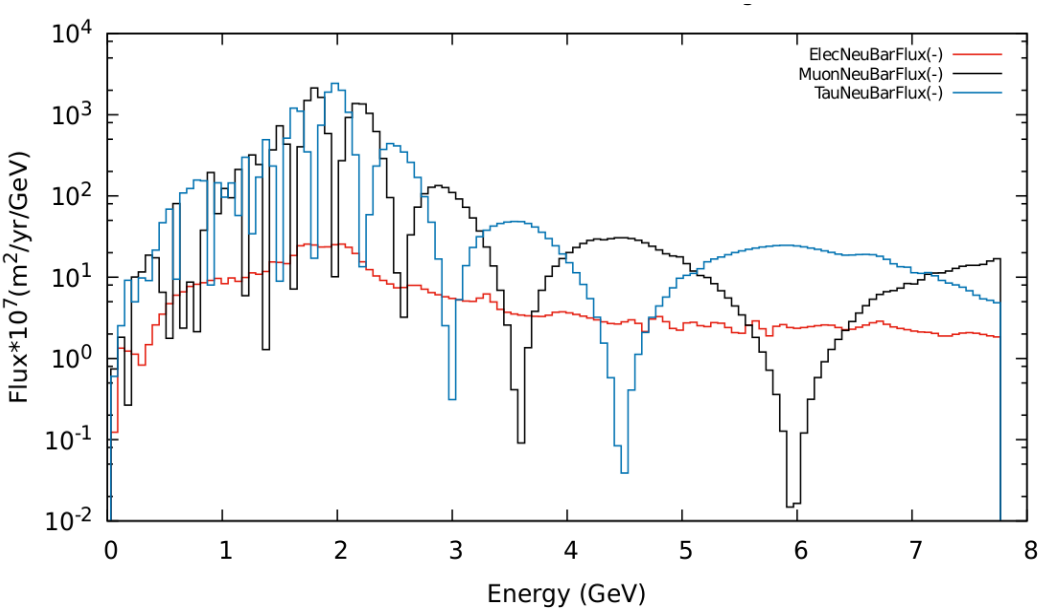

Figure 5.13: Total Anti-Neutrino Flux at INO from Fermilab for **Minus** Horn Focusing.

5.2.3 Oscillation Probabilities

Different Oscillations probabilities for neutrinos and anti-neutrinos propagating from Fermilab to INO site, India.

Legends:

- **Neutrino:** $P\alpha\beta \rightarrow \alpha = Initial\ Flavor$ and $\beta = Final\ Flavor$; e = Electron Neutrino , m = Muon Neutrino ,t = Tau Neutrino

- **Anti-neutrino:** $Pbar\alpha\beta \rightarrow \alpha = Initial\ Flavor$ and $\beta = Final\ Flavor$; e = Electron Neutrino , m = Muon Neutrino ,t = Tau Neutrino

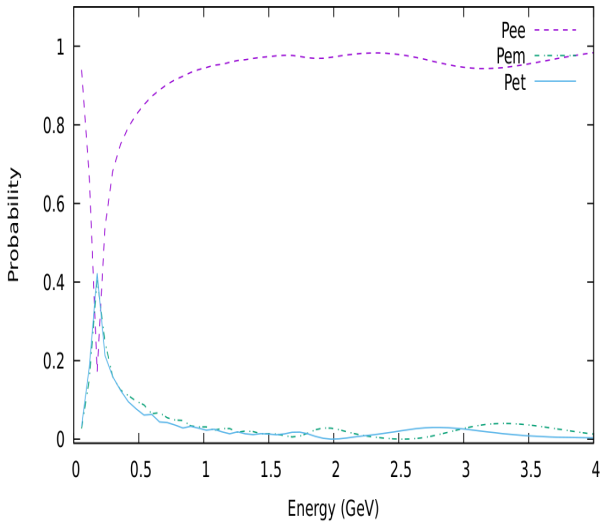

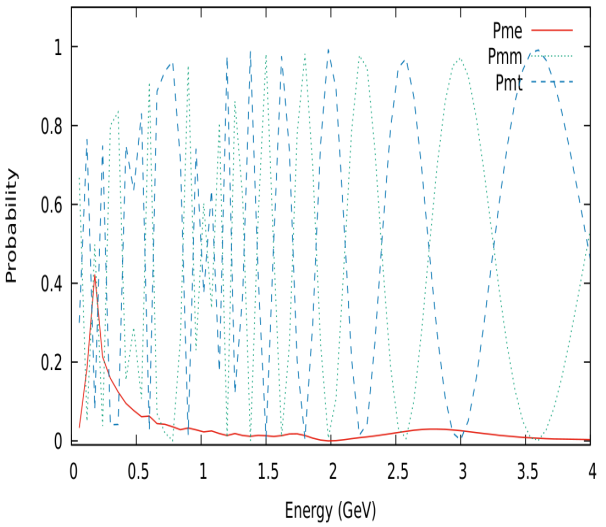

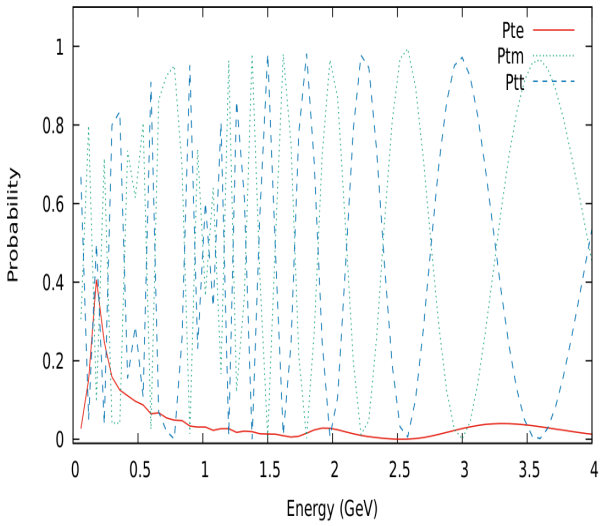

Figure 5.14: Neutrino Transition Probability Values for Fermilab to INO Baseline.

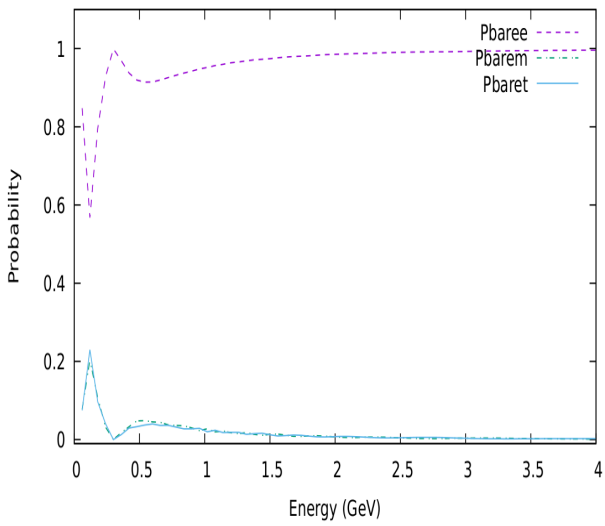

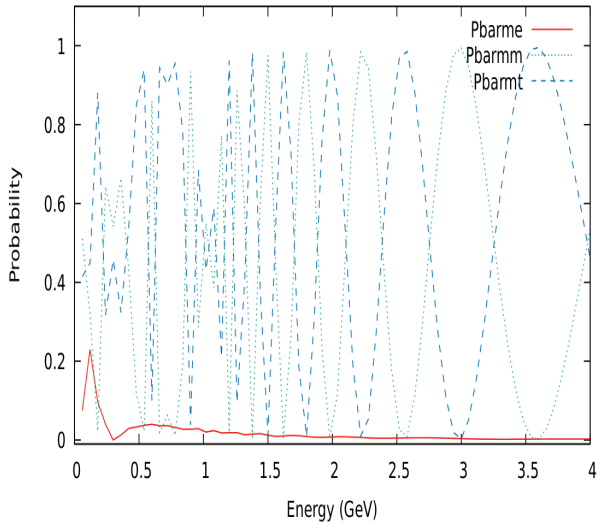

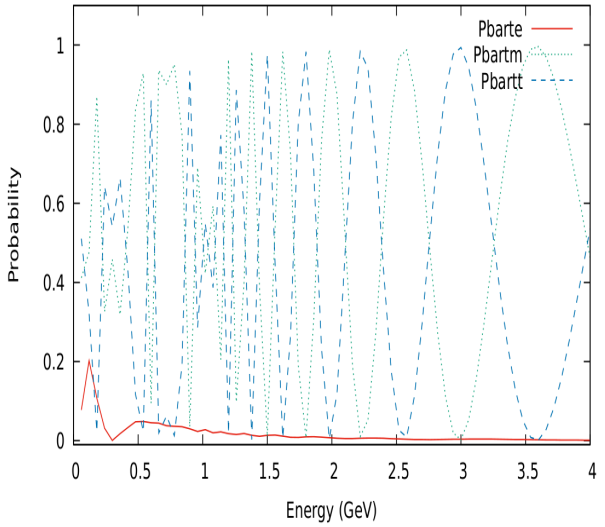

Figure 5.15: Anti-Neutrino Transition Probability Values for Fermilab to INO Baseline.

5.3 Source: J-PARC

Similar to the two previous cases, using GLoBES the neutrino flux was calculated for all flavors at INO site, for Plus and Minus Horn Focussing, coming from Fermilab Near detector. The baseline length is 6637.53 Km, with density profile for the propagation length given by

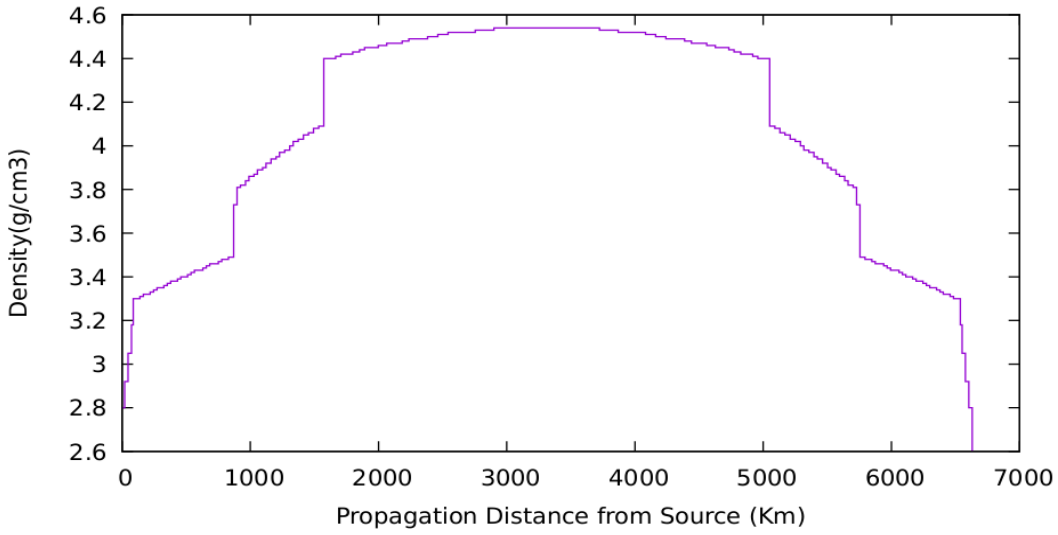

Figure 5.16: Matter Density Profile for neutrino propagating from J-PARC to INO.

5.3.1 Plus Focussing

Neutrino → Legends: ElecNeuFlux = Electron Neutrino Flux, MuonNeuFlux = Muon Neutrino Flux, TauNeuFlux = Tau Neutrino Flux.

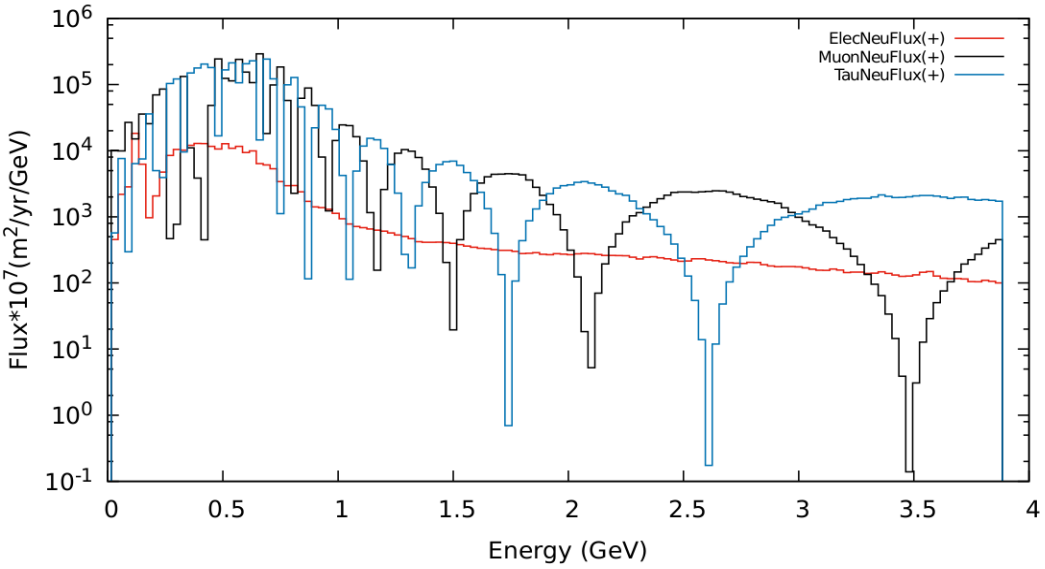

Figure 5.17: Total Neutrino Flux at INO from J-PARC for **Plus** Horn Focusing.

Anti-neutrino → Legends: ElecNeuBarFlux = Electron Anti-neutrino Flux, MuonNeuBarFlux = Muon Anti-neutrino Flux, TauNeuBarFlux = Tau Anti-neutrino Flux.

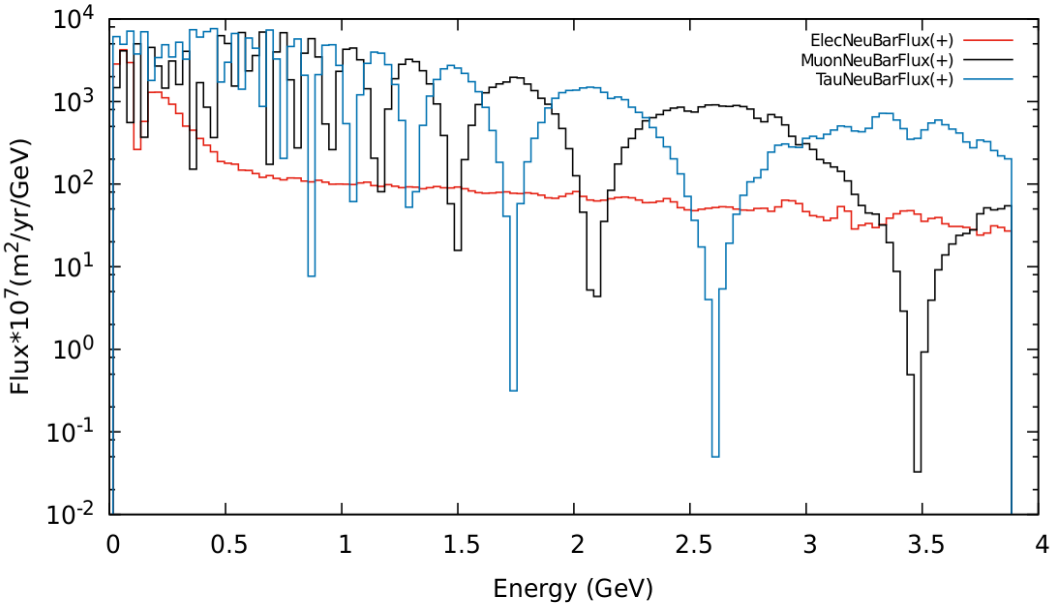

Figure 5.18: Total Anti-Neutrino Flux at INO from J-PARC for **Plus** Horn Focusing.

5.3.2 Minus Focussing

Neutrino → Legends: ElecNeuFlux = Electron Neutrino Flux, MuonNeuFlux = Muon Neutrino Flux, TauNeuFlux = Tau Neutrino Flux.

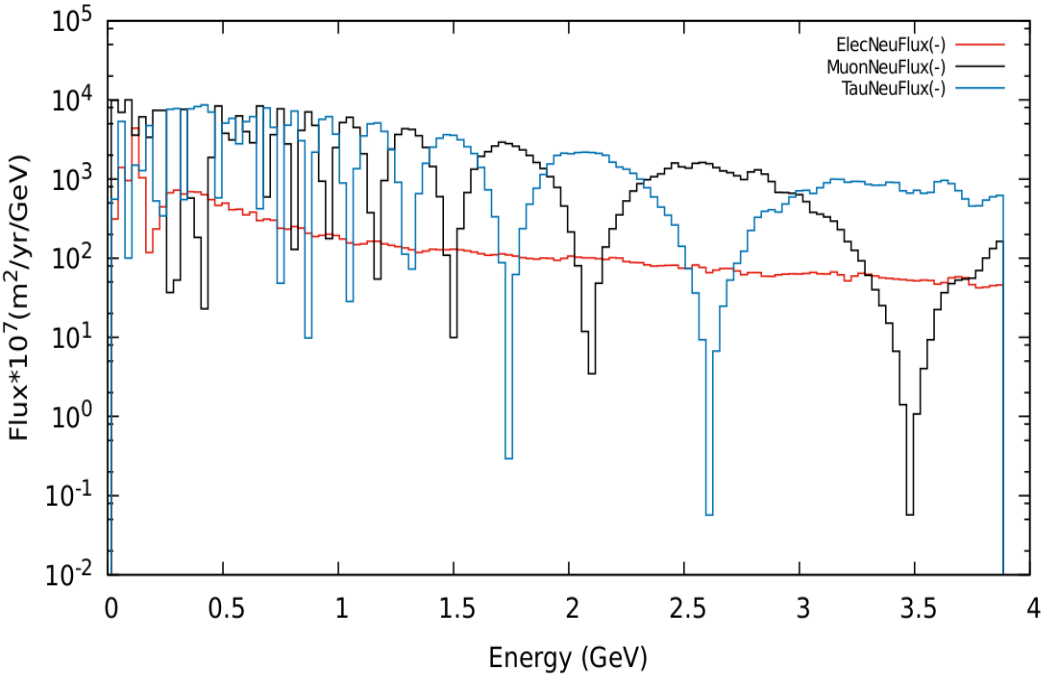

Figure 5.19: Total Neutrino Flux at INO from J-PARC for **Minus** Horn Focusing.

Anti-neutrino → Legends: ElecNeuBarFlux = Electron Anti-neutrino Flux, MuonNeuBarFlux = Muon Anti-neutrino Flux, TauNeuBarFlux = Tau Anti-neutrino Flux.

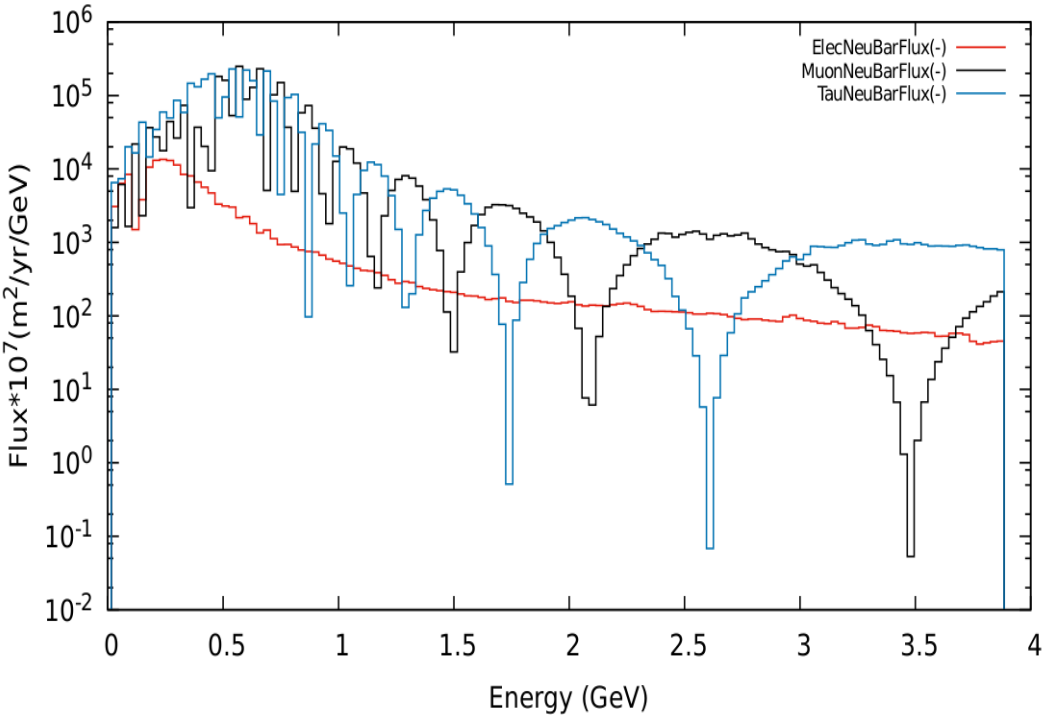

Figure 5.20: Total Anti-Neutrino Flux at INO from J-PARC for **Minus** Horn Focusing.

5.3.3 Oscillation Probabilities

Different Oscillations probabilities for neutrinos and anti-neutrinos propagating from J-PARC to INO site, India.

Legends:

- **Neutrino:** $P\alpha\beta \rightarrow \alpha = Initial\ Flavor$ and $\beta = Final\ Flavor$; e = Electron Neutrino , m = Muon Neutrino ,t = Tau Neutrino

- **Anti-neutrino:** $Pbar\alpha\beta \rightarrow \alpha = Initial\ Flavor$ and $\beta = Final\ Flavor$; e = Electron Neutrino , m = Muon Neutrino ,t = Tau Neutrino

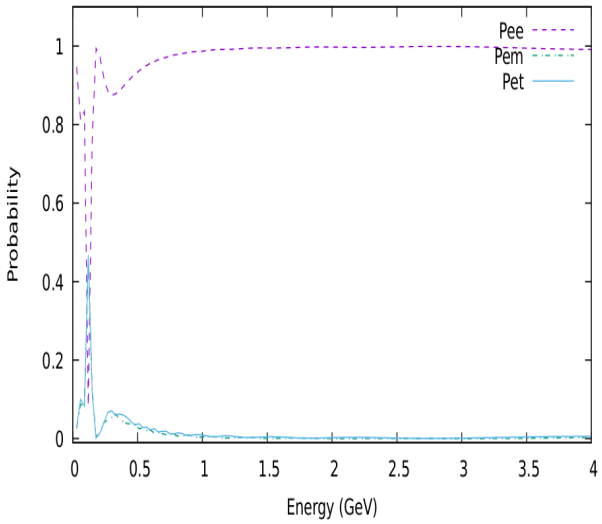

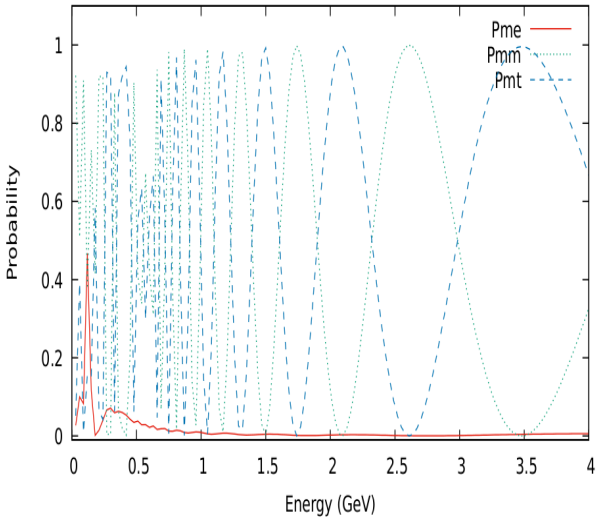

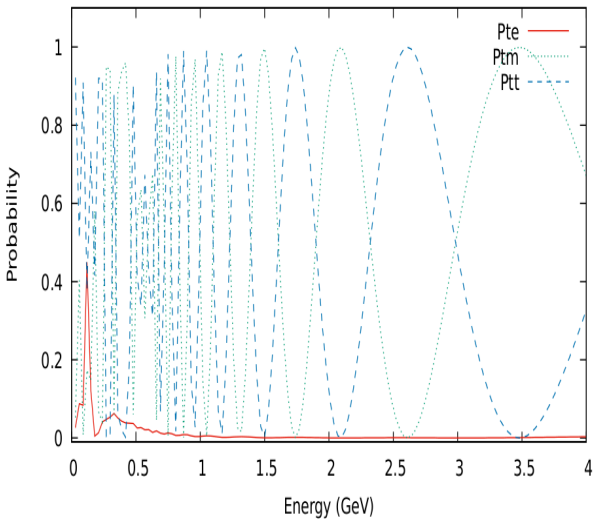

Figure 5.21: Neutrino Transition Probability Values for J-PARC to INO Baseline

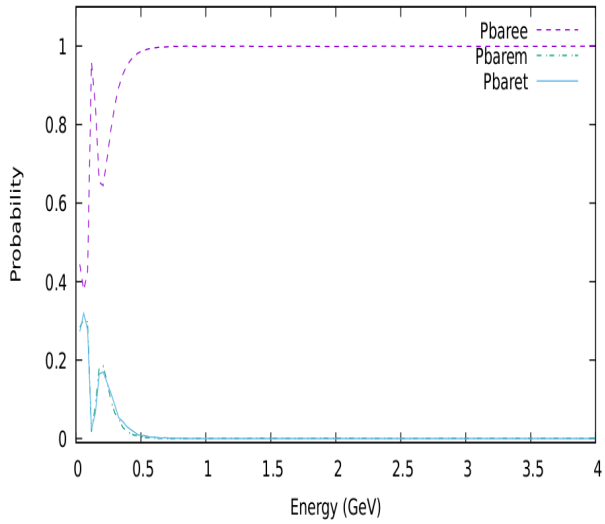

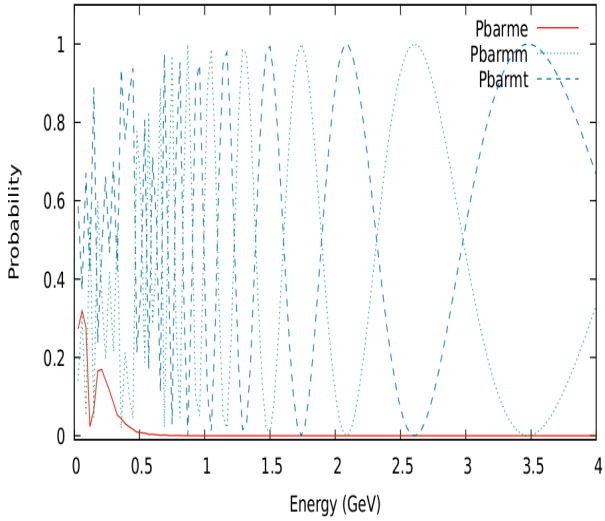

Figure 5.22: Anti-Neutrino Transition Probability Values for J-PARC to INO Baseline

Chapter 6

EHEP Lab, IISER Mohali

EHEP (Experimental High Energy Physics) Lab at IISER Mohali, India is actively involved in various detector R&D programs at the technological frontiers for current and future particle physics experiments via national and international mega-science programs. It is also working towards the development of gas-ionizing detectors like RPC, PMD, MWPC and silicon detectors. These technological developments have numerous applications over a wide range of disciplines starting from physical sciences, nuclear physics experiments, radiation physics, accelerator driven research to medical imaging and applications. Individuals at EHEP lab are also involved in the study of the phase transition from hadronic matter to quark-gluon plasma in heavy ion-collisions and to the experimental investigation of soft non-perturbative QCD in high-energy collisions in a large accelerator like LHC. Finally, the lab is also involved in the study of neutrinos and detector R&D activities in INO collaboration.
The neutrino flux was calculated at the location for test and estimation purposes.

Figure 6.1: Location of Detector (Blue Dot) in IISER Mohali, India Campus.

6.1 Source: CERN

Using GLoBES the neutrino flux was calculated for all flavors at EHEP Lab, for Plus and Minus Horn Focussing. The baseline length from CERN Near Detector to EHEP Lab Far detector is 5945.56 Km, with density profile for the propagation length given by

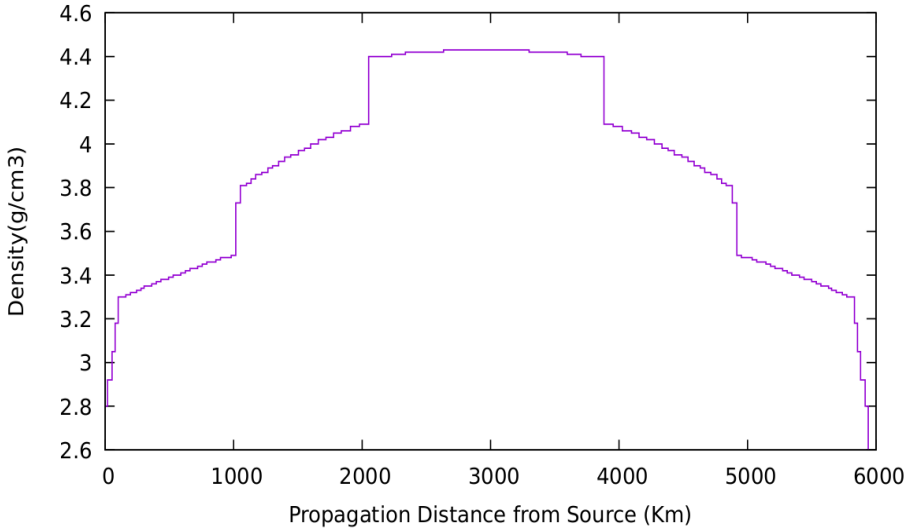

Figure 6.2: Matter Density Profile for neutrino propagating from CERN-SPL to EHEP Lab, IISER Mohali.

6.1.1 Plus Focussing

Neutrino → Legends: ElecNeuFlux = Electron Neutrino Flux, MuonNeuFlux = Muon Neutrino Flux, TauNeuFlux = Tau Neutrino Flux.

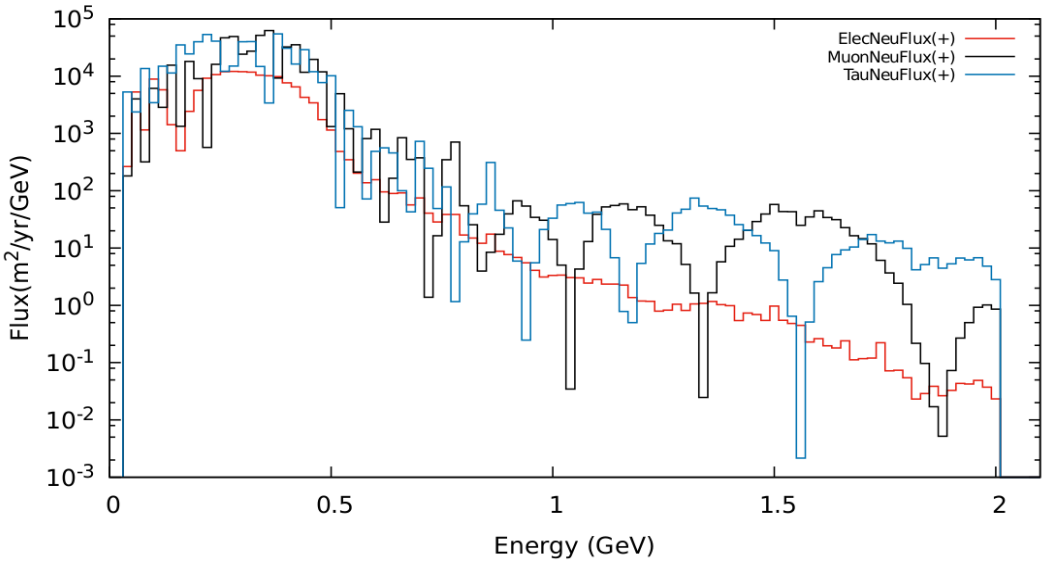

Figure 6.3: Total Neutrino Flux at EHEP Lab, IISER Mohali from CERN for **Plus** Horn Focusing.

Anti-neutrino → Legends: ElecNeuBarFlux = Electron Anti-neutrino Flux, MuonNeuBarFlux = Muon Anti-neutrino Flux, TauNeuBarFlux = Tau Anti-neutrino Flux.

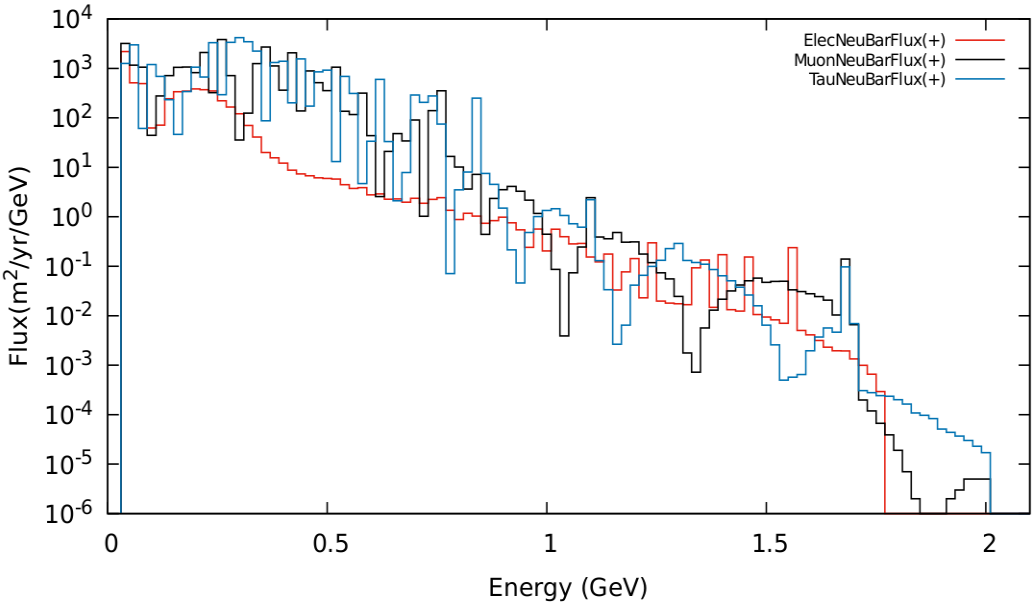

Figure 6.4: Total Anti-Neutrino Flux at EHEP Lab, IISER Mohali from CERN for **Plus** Horn Focusing.

6.1.2 Minus Focussing

Neutrino → Legends: ElecNeuFlux = Electron Neutrino Flux, MuonNeuFlux = Muon Neutrino Flux, TauNeuFlux = Tau Neutrino Flux.

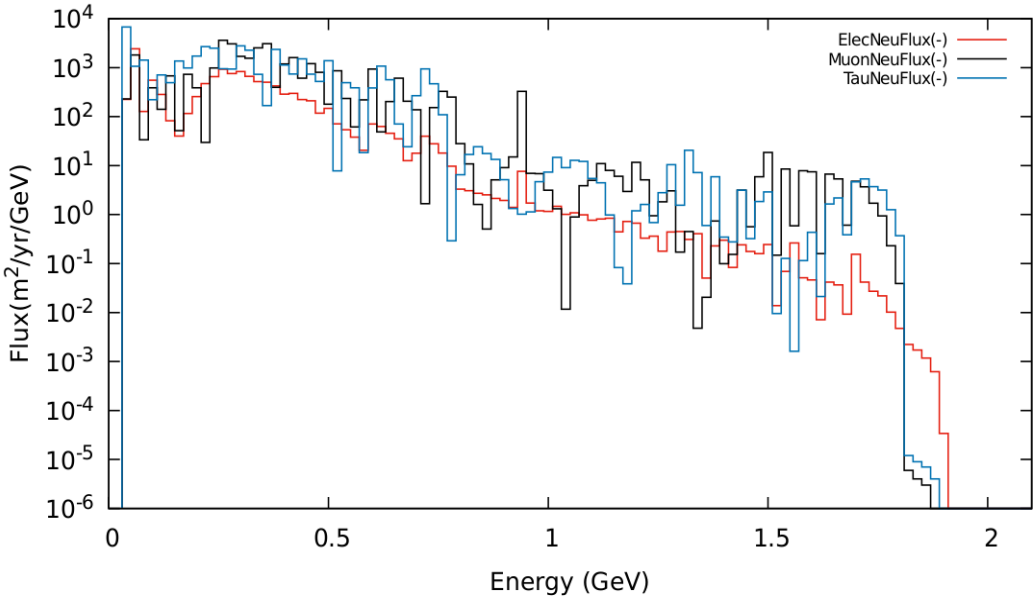

Figure 6.5: Total Neutrino Flux at EHEP Lab, IISER Mohali from CERN for **Minus** Horn Focusing.

Anti-neutrino → Legends: ElecNeuBarFlux = Electron Anti-neutrino Flux, MuonNeuBarFlux

= Muon Anti-neutrino Flux, TauNeuBarFlux = Tau Anti-neutrino Flux.

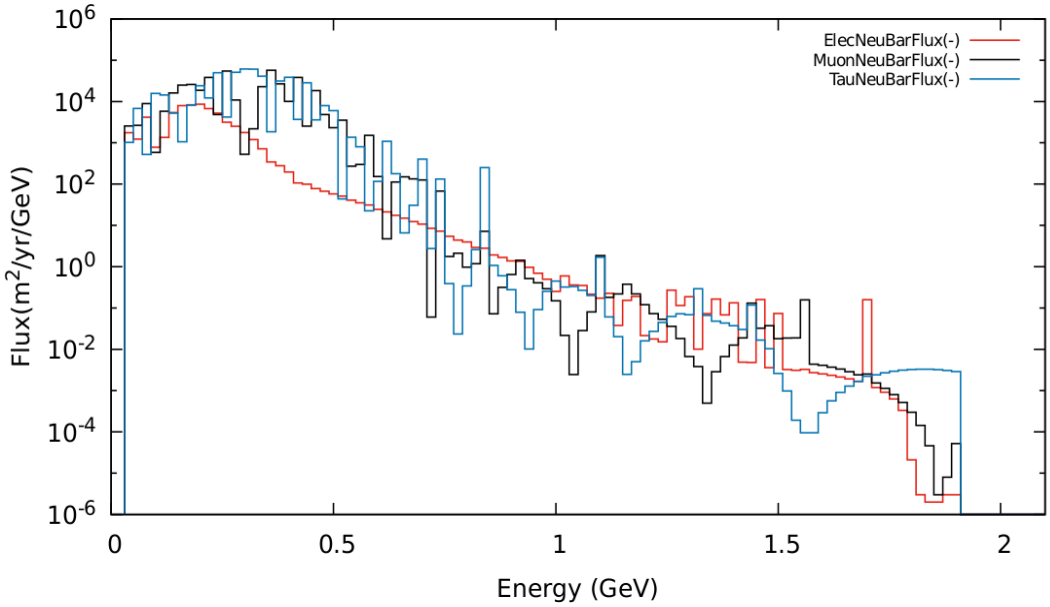

Figure 6.6: Total Anti-Neutrino Flux at EHEP Lab, IISER Mohali from CERN for **Minus** Horn Focusing.

6.1.3 Oscillation Probabilities

Different Oscillations probabilities for neutrinos and anti-neutrinos propagating from CERN to EHEP-Lab, IISER Mohali, India.

Legends:

- **Neutrino:** $P\alpha\beta \rightarrow \alpha = Initial\ Flavor$ and $\beta = Final\ Flavor$; e = Electron Neutrino , m = Muon Neutrino ,t = Tau Neutrino

- **Anti-neutrino:** $Pbar\alpha\beta \rightarrow \alpha = Initial\ Flavor$ and $\beta = Final\ Flavor$; e = Electron Neutrino , m = Muon Neutrino ,t = Tau Neutrino

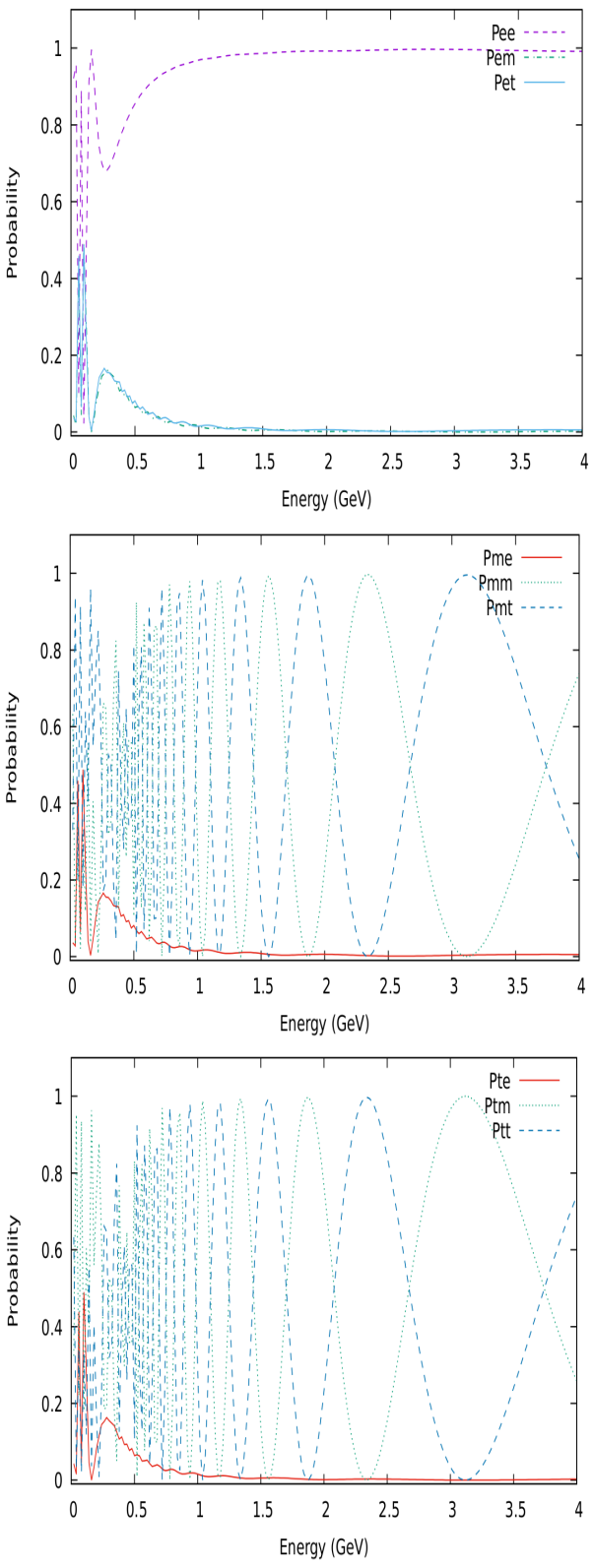

Figure 6.7: Neutrino Transition Probability Values for CERN to EHEP Lab, IISER Mohali Baseline.

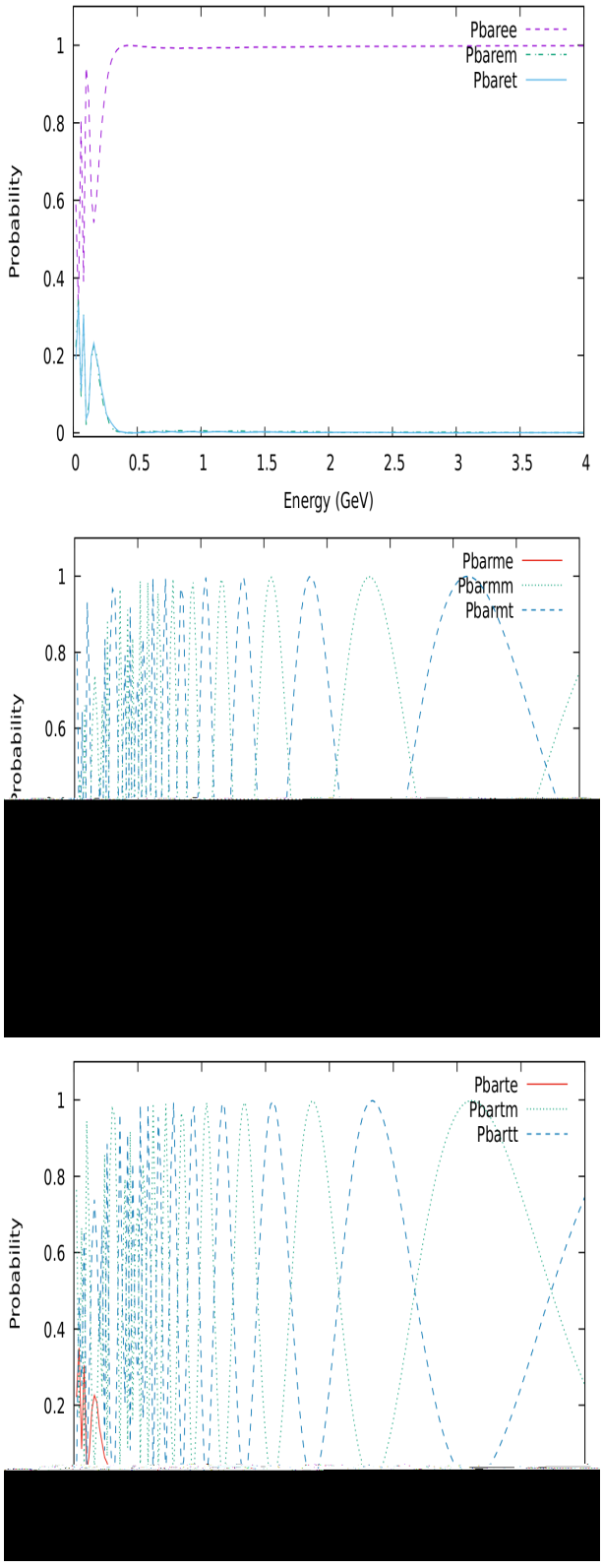

Figure 6.8: Anti-Neutrino Transition Probability Values for CERN to EHEP Lab, IISER Mohali Baseline.

6.2 Source: Fermilab

Similar to previous case, using GLoBES the neutrino flux was calculated for all flavors at EHEP Lab, for Plus and Minus Horn Focussing, propagating from Fermilab Near detector to EHEP Lab, IISER Mohali, India. The baseline length is 10200.28 Km, with density profile for the propagation length given by

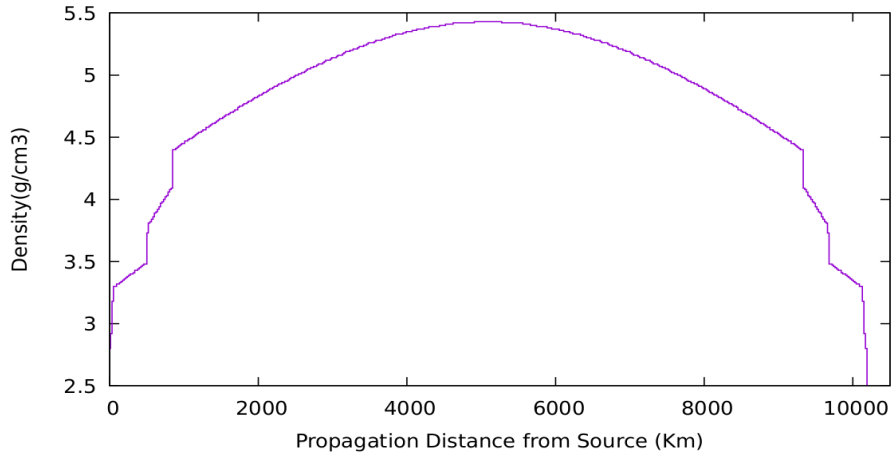

Figure 6.9: Matter Density Profile for neutrino propagating from Fermilab to EHEP Lab, IISER Mohali, India .

6.2.1 Plus Focussing

Neutrino $\rightarrow$ Legends: ElecNeuFlux = Electron Neutrino Flux, MuonNeuFlux = Muon Neutrino Flux, TauNeuFlux = Tau Neutrino Flux.

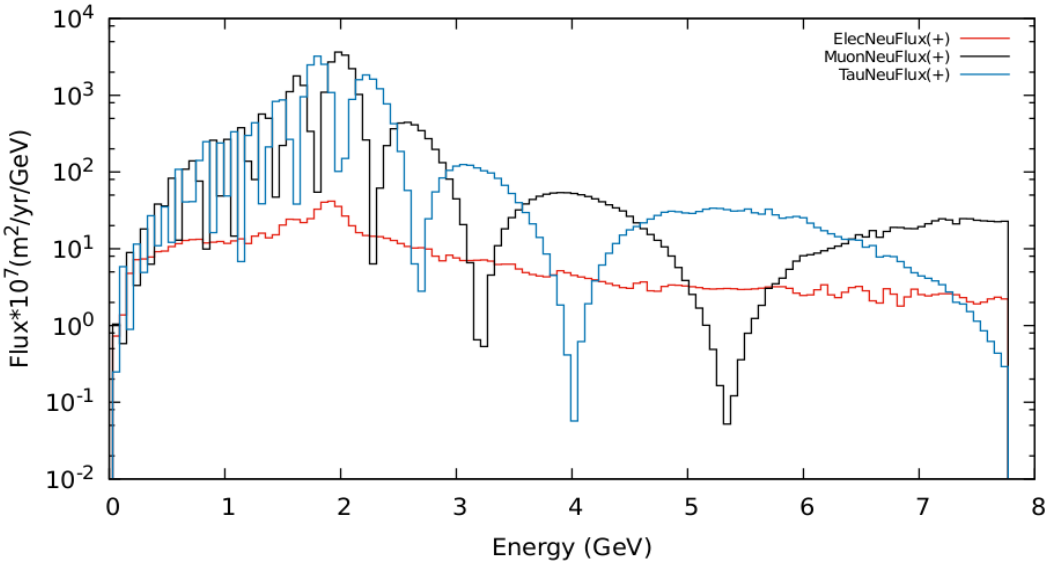

Figure 6.10: Total Neutrino Flux at EHEP Lab, IISER Mohali from Fermilab for **Plus** Horn Focusing.

Anti-neutrino → Legends: ElecNeuBarFlux = Electron Anti-neutrino Flux, MuonNeuBarFlux = Muon Anti-neutrino Flux, TauNeuBarFlux = Tau Anti-neutrino Flux.

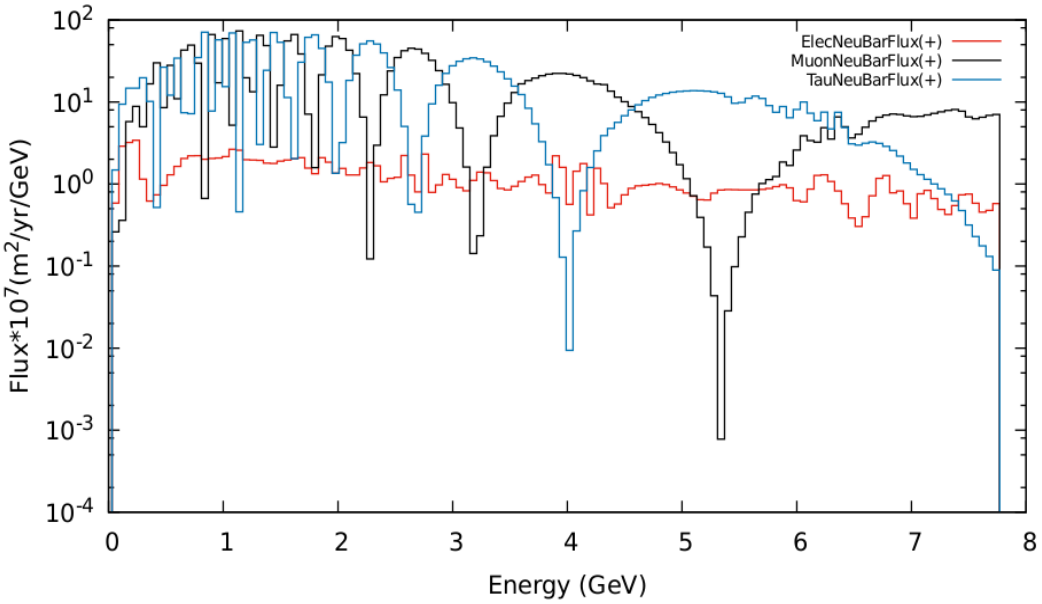

Figure 6.11: Total Anti-Neutrino Flux at EHEP Lab, IISER Mohali from Fermilab for **Plus** Horn Focusing.

6.2.2 Minus Focussing

Neutrino → Legends: ElecNeuFlux = Electron Neutrino Flux, MuonNeuFlux = Muon Neutrino Flux, TauNeuFlux = Tau Neutrino Flux.

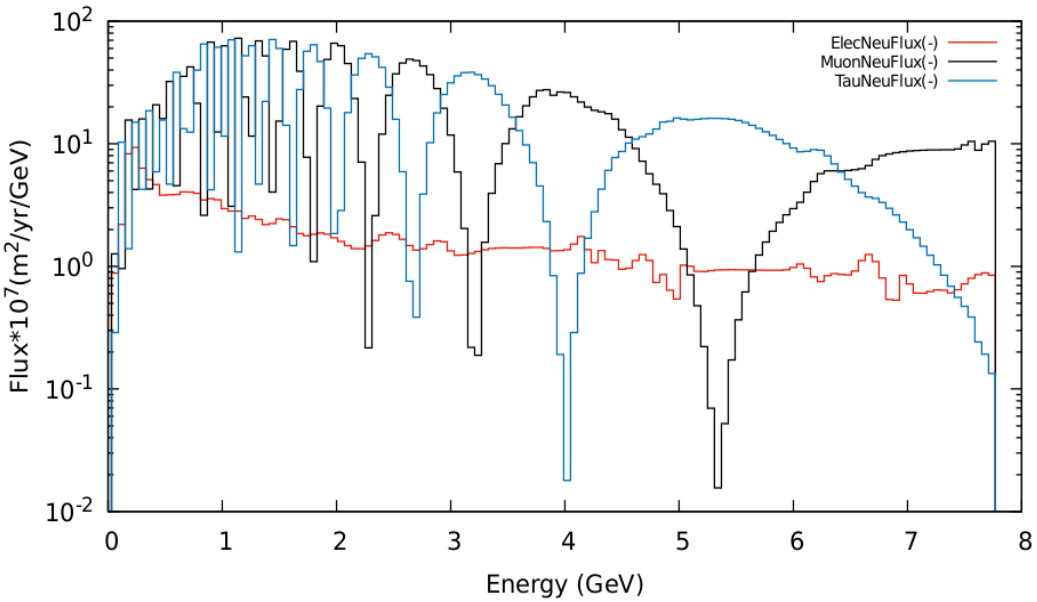

Figure 6.12: Total Neutrino Flux at EHEP Lab, IISER Mohali from Fermilab for **Minus** Horn Focusing.

Anti-neutrino → Legends: ElecNeuBarFlux = Electron Anti-neutrino Flux, MuonNeuBarFlux = Muon Anti-neutrino Flux, TauNeuBarFlux = Tau Anti-neutrino Flux.

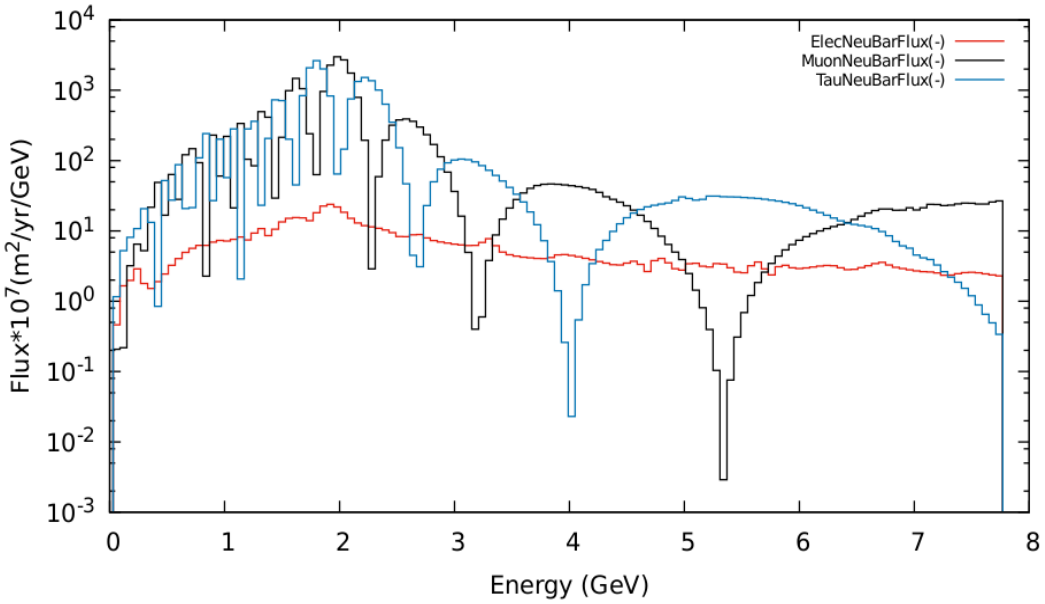

Figure 6.13: Total Anti-Neutrino Flux at EHEP Lab, IISER Mohali from Fermilab for **Minus** Horn Focusing.

6.2.3 Oscillation Probabilities

Different Oscillations probabilities for neutrinos and anti-neutrinos propagating from Fermilab to EHEP-Lab, IISER Mohali, India.

Legends:

- **Neutrino:** $P\alpha\beta \rightarrow \alpha = Initial\ Flavor$ and $\beta = Final\ Flavor$; e = Electron Neutrino , m = Muon Neutrino ,t = Tau Neutrino

- **Anti-neutrino:** $Pbar\alpha\beta \rightarrow \alpha = Initial\ Flavor$ and $\beta = Final\ Flavor$; e = Electron Neutrino , m = Muon Neutrino ,t = Tau Neutrino

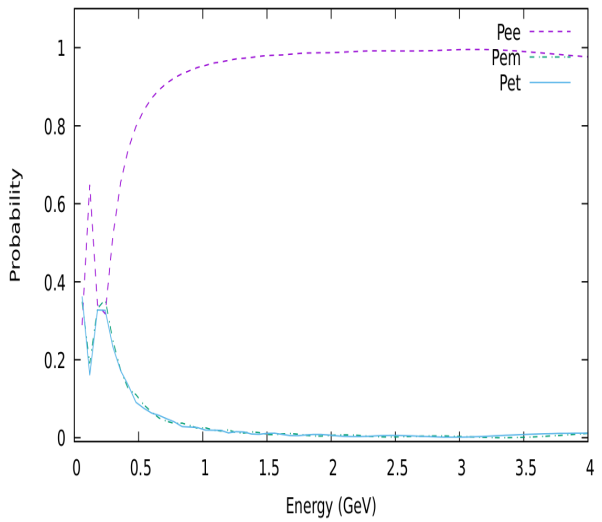

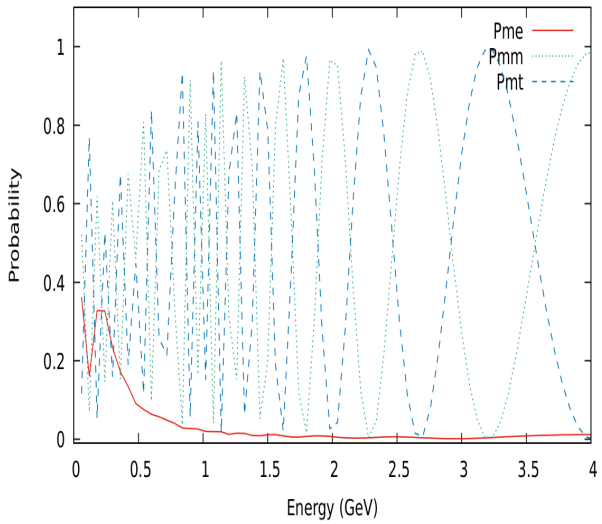

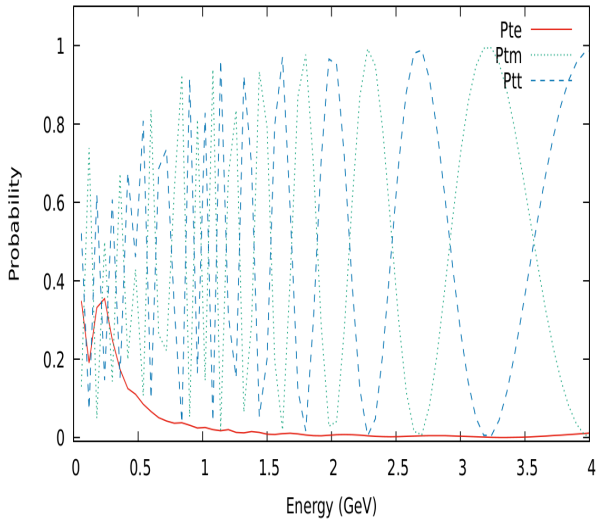

Figure 6.14: Neutrino Transition Probability Values for Fermilab to EHEP Lab, IISER Mohali Baseline

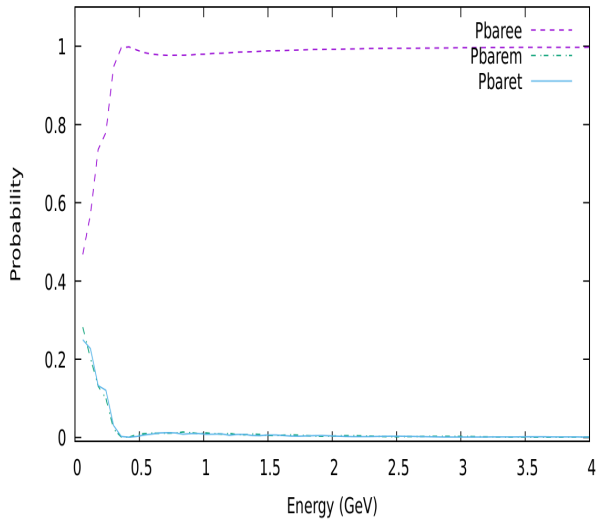

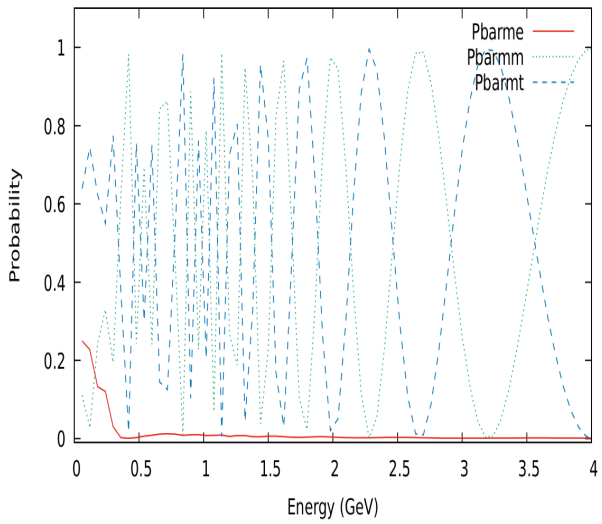

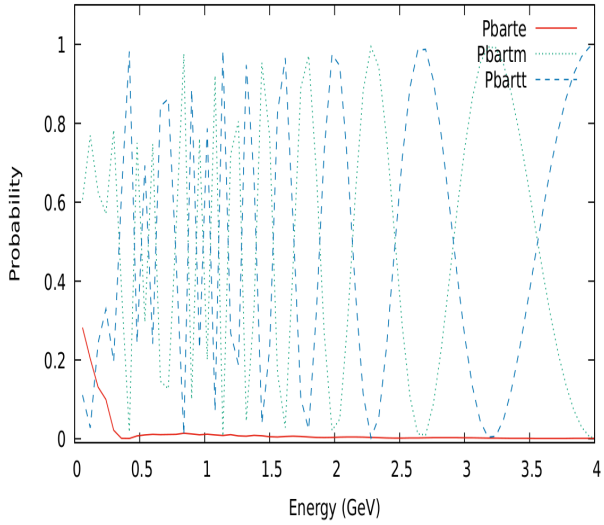

Figure 6.15: Anti-Neutrino Transition Probability Values for Fermilab to EHEP Lab, IISER Mohali Baseline.

6.3 Source: J-PARC

Similar to the two previous cases, using GLoBES the neutrino flux was calculated for all flavors at EHEP Lab, for Plus and Minus Horn Focussing, coming from J-PARC Near detector. The baseline length is 5649.37 Km, with density profile for the propagation length given by

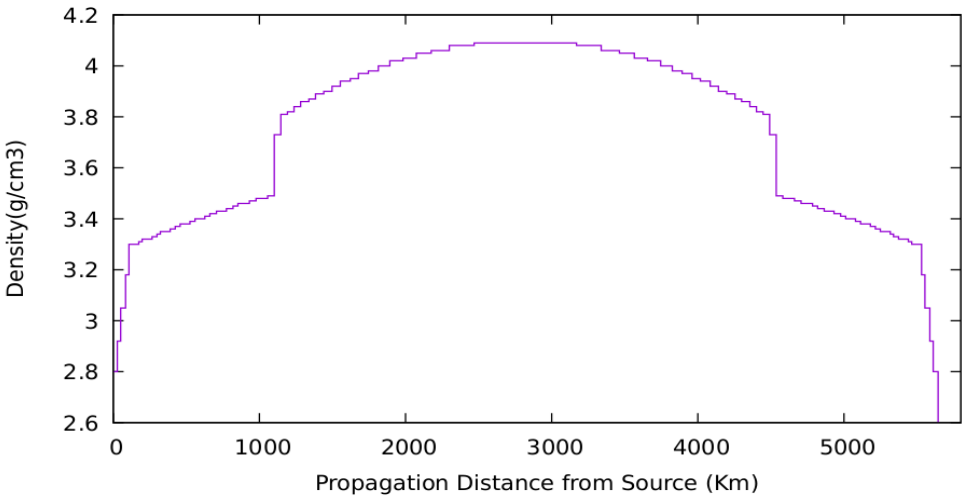

Figure 6.16: Matter Density Profile for neutrino propagating from J-PARC to EHEP Lab, IISER Mohali.

6.3.1 Plus Focussing

Neutrino → Legends: ElecNeuFlux = Electron Neutrino Flux, MuonNeuFlux = Muon Neutrino Flux, TauNeuFlux = Tau Neutrino Flux.

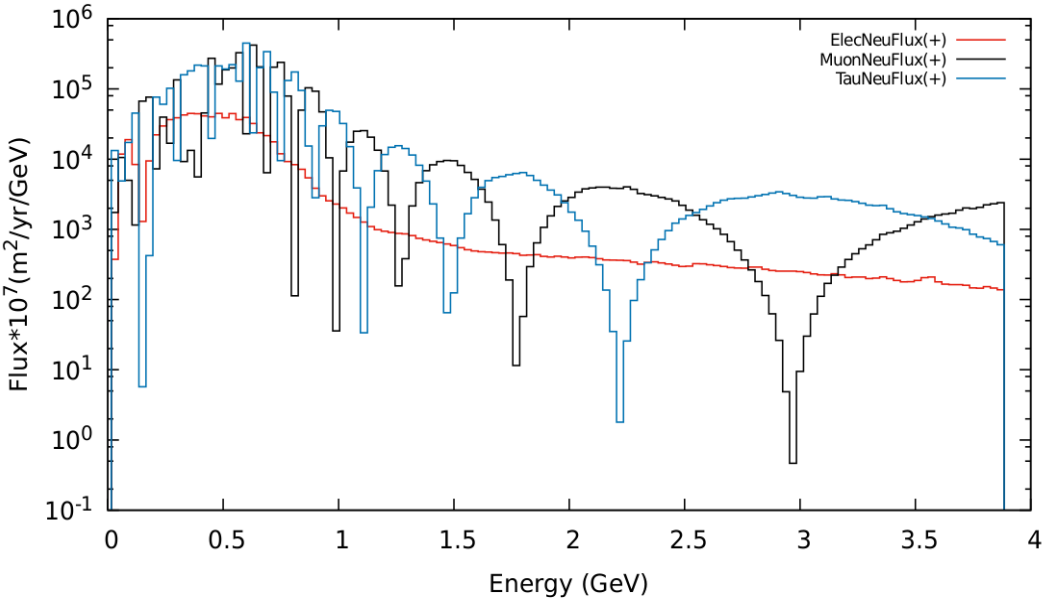

Figure 6.17: Total Neutrino Flux at EHEP Lab, IISER Mohali from J-PARC for **Plus** Horn Focusing.

Anti-neutrino → Legends: ElecNeuBarFlux = Electron Anti-neutrino Flux, MuonNeuBarFlux = Muon Anti-neutrino Flux, TauNeuBarFlux = Tau Anti-neutrino Flux.

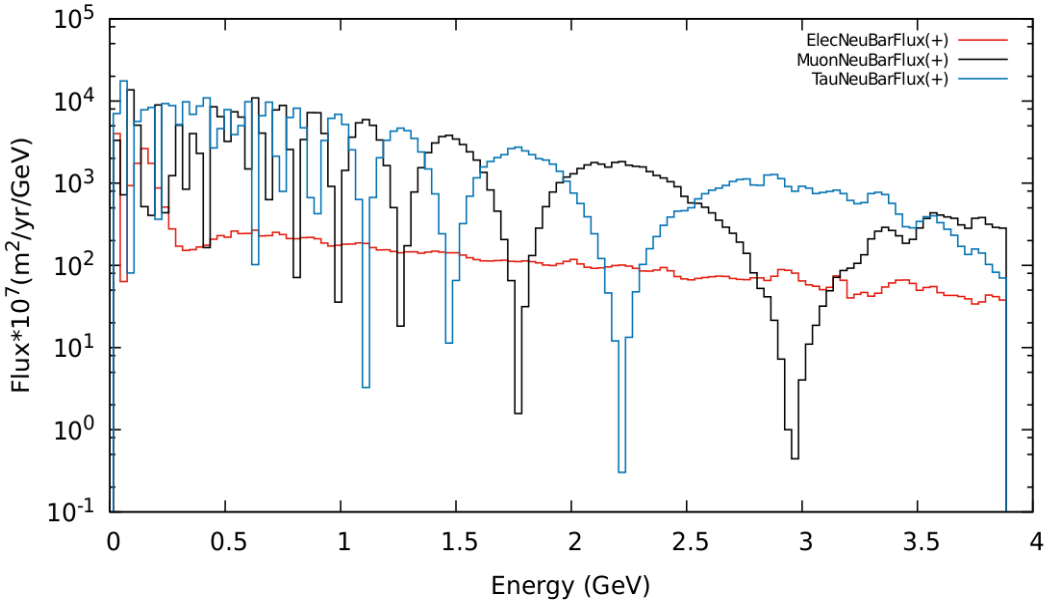

Figure 6.18: Total Anti-Neutrino Flux at EHEP Lab, IISER Mohali from J-PARC for **Plus** Horn Focusing.

6.3.2 Minus Focussing

Neutrino → Legends: ElecNeuFlux = Electron Neutrino Flux, MuonNeuFlux = Muon Neutrino Flux, TauNeuFlux = Tau Neutrino Flux.

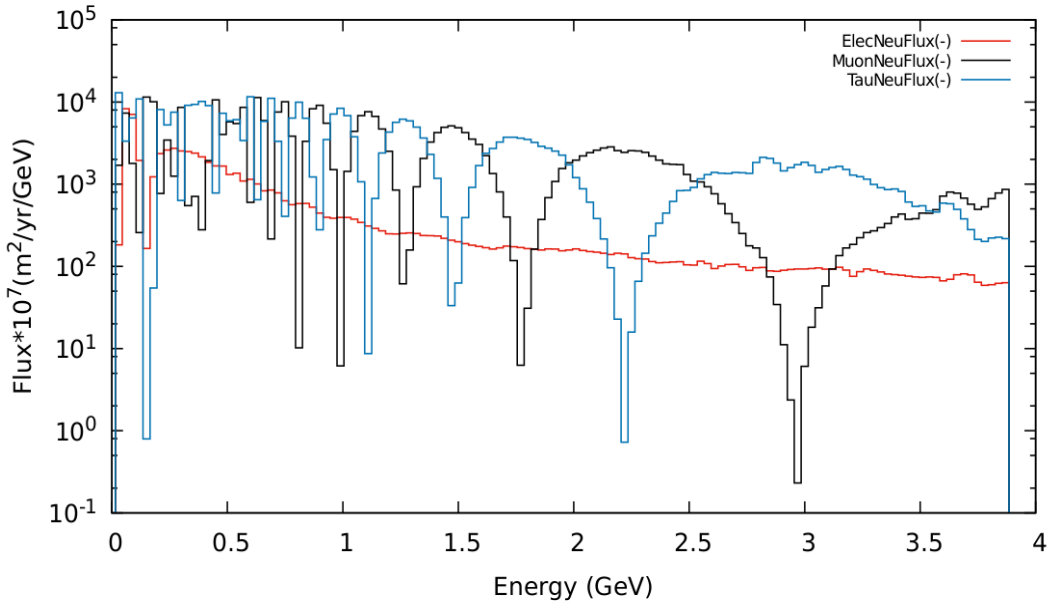

Figure 6.19: Total Neutrino Flux at EHEP Lab, IISER Mohali from J-PARC for **Minus** Horn Focusing.

Anti-neutrino → Legends: ElecNeuBarFlux = Electron Anti-neutrino Flux, MuonNeuBarFlux = Muon Anti-neutrino Flux, TauNeuBarFlux = Tau Anti-neutrino Flux.

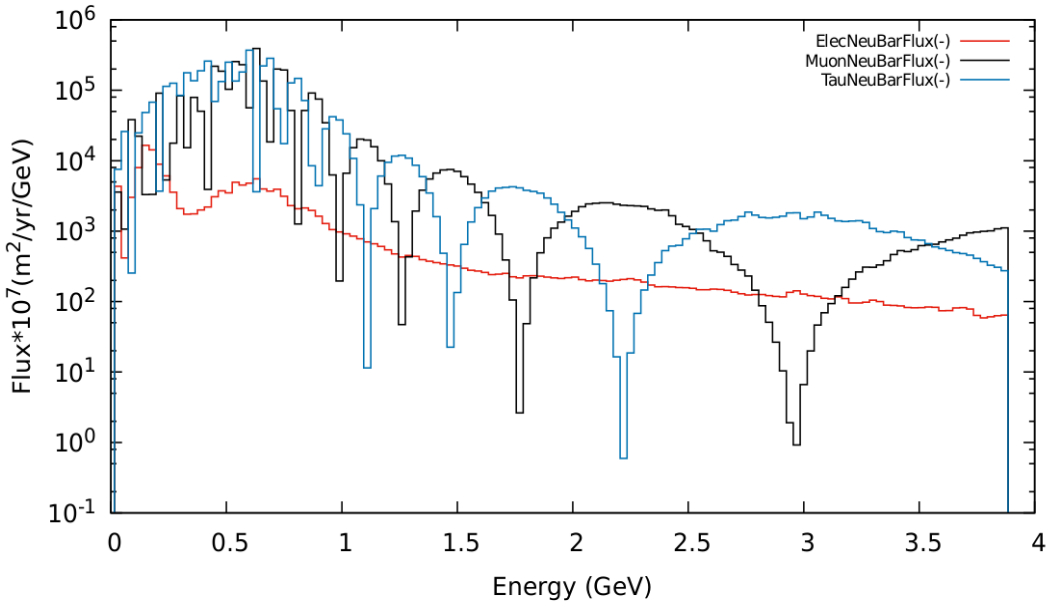

Figure 6.20: Total Anti-Neutrino Flux at EHEP Lab, IISER Mohali from J-PARC for **Minus** Horn Focusing.

6.3.3 Oscillation Probabilities

Different Oscillations probabilities for neutrinos and anti-neutrinos propagating from J-PARC to EHEP-Lab, IISER Mohali, India.

Legends:

- **Neutrino:** $P\alpha\beta \rightarrow \alpha = Initial\ Flavor$ and $\beta = Final\ Flavor$; e = Electron Neutrino , m = Muon Neutrino ,t = Tau Neutrino

- **Anti-neutrino:** $Pbar\alpha\beta \rightarrow \alpha = Initial\ Flavor$ and $\beta = Final\ Flavor$; e = Electron Neutrino , m = Muon Neutrino ,t = Tau Neutrino

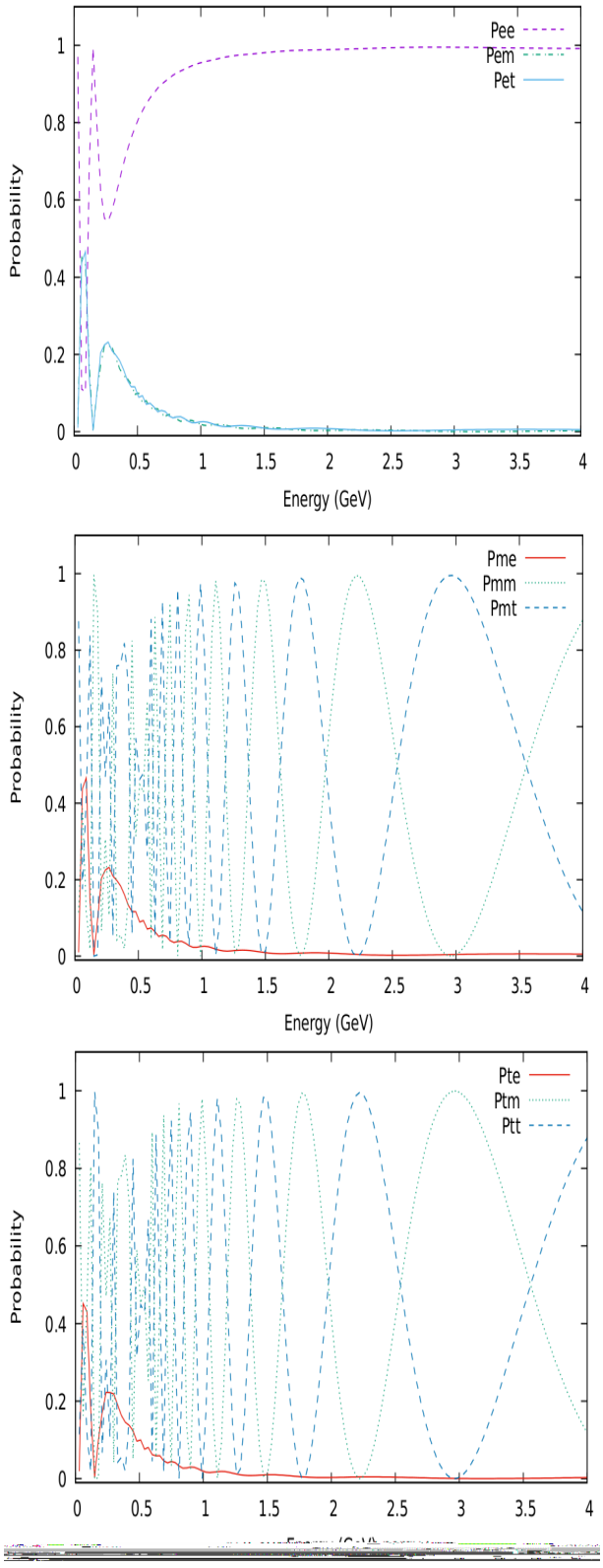

Figure 6.21: Neutrino Transition Probability Values for J-PARC to EHEP Lab, IISER Mohali Baseline.

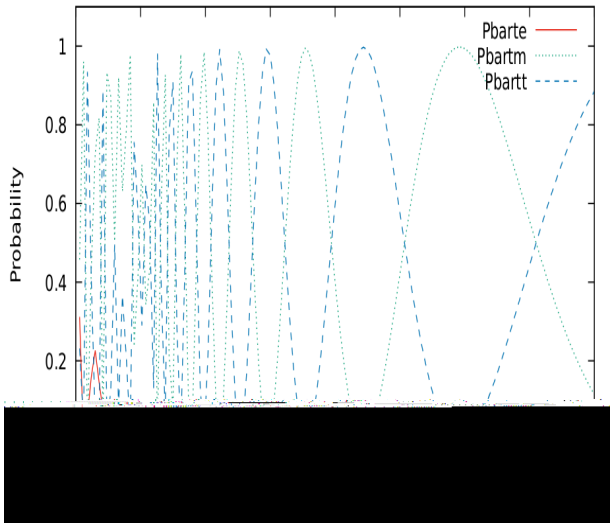

Figure 6.22: Anti-Neutrino Transition Probability Values for J-PARC to EHEP Lab, IISER Mohali Baseline.

Chapter 7

Conclusions

Neutrino Oscillation provide us a way to probe Beyond Standard Model Physics and a satisfactory explanation to solar and atmospheric neutrino deficits. It now plans to solve probe parameters which could shed light on why is the Universe dominated by matter over anti-matter(by the measurement of δ_{CP}). This long-lasting important question of Physics could be answered if neutrinos and anti-neutrinos behave differently. To do this, we need simultaneous knowledge of neutrino and anti-neutrino fluxes at the same detector location. Few other unsolved problems in neutrino physics like Octant issue, sterile neutrinos can also benefit from the simultaneous knowledge of neutrino flux for various flavors. Understanding of matter effects is crucial for many of the experiments trying to solve the mentioned problems. This was the primary reason for us to study matter effects on neutrino oscillations.

A significant part of this thesis focused on the estimation of neutrino and anti-neutrino flux (for both Plus and Minus Horn focussing) using two detector setup. This involves measuring the neutrino flux near the production site and then at the far detector where the peak of oscillation probability lies. After including the near detector data into the analysis of the oscillation signals, it was extrapolated using GLoBES simulation software to get the flux at the far detector. This was done taking data from the near detector at three accelerator facilities namely: CERN, Fermilab, and J-PARC.

After analysis, it was realized that although oscillation peaks existed for various transition channels at both the detector locations (Indian Neutrino Observatory and EHEP-Lab, IISER Mohali, India), considerable neutrino flux contribution for all flavors is only from CERN neutrino facility. The flux from other accelerator facilities is too less to make any measurement by a detector.

This is mainly because of CERN operating at intensity frontier of neutrino physics, producing neutrinos with intensity several orders higher than other accelerator facilities. On the other hand, Fermilab and J-PARC function on energy frontier, with neutrino production over a higher energy range but with low intensity.

It will be interesting to apply some of the ideas developed in this thesis, to establish new neutrino detectors which can benefit from the multiple baselines and probe the properties of neutrinos and improve the precision of already established parameters. I also further plan to modify my work to develop a setup which can easily itself give suitable detector location on earth having considerable flux to make measurements and still benefiting from the multiple baselines.

Appendices

Appendix A

Solar and Atmospheric Neutrino Problem

Neutrino flux is mainly measured by two processes listed as:

- **Radiochemical Detection:** This method involves exposing the detection element to the flux of neutrinos and later extracting the signals (using radiochemical techniques) and counting them. This method uses the Inverse $\beta-$decay process as its detection process. Since it's a passive detection process, it loses the information of direction.
- **Cerenkov Detection:** This method uses the elastic scattering processes as its detection process. The charged leptons produced from neutrino interactions produce Cerenkov light while passing through the detector. By analyzing this Cerenkov Light, we can reconstruct the neutrino track. The recoil particle's energy distribution gives information about the incident neutrino energy spectrum. It's a real-time detection process.

A.1 Solar Neutrino Problem:

A.1.1 Homestake Experiment:

Ray Davis's Homestake experiment(1965) [Dav94] was the first experiment to measure solar neutrino flux. This experiment used the radiochemical detection method and consisted of 400,000 liters of Perchloroethylene (C_2Cl_4). The reaction involved in the detection process is:

$$\nu_e + {}^{37}Cl \rightarrow {}^{37}Ar + e^-$$

This reaction has a threshold 0.814 MeV.

Surprising Result: Homestake experiment noted an average capture rate of solar neutrinos

of 2.56±0.25 SNU (1 SNU = 10^{-36} neutrino interactions per target atom per second). However Standard Solar Model predicted that Homestake should have seen about 8.1±1.2 SNU. This was the birth of "**Solar Neutrino Problem**". Since the Homestake experiment had no information about directionality, the results were not widely accepted by the scientific community at that time.

A.1.2 Super Kamiokande Experiment:

Solar Neutrino Problem was only reconfirmed 20 years later when S-Kamiokande [Smy01] in 1985 measured the solar neutrino flux again. They used the Cerenkov detection process and obtained a clear amount of excess events in the direction of the sun, confirming that the neutrinos detected were, in fact, solar neutrinos. Much similar to the Homestake Experiment they also observed around 50% deficit in the neutrino flux. The experiment had a high threshold of 7.5 MeV.

After S-Kamiokande it was clear that there was in fact some deficit in the solar neutrino flux. However, later a problem was realized with these experiments. They had a high energy threshold for detection. However, most of the neutrino flux was released at lower energies through the pp-chain in the sun. So the previous experiments were insensitive to the majority of the solar neutrino flux.

To cover-up for the Homestake and S-Kamiokande, Gallium [A^{+}94] [Vig98] experiments were proposed. These experiments because of their low threshold were sensitive to most of the solar neutrino flux.

A.1.3 SAGE and GALLEX:

These were radiochemical detectors, using Gallium as their main detector element. These experiments also observed a deficit in the neutrino flux.

After the unexpected neutrino flux measurements measured by above-mentioned experiments, questions were raised whether the model we are using, i.e., "Standard Solar Model" to estimate Neutrino flux is correct or not. Helioseismology results turned the decision in favor of "Standard Solar Model." The results were matching with the expectations to better than 99.5%. So it was concluded that there was still some problem with the measurement process only.

It was realized that the previous experiments had sensitivity exclusively to electron neutrinos

only. So we might be getting other flavors, but the experiment was unable to detect those. **Sudbury Neutrino Observatory (SNO)** was used for this.

A.1.4 Sudbury Neutrino Observatory (SNO):

SNO is a "Heavy-Water" Cerenkov detector. SNO used heavy water since deuteron is a very fragile nucleus. It only takes about 2 MeV to break it apart into a proton and a neutron. The deuterium in heavy water allows the detection of all types of neutrinos.SNO was able to detect neutrino via three different interactions:

- The Charged Current (CC) channel :

$$\nu_e + d \rightarrow p + p + e^-$$

  This reaction can only be initiated by electron neutrinos and therefore only measure flux of electron neutrinos $(\phi(\nu_e))$.

- The Elastic Scattering (ES) channel :

$$\nu_e + e^- \rightarrow \nu_e + e^-$$

  This channel is most sensitive to electron neutrinos.It measures,$\phi(\nu_e) + .15\left[\phi(\nu_\mu) + \phi(\nu_\tau)\right]$

- The Neutral Current (NC) channel :

$$\nu + d \rightarrow n + p + \nu$$

  This channel was the unique feature of SNO. It is equally sensitive to all flavors of neutrinos.Hence it measures the total flux $\phi(\nu_e) + \phi(\nu_\mu) + \phi(\nu_\tau)$.

SNO used the measurements [Ske02] of the these three independent reaction channels to get individual fluxes of neutrinos.Their measurement of the neutrino fluxes (in units of $10^{-8} cm^{-2} s^{-1}$) was:

$$\phi_{CC} = \phi(\nu_e) = 1.76 \pm 0.01$$

$$\phi_{ES} = \phi(\nu_e) + .15\left[\phi(\nu_\mu) + \phi(\nu_\tau)\right] = 2.39 \pm 0.26$$

$$\phi_{NC} = \phi(\nu_e) + \phi(\nu_\mu) + \phi(\nu_\tau) = 5.09 \pm 0.63$$

The total flux of muon and tau neutrinos from the Sun $\phi(\nu_\mu) + \phi(\nu_\tau)$ is $(3.33 \pm 0.63)10^{-8} cm^{-2} s^{-1}$. This is roughly three times larger than the flux of ν_e. Since we know the Sun only produces electron neutrinos, the only conclusion is that **neutrinos must change flavor** between the Sun and the Earth. Further, the SSM predicts a total flux of neutrinos with energies greater than 2 MeV (the deuteron break-up energy) of $\phi_{SSM} = (5.05 \pm 1.01)10^{-8} cm^{-2} s^{-1}$, which is in very good agreement with the NC flux measured by SNO. Hence the Solar Neutrino Problem was solved.

A.2 Atmospheric Neutrino Problem

The atmosphere is constantly bombarded by cosmic rays. When cosmic rays (mostly composed of protons and helium nuclei) hit air nuclei in the atmosphere they produce secondary particles like pions, kaons etc.. When these secondary particles decay, it produces neutrinos. Neutrinos in atmosphere are predominantly produced in two flavors (ν_e , ν_μ).The decay chain is:

$$\pi^\pm \rightarrow \mu^\pm + \nu_\mu(\bar{\nu_\mu})$$

$$\mu^\pm \rightarrow e^\pm + \bar{\nu_\mu}(\nu_\mu) + \nu_e(\bar{\nu_e})$$

As described in chapter 1, the value of parameter **Double Ratio** R should be near unity but various experiments showed a significant deviation from unity for the **R** value.
This deviation from the unity signifies a deficit in the observed flux and was refereed as the **Atmospheric Neutrino Anomaly**. Super-Kamiokande in addition to confirming the anomaly with high statistics, also gave evidence of **Neutrino Oscillation**. Many other models to justify the anomalies, such as neutrino decay etc. have been ruled out because of their inability to justify all experimental measurements.

A.2.1 Super-Kamiokande(SK) Observations

Located in Kamioka mines of Japan, it is a water Cerenkov detector. Cerenkov light produced in water is detected by 7650 photomultiplier tubes (PMT) mounted on the walls of the detector. The trajectory of the charged particle (such as e, μ, τ) propagating in water is recreated by analyzing the Cerenkov ring's timing and pulse data from PMTs.

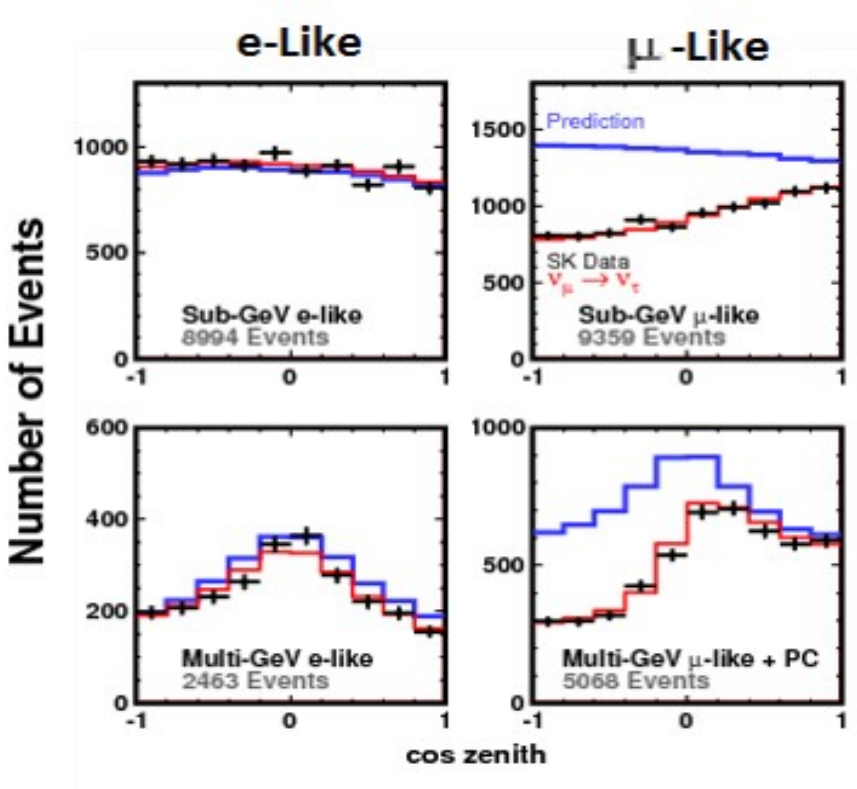

Figure A.1: Zenith Angle distribution of observed number of events in sub-MeV and multi-GeV range for electron and muon like events [F+98]

Since the flux of cosmic rays is almost isotropic, the flux reaching a detector in the upward and downward direction is expected to be the same (little asymmetry for $E_\nu < 3GeV$). Hence we expect observed number of events to be symmetric about $cos(\theta) = 0$ .As can be seen from **Figure A.1**; there is consistency between observed and expected observation in case of electron type events. However in case of muon-type, a distinct asymmetry is observed around the horizon ($cos(\theta) = 0$) . This is referred as up-down asymmetry in muon flux. These observations suggest Beyond Standard Model Physics. One of the most convincing and promising explanations for these was suggested as **Neutrino Oscillation**. Many other models such as neutrino decay etc. have been ruled out to a good extent by experimental measurements.

Appendix B

Standard Derivation of Neutrino Oscillations

Let $|\nu_\alpha\rangle$ represent the flavor states and $|\nu_k\rangle$ represent the mass states. Writing the flavor states as superposition of mass states we get:

$$|\nu_\alpha\rangle = U^*_{\alpha k}|\nu_k\rangle \tag{B.1}$$

Here $\alpha = e, \nu, \tau$ and $k = 1, 2, 3$

Where $U_{\alpha k}$ is the (α, k) component of Unitary matrix **U**.

The transition probability of any general neutrino flavor ν_α to ν_β is given by:

$$P_{\nu_\alpha \to \nu_\beta}(L,E) = \sum_k |\, U_{\alpha k}\,|^2 |\, U_{\beta k}\,|^2 + 2 * Re \sum_{k>j} U^*_{\alpha k} U_{\beta k} U_{\alpha j} U^*_{\beta j} * \exp\left(-2\pi\imath \frac{L}{L^{osc}_{kj}}\right) \tag{B.2}$$

Here

E = Energy of the neutrino

L = Distance between source and detector

L^{osc}_{kj} = Oscillation Length = $\frac{4\pi E}{\Delta m^2_{kj}} = 2.47 * \frac{E(GeV)}{\Delta m^2(eV^2)}$km

Using the identity:

$$\sum_k |\, U_{\alpha k}\,|^2 |\, U_{\beta k}\,|^2 = \delta_{\alpha\beta} - 2 * Re \sum_{k>j} U^*_{\alpha k} U_{\beta k} U_{\alpha j} U^*_{\beta j} \tag{B.3}$$

Using **Equation(B.3)** in **Equation(B.2)** we get:

$$
\begin{aligned}
P_{\nu_\alpha \to \nu_\beta}(L,E) &= \delta_{\alpha\beta} - 2 * \sum_{k>j} Re[U^*_{\alpha k} U_{\beta k} U_{\alpha j} U^*_{\beta j}] + \\
&\quad 2 * Re\left[\sum_{k>j} U^*_{\alpha k} U_{\beta k} U_{\alpha j} U^*_{\beta j} \left(\cos\left(\frac{\Delta m^2_{kj} L}{2E}\right) - \iota \sin\left(\frac{\Delta m^2_{kj} L}{2E}\right)\right)\right] \\
&= \delta_{\alpha\beta} - 2 * \sum_{k>j} Re[U^*_{\alpha k} U_{\beta k} U_{\alpha j} U^*_{\beta j}] * \left(1 - \cos\left(\frac{\Delta m^2_{kj} L}{2E}\right)\right) + \\
&\quad 2 * \sum_{k>j} Im[U^*_{\alpha k} U_{\beta k} U_{\alpha j} U^*_{\beta j}] * \sin\left(\frac{\Delta m^2_{kj} L}{2E}\right) \\
\textit{So}\ \ P_{\nu_\alpha \to \nu_\beta}(L,E) &= \delta_{\alpha\beta} - 4 * \sum_{k>j} Re[U^*_{\alpha k} U_{\beta k} U_{\alpha j} U^*_{\beta j}] * \sin^2\left(\frac{\Delta m^2_{kj} L}{4E}\right) + \\
&\quad 2 * \sum_{k>j} Im[U^*_{\alpha k} U_{\beta k} U_{\alpha j} U^*_{\beta j}] \left(\sin\left(\frac{\Delta m^2_{kj} L}{2E}\right)\right)
\end{aligned}
\tag{B.4}
$$

When $\alpha = \beta$ its called the **"Survival Probability"** and when $\alpha \neq \beta$ its called the **"Transition Probability"**

Appendix C

General Survival and Transition Probability Expressions

The general probability expression is given by:

$$P_{\alpha\beta} = \delta_{\alpha\beta} - 4 * \sum_{k>j} Re[U^*_{\alpha k} U_{\beta k} U_{\alpha j} U^*_{\beta j}] * \sin^2\left(\frac{\Delta m^2_{kj} L}{4E}\right) + 2 * \sum_{k>j} Im[U^*_{\alpha k} U_{\beta k} U_{\alpha j} U^*_{\beta j}] * \sin\left(\frac{\Delta m^2_{kj} L}{2E}\right) \tag{C.1}$$

C.1 Expression for Survival Probability, $\alpha = \beta$

Consider three neutrino flavors.

$$\begin{aligned} P_{\alpha\alpha} &= 1 - 4 \sum_{k>j} |U_{\alpha k}|^2 |U_{\alpha j}|^2 sin^2\left(\frac{\Delta m^2_{kj} L}{4E}\right) \\ &= 1 - 4\left[|U_{\alpha 2}|^2 |U_{\alpha 1}|^2 sin^2\left(\frac{\Delta m^2_{21} L}{4E}\right) + |U_{\alpha 3}|^2 |U_{\alpha 2}|^2 sin^2\left(\frac{\Delta m^2_{32} L}{4E}\right) + \right. \\ &\quad \left. |U_{\alpha 3}|^2 |U_{\alpha 1}|^2 sin^2\left(\frac{\Delta m^2_{31} L}{4E}\right)\right] \end{aligned} \tag{C.2}$$

But

$$\Delta m^2_{ij} = m^2_i - m^2_j$$

$$\Longrightarrow \Delta m^2_{32} = \Delta m^2_{31} - \Delta m^2_{21}$$

Let

$$\nabla_{ij} = \frac{\Delta m^2_{ij} L}{2E} \Longrightarrow \nabla_{32} = \nabla_{31} - \nabla_{21}$$

Putting these in above expression we get:

$$P_{\alpha\alpha} = 1 - 4\left[|U_{\alpha 2}|^2|U_{\alpha 1}|^2 sin^2\left(\frac{\nabla_{21}}{2}\right) + |U_{\alpha 3}|^2|U_{\alpha 2}|^2 sin^2\left(\frac{\nabla_{31}-\nabla_{21}}{2}\right) + |U_{\alpha 3}|^2|U_{\alpha 1}|^2 sin^2\left(\frac{\nabla_{31}}{2}\right)\right]$$

Use identity of unitary matrix i.e.:

$$|U_{\alpha 1}|^2 + |U_{\alpha 2}|^2 + |U_{\alpha 3}|^2 = 1$$

Using the unitary matrix identity, the probability expression can be written as: expression we get:

$$\begin{aligned}
P_{\alpha\alpha} &= 1 - 4|U_{\alpha 2}|^2(1-|U_{\alpha 2}|^2) sin^2\left(\frac{\nabla_{21}}{2}\right) - 4|U_{\alpha 3}|^2(1-|U_{\alpha 3}|^2) sin^2\left(\frac{\nabla_{31}}{2}\right) + \\
&\quad 4|U_{\alpha 2}|^2|U_{\alpha 3}|^2 sin^2\left(\frac{\nabla_{21}}{2}\right) + 4|U_{\alpha 2}|^2|U_{\alpha 3}|^2 sin^2\left(\frac{\nabla_{31}}{2}\right) - \\
&\quad 4|U_{\alpha 2}|^2|U_{\alpha 3}|^2 sin^2\left(\frac{\nabla_{31}-\nabla_{21}}{2}\right) \\
&= 1 - 4|U_{\alpha 2}|^2(1-|U_{\alpha 2}|^2) sin^2\left(\frac{\nabla_{21}}{2}\right) - 4|U_{\alpha 3}|^2(1-|U_{\alpha 3}|^2) sin^2\left(\frac{\nabla_{31}}{2}\right) + \\
&\quad 4|U_{\alpha 2}|^2|U_{\alpha 3}|^2\left(sin^2\left(\frac{\nabla_{21}}{2}\right) + sin^2\left(\frac{\nabla_{31}}{2}\right) - sin^2\left(\frac{\nabla_{31}-\nabla_{21}}{2}\right)\right) \\
&= 1 - 4|U_{\alpha 2}|^2(1-|U_{\alpha 2}|^2) sin^2\left(\frac{\nabla_{21}}{2}\right) - 4|U_{\alpha 3}|^2(1-|U_{\alpha 3}|^2) sin^2\left(\frac{\nabla_{31}}{2}\right) + \\
&\quad 4|U_{\alpha 2}|^2|U_{\alpha 3}|^2\left[sin^2\left(\frac{\nabla_{21}}{2}\right) + sin^2\left(\frac{\nabla_{31}}{2}\right) - \left(sin\left(\frac{\nabla_{31}}{2}\right) cos\left(\frac{\nabla_{21}}{2}\right) - \right.\right. \\
&\quad \left.\left. cos\left(\frac{\nabla_{31}}{2}\right) sin\left(\frac{\nabla_{21}}{2}\right)\right)^2\right] \\
&= 1 - 4|U_{\alpha 2}|^2(1-|U_{\alpha 2}|^2) sin^2\left(\frac{\nabla_{21}}{2}\right) - 4|U_{\alpha 3}|^2(1-|U_{\alpha 3}|^2) sin^2\left(\frac{\nabla_{31}}{2}\right) + \\
&\quad 4|U_{\alpha 2}|^2|U_{\alpha 3}|^2\left[2sin^2\left(\frac{\nabla_{21}}{2}\right) sin^2\left(\frac{\nabla_{31}}{2}\right) + \frac{1}{2} sin(\nabla_{31}) sin(\nabla_{21})\right]
\end{aligned}$$

Hence

$$\begin{aligned}
P_{\alpha\alpha} &= 1 - 4|U_{\alpha 2}|^2(1-|U_{\alpha 2}|^2) sin^2\left(\tfrac{\nabla_{21}}{2}\right) - 4|U_{\alpha 3}|^2(1-|U_{\alpha 3}|^2) sin^2\left(\tfrac{\nabla_{31}}{2}\right) + \\
&\quad 2|U_{\alpha 2}|^2|U_{\alpha 3}|^2\left[4sin^2\left(\tfrac{\nabla_{21}}{2}\right) sin^2\left(\tfrac{\nabla_{31}}{2}\right) + sin(\nabla_{31}) sin(\nabla_{21})\right] \qquad \text{(C.3)}
\end{aligned}$$

C.2 Expression for Transition Probability, $\alpha \neq \beta$

Consider three neutrino flavors.

$$\begin{aligned} P_{\alpha\beta} &= -4\sum_{k>j} Re[U^*_{\alpha k}U_{\beta k}U_{\alpha j}U^*_{\beta j}]sin^2\left(\frac{\nabla_{kj}}{2}\right) + 2\sum_{k>j} Im[U^*_{\alpha k}U_{\beta k}U_{\alpha j}U^*_{\beta j}]sin(\nabla_{kj}) \\ &= -4Re[U^*_{\alpha 3}U_{\beta 3}U_{\alpha 2}U^*_{\beta 2}]sin^2\left(\frac{\nabla_{32}}{2}\right) - 4Re[U^*_{\alpha 2}U_{\beta 2}U_{\alpha 1}U^*_{\beta 1}]sin^2\left(\frac{\nabla_{21}}{2}\right) \\ &\quad - 4Re[U^*_{\alpha 3}U_{\beta 3}U_{\alpha 1}U^*_{\beta 1}]sin^2\left(\frac{\nabla_{31}}{2}\right) + 2Im[U^*_{\alpha 3}U_{\beta 3}U_{\alpha 2}U^*_{\beta 2}]sin(\nabla_{32}) \\ &\quad + 2Im[U^*_{\alpha 2}U_{\beta 2}U_{\alpha 1}U^*_{\beta 1}]sin(\nabla_{21}) + 2Im[U^*_{\alpha 3}U_{\beta 3}U_{\alpha 1}U^*_{\beta 1}]sin(\nabla_{31}) \end{aligned} \tag{C.4}$$

Use the identity of Unitary matrix:

$$U_{\alpha 1}U^*_{\beta 1} + U_{\alpha 2}U^*_{\beta 2} + U_{\alpha 3}U^*_{\beta 3} = 0$$

We get:

$$\begin{aligned} P_{\alpha\beta} &= 4|U_{\alpha 2}|^2|U_{\beta 2}|^2 sin^2\left(\frac{\nabla_{21}}{2}\right) + 4|U_{\alpha 3}|^2|U_{\beta 3}|^2 sin^2\left(\frac{\nabla_{31}}{2}\right) - 4Re[U^*_{\alpha 3}U_{\beta 3}U_{\alpha 2}U^*_{\beta 2}]sin^2\left(\frac{\nabla_{32}}{2}\right) \\ &\quad + 4Re[U^*_{\alpha 3}U_{\beta 3}U_{\alpha 2}U^*_{\beta 2}]sin^2\left(\frac{\nabla_{31}}{2}\right) + 4Re[U^*_{\alpha 2}U_{\beta 2}U_{\alpha 1}U^*_{\beta 1}]sin^2\left(\frac{\nabla_{21}}{2}\right) + \\ &\quad 2Im[U^*_{\alpha 3}U_{\beta 3}U_{\alpha 2}U^*_{\beta 2}](-sin(\nabla_{31}) + sin(\nabla_{32})) - 2Im[U^*_{\alpha 2}U_{\beta 2}U_{\alpha 3}U^*_{\beta 3}]sin(\nabla_{21}) \end{aligned}$$

Note:

$$|U_{\alpha 2}U^*_{\beta 2} + U_{\alpha 3}U^*_{\beta 3}|^2 = |U_{\alpha 2}|^2|U_{\beta 2}|^2 + |U_{\alpha 3}|^2|U_{\beta 3}|^2 + U_{\alpha 2}U^*_{\beta 2}U^*_{\alpha 3}U_{\beta 3} + U_{\alpha 3}U^*_{\beta 3}U^*_{\alpha 2}U_{\beta 2}$$

But it can also be expanded using the following identity:

$$|z_1 + z_2|^2 = \sum_k |z_k|^2 + 2Re\sum_{k>j} z_k z^*_j$$

$$So, \quad |U_{\alpha 2}U^*_{\beta 2} + U_{\alpha 3}U^*_{\beta 3}|^2 = |U_{\alpha 2}|^2|U_{\beta 2}|^2 + |U_{\alpha 3}|^2|U_{\beta 3}|^2 + 2Re[U^*_{\alpha 2}U_{\beta 2}U_{\alpha 3}U^*_{\beta 3}]$$

Hence

$$2Re[U^*_{\alpha 2}U_{\beta 2}U_{\alpha 3}U^*_{\beta 3}] = U_{\alpha 2}U^*_{\beta 2}U^*_{\alpha 3}U_{\beta 3} + U_{\alpha 3}U^*_{\beta 3}U^*_{\alpha 2}U_{\beta 2}$$

Use this in transition probability formula.

$$
\begin{aligned}
P_{\alpha\beta} = {} & 4|U_{\alpha 2}|^2|U_{\beta 2}|^2 sin^2\left(\frac{\nabla_{21}}{2}\right) + 4|U_{\alpha 3}|^2|U_{\beta 3}|^2 sin^2\left(\frac{\nabla_{31}}{2}\right) \\
& + 4Re[U^*_{\alpha 3}U_{\beta 3}U_{\alpha 2}U^*_{\beta 2}]\left(sin^2\left(\frac{\nabla_{31}}{2}\right) + sin^2\left(\frac{\nabla_{21}}{2}\right) - sin^2\left(\frac{\nabla_{32}}{2}\right)\right) + \\
& - 2Im[U^*_{\alpha 3}U_{\beta 3}U_{\alpha 2}U^*_{\beta 2}](-sin(\nabla_{31}) + sin(\nabla_{21}) - sin(\nabla_{32}))
\end{aligned}
$$

Using $\nabla_{32} = \nabla_{31} - \nabla_{21}$, we can obtain transition probability as:

$$
\begin{aligned}
P_{\alpha\beta} = {} & 4|U_{\alpha 2}|^2|U_{\beta 2}|^2 sin^2\left(\tfrac{\nabla_{21}}{2}\right) + 4|U_{\alpha 3}|^2|U_{\beta 3}|^2 sin^2\left(\tfrac{\nabla_{31}}{2}\right) + \\
& 2Re[U^*_{\alpha 3}U_{\beta 3}U_{\alpha 2}U^*_{\beta 2}]\left(4sin^2\left(\tfrac{\nabla_{21}}{2}\right) sin^2\left(\tfrac{\nabla_{31}}{2}\right) + sin(\nabla_{31})sin(\nabla_{21})\right) \\
& -4J_{(\alpha\beta)}\left(4sin^2(\nabla_{31})sin^2\left(\tfrac{\nabla_{21}}{2}\right) - sin(\nabla_{21})sin\left(\tfrac{\nabla_{31}}{2}\right)\right)
\end{aligned} \tag{C.5}
$$

where $J_{(\alpha\beta)}$ is called the Jarlskog Invariant:

$$
\begin{aligned}
J_{\alpha\beta} & = Im[U^*_{\alpha 1}U_{\beta 1}U_{\alpha 2}U^*_{\beta 2}] = Im[U^*_{\alpha 2}U_{\beta 2}U_{\alpha 3}U^*_{\beta 3}] = Im[U^*_{\alpha 3}U_{\beta 3}U_{\alpha 1}U^*_{\beta 1}] \\
& = -Im[U^*_{\alpha 2}U_{\beta 2}U_{\alpha 1}U^*_{\beta 1}] = -Im[U^*_{\alpha 1}U_{\beta 1}U_{\alpha 3}U^*_{\beta 3}] = -Im[U^*_{\alpha 3}U_{\beta 3}U_{\alpha 2}U^*_{\beta 2}] \\
& = -J_{\beta\alpha}
\end{aligned} \tag{C.6}
$$

Using the standard parametrization i.e. U_{PMNS}, we have:

$$
J_{\mu e} = -J_{e\mu} = J_{e\tau} = J_{\tau\mu} = -J_{\mu\tau} = \hat{J}sin(\delta_{CP})
$$

with

$$
\hat{J} = s_{12}c_{12}s_{13}c^2_{13}s_{23}c_{23}
$$

Appendix D

Few Survival and Transition Probability Expressions

We know that probability expression can also be written as:

$$P_{\alpha\beta} = \sum_j \left| U_{\beta j} U^*_{\alpha j} exp\left[-\iota \frac{m_j^2 L}{2E} \right] \right|^2 \tag{D.1}$$

Use the standard PMNS Parametrization:

$$U_{PMNS} = \begin{pmatrix} c_{12}c_{13} & s_{12}c_{13} & s_{13}e^{-\iota\delta_{CP}} \\ -s_{12}c_{23} - c_{12}s_{13}s_{23}e^{\iota\delta_{CP}} & c_{12}c_{23} - s_{12}s_{13}s_{23}e^{\iota\delta_{CP}} & c_{13}s_{23} \\ s_{12}s_{23} - c_{12}s_{13}c_{23}e^{\iota\delta_{CP}} & -c_{12}s_{23} - s_{12}s_{13}c_{23}e^{\iota\delta_{CP}} & c_{13}c_{23} \end{pmatrix}$$

Also use the following change of variables:

$$\alpha = \frac{\Delta m_{21}^2}{\Delta m_{31}^2} \approx 0.026 \;\; and \;\; \Delta = \frac{\Delta m_{31}^2 L}{4E}$$

D.1 ν_e-ν_e Channel

$$\begin{aligned} P_{ee} &= |c_{12}^2 c_{13}^2 + s_{12}^2 c_{13}^2 e^{-\iota 2\alpha\Delta} + s_{13}^2 e^{-\iota 2\Delta}|^2 \\ &= (c_{12}c_{13})^4 + s_{13}^4 + (s_{12}c_{13})^4 + c_{12}^2 c_{13}^2 s_{12}^2 c_{13}^2 (e^{\iota 2\alpha\Delta} + e^{-\iota 2\alpha\Delta}) + c_{12}^2 c_{13}^2 s_{13}^2 (e^{\iota 2\Delta} + e^{-\iota 2\Delta}) \\ &\quad + s_{12}^2 c_{13}^2 s_{13}^2 (e^{-\iota 2\alpha\Delta} e^{\iota 2\Delta} + e^{\iota 2\alpha\Delta} e^{-\iota 2\Delta}) \\ &= (c_{12}c_{13})^4 + s_{13}^4 + (s_{12}c_{13})^4 + 2c_{12}^2 c_{13}^2 s_{12}^2 c_{13}^2 cos(2\alpha\Delta) + 2c_{12}^2 c_{13}^2 s_{13}^2 cos(2\Delta) \\ &\quad + 2s_{12}^2 c_{13}^2 s_{13}^2 cos(2(\alpha-1)\Delta) \end{aligned}$$

Use the identity:

$$c_{12}^4 + s_{12}^4 = 1 - 2c_{12}^2 s_{12}^2 = 1 - \frac{1}{2} sin^2(2\theta_{12})$$

Hence:

$$\begin{aligned}
P_{ee} &= c_{13}^4 - 2c_{13}^4 s_{12}^2 c_{12}^2 + s_{13}^4 + (s_{12}c_{13})^4 + 2c_{12}^2 c_{13}^2 s_{12}^2 c_{13}^2 cos(2\alpha\Delta) + 2c_{12}^2 c_{13}^2 s_{13}^2 cos(2\Delta) \\
&\quad + 2s_{12}^2 c_{13}^2 s_{13}^2 cos(2(\alpha-1)\Delta) \\
&= c_{13}^4 \left(1 - \frac{1}{2} sin^2(2\theta_{12})\right) + s_{13}^4 + \frac{1}{2} sin^2(2\theta_{12})[c_{12}^2 cos(2\Delta) + (1-c_{12}^2) cos(2(\alpha-1)\Delta)] \\
&\quad + \frac{1}{2} sin^2(2\theta_{12}) c_{13}^4 cos(2\alpha\Delta) \\
&= 1 - \frac{1}{2} sin^2(2\theta_{13}) - \frac{1}{2} c_{13}^4 sin^2(2\theta_{12}) + \frac{1}{2} sin^2(2\theta_{12}) c_{12}^2 [cos(2\Delta) - cos(2(\alpha-1)\Delta)] \\
&\quad + \frac{1}{2} sin^2(2\theta_{13}) cos(2(\alpha-1)\Delta)
\end{aligned}$$

Pairing the second and last term we get:

$$\begin{aligned}
P_{ee} &= 1 - sin^2(2\theta_{13}) sin^2((\alpha-1)\Delta) + \frac{1}{2} sin^2(2\theta_{12}) c_{12}^2 [cos(2\Delta) - cos(2(\alpha-1)\Delta)] \\
&\quad + \frac{1}{2} sin^2(2\theta_{12}) c_{13}^4 cos(2\alpha\Delta) - \frac{1}{2} c_{13}^4 sin^2(2\theta_{12})
\end{aligned}$$

Hence

$$\begin{aligned}
P_{ee} &= 1 - sin^2(2\theta_{13}) sin^2((\alpha-1)\Delta) - c_{13}^4 sin^2(2\theta_{12}) sin^2(\alpha\Delta) \\
&\quad + \tfrac{1}{2} sin^2(2\theta_{12}) c_{12}^2 [cos(2\Delta) - cos(2(\alpha-1)\Delta)]
\end{aligned} \tag{D.2}$$

D.2 ν_e-ν_μ Channel

$$\begin{aligned}
P_{e\mu} &= |c_{12}c_{13}(-s_{12}c_{23} - c_{12}s_{23}s_{13}e^{\iota\delta_{CP}}) + s_{12}c_{13}(c_{12}c_{23} - s_{12}s_{23}s_{13}e^{\iota\delta_{CP}})e^{-\iota 2\alpha\Delta} + \\
&\quad s_{13}s_{23}c_{13}e^{-\iota 2\Delta}|^2 \\
&= |c_{12}c_{13}s_{12}c_{23}(-1+e^{-\iota 2\alpha\Delta}) - s_{23}c_{13}s_{13}e^{\iota\delta}(c_{12}^2 + s_{12}^2 e^{-\iota 2\alpha\Delta} - e^{-\iota 2\Delta})|^2 \\
&= c_{13}^2 (c_{12}s_{12}c_{23}(-1+e^{-\iota 2\alpha\Delta}) - s_{23}s_{13}e^{\iota\delta}(c_{12}^2 + s_{12}^2 e^{-\iota 2\alpha\Delta} - e^{-\iota 2\Delta})) * \\
&\quad (c_{12}s_{12}c_{23}(-1+e^{\iota 2\alpha\Delta}) - s_{23}s_{13}e^{-\iota\delta}(c_{12}^2 + s_{12}^2 e^{\iota 2\alpha\Delta} - e^{\iota 2\Delta})) \\
&= c_{13}^2 \left[c_{12}^2 s_{12}^2 c_{23}^2 (2 - 2\cos(2\alpha\Delta)) + s_{13}^2 s_{23}^2 (\ c_{12}^4 + s_{12}^4 + 1 + c_{12}^2 s_{12}^2 (2\cos(2\alpha\Delta)) - 2c_{12}^2 \cos(2\Delta) \right. \\
&\quad \left. -2s_{12}^2 \cos(2(\alpha-1)\Delta)\ )\right] + e^{-\iota\delta}(c_{12}^2 + s_{12}^2 e^{\iota 2\alpha\Delta} - e^{\iota 2\Delta})(e^{-\iota 2\alpha\Delta} - 1)\ ] \\
&\quad - c_{12}s_{12}c_{23}s_{23}s_{13}c_{13}^2 [\ e^{\iota\delta}(c_{12}^2 + s_{12}^2 e^{-\iota 2\alpha\Delta} - e^{-\iota 2\Delta})(e^{\iota 2\alpha\Delta} - 1)
\end{aligned}$$

Let's denote the cross terms in above equation as "**C.T.**". Solving the above equation then gives:

$$\begin{aligned}
P_{e\mu} &= \textbf{C.T.} + \sin^2(2\theta_{12}c_{23}^2c_{13}^2\sin^2(\alpha\Delta)) + \frac{1}{4}\sin^2(2\theta_{13})s_{23}^2[1 + c_{12}^4 + s_{12}^4 - 2c_{12}^2\cos(2\Delta) - \\
&\quad 2s_{12}^2\cos(2(\alpha-1)\Delta) + 2c_{12}^2s_{12}^2\cos(2\alpha\Delta)] \\
&= \textbf{C.T.} + \sin^2(2\theta_{12}c_{23}^2c_{13}^2\sin^2(\alpha\Delta)) + \frac{1}{4}\sin^2(2\theta_{13})s_{23}^2[2 - 2s_{12}^2c_{12}^2 - 2c_{12}^2\cos(2\Delta) \\
&\quad - 2s_{12}^2\cos(2(\alpha-1)\Delta) + 2c_{12}^2s_{12}^2\cos(2\alpha\Delta)] \\
&= \textbf{C.T.} + \sin^2(2\theta_{12}c_{23}^2c_{13}^2\sin^2(\alpha\Delta)) + \frac{1}{4}\sin^2(2\theta_{13})s_{23}^2[2 - 2\sin^2(2\theta_{12})\sin^2(\alpha\Delta) - 2c_{12}^2\cos(2\Delta) \\
&\quad - 2s_{12}^2\cos(2(\alpha-1)\Delta)]
\end{aligned} \tag{D.3}$$

Solving for cross terms **C.T.** now:

$$\begin{aligned}
\textbf{C.T.} &= -c_{12}s_{12}c_{23}s_{13}c_{13}^2[e^{\iota\delta}(c_{12}^2 + s_{12}^2e^{-\iota 2\alpha\Delta} - e^{-\iota 2\Delta})(e^{\iota 2\alpha\Delta} - 1) + \\
&\quad e^{-\iota\delta}(c_{12}^2 + s_{12}^2e^{\iota 2\alpha\Delta} - e^{\iota 2\Delta})(e^{-\iota 2\alpha\Delta} - 1)] \\
&= -\frac{1}{8}c_{13}sin(2\theta_{12})sin(2\theta_{23})sin(2\theta_{13})[\, e^{\iota\delta}(e^{-\iota 2\Delta} - e^{\iota 2(\alpha-1)\Delta}) + e^{\iota\delta}c_{12}^2(e^{\iota 2\alpha\Delta} - 1) + \\
&\quad e^{\iota\delta}s_{12}^2(-e^{-\iota 2\alpha\Delta} + 1) + e^{-\iota\delta}(e^{\iota 2\Delta} - e^{-\iota 2(\alpha-1)\Delta}) + e^{-\iota\delta}c_{12}^2(e^{-\iota 2\alpha\Delta} - 2) + \\
&\quad e^{-\iota\delta}s_{12}^2(-e^{\iota 2\alpha\Delta} + 1)\,] \\
&= -\frac{1}{8}c_{13}sin(2\theta_{12})sin(2\theta_{23})sin(2\theta_{13})[\, 2(cos(2\Delta - \delta) - cos(2(\alpha-1)\Delta + \delta)) + \\
&\quad 2c_{12}^2(cos(2\alpha\Delta + \delta) - cos(\delta)) + 2s_{12}^2(cos(2\alpha\Delta - \delta) + cos(\delta))\,] \\
&= -\frac{1}{8}c_{13}sin(2\theta_{12})sin(2\theta_{23})sin(2\theta_{13})[\, 4sin(\alpha\Delta)sin((\alpha-2)\Delta + \delta) - 2cos(\delta)(c_{12}^2 - s_{12}^2) \\
&\quad + 2(1 - s_{12}^2)cos(2\alpha\Delta + \delta) - 2s_{12}^2cos(2\alpha\Delta - \delta)\,] \\
&= -\frac{1}{8}c_{13}sin(2\theta_{12})sin(2\theta_{23})sin(2\theta_{13})[\, 4sin(\alpha\Delta)sin((\alpha-2)\Delta + \delta) - 2cos(\delta)(c_{12}^2 - s_{12}^2) \\
&\quad + 2cos(2\alpha\Delta + \delta) - 2s_{12}^2(cos(2\alpha\Delta - \delta) + cos(2\alpha\Delta + \delta))\,] \\
&= -\frac{1}{8}c_{13}sin(2\theta_{12})sin(2\theta_{23})sin(2\theta_{13})[\, 4sin(\alpha\Delta)sin((\alpha-2)\Delta + \delta) - 2cos(\delta)(c_{12}^2 - s_{12}^2) \\
&\quad - 4s_{12}^2cos(2\alpha\Delta)cos(\delta) + 2cos(2\alpha\Delta)cos(\delta) - 2sin(2\alpha\Delta)sin(\delta)\,] \\
&= -\frac{1}{8}c_{13}sin(2\theta_{12})sin(2\theta_{23})sin(2\theta_{13})[\, 4sin(\alpha\Delta)sin((\alpha-2)\Delta + \delta) - 2cos(\delta)(c_{12}^2 - s_{12}^2) \\
&\quad + 2cos(2\alpha\Delta)cos(\delta)cos(2\theta_{12}) - 2sin(2\alpha\Delta)sin(\delta)\,] \\
&= -\frac{1}{2}c_{13}sin(2\theta_{12})sin(2\theta_{23})sin(2\theta_{13})sin(\alpha\Delta)[\, sin((\alpha-2)\Delta + \delta) - sin(\delta)cos(\alpha\Delta) \\
&\quad - cos(2\theta_{12})cos(\delta)sin(\alpha\Delta)\,]
\end{aligned} \tag{D.4}$$

Putting term obtained in **Equation (D.4)** into in **Equation (D.3)**, we get transition probability as:

$$\begin{aligned} P_{e\mu} &= sin^2(2\theta_{12})c_{23}^2c_{13}^2sin^2(\alpha\Delta) + \tfrac{1}{4}sin^2(2\theta_{13})s_{23}^2\big[2 - sin^2(2\theta_{12})sin^2(\alpha\Delta) - 2c_{12}^2cos(2\Delta) \\ &\quad -2s_{12}^2(cos(2\Delta) - cos(2(\alpha-1)\Delta))\big] - \tfrac{1}{2}c_{13}sin(2\theta_{12})sin(2\theta_{13})sin(2\theta_{23})sin(\alpha\Delta) \\ &\quad \big[sin((\alpha-2)\Delta+\delta) - sin(\delta)cos(\alpha\Delta) - cos(2\theta_{12})cos(\delta)sin(\alpha\Delta)\big] \end{aligned} \tag{D.5}$$

Appendix E

Matter Modified Neutrino Oscillation

E.1 Two Flavor Case

$$UHU^{\dagger} = \frac{1}{4E}\begin{bmatrix} \cos\theta & \sin\theta \\ -\sin\theta & \cos\theta \end{bmatrix}\begin{bmatrix} -\Delta & 0 \\ 0 & \Delta \end{bmatrix}\begin{bmatrix} \cos\theta & -\sin\theta \\ \sin\theta & \cos\theta \end{bmatrix} \tag{E.1}$$

$$= \frac{1}{4E}\begin{bmatrix} -\Delta\cos 2\theta & \Delta\sin 2\theta \\ \Delta\sin 2\theta & \Delta\cos 2\theta \end{bmatrix} \tag{E.2}$$

$$H^m = U_m^{\dagger}[UHU^{\dagger} + V]U_m \tag{E.3}$$

$$= U_m^{\dagger}\left(\frac{1}{4E}\begin{bmatrix} -\Delta\cos 2\theta & \Delta\sin 2\theta \\ \Delta\sin 2\theta & \Delta\cos 2\theta \end{bmatrix} + \begin{bmatrix} V_{NC}+V_{CC} & 0 \\ 0 & V_{NC} \end{bmatrix}\right)U_m \tag{E.4}$$

$$= U_m^{\dagger}\left(\frac{1}{4E}\begin{bmatrix} -\Delta\cos 2\theta & \Delta\sin 2\theta \\ \Delta\sin 2\theta & \Delta\cos 2\theta \end{bmatrix} + \left(V_{NC}+\frac{V_{CC}}{2}\right)\mathbb{1} + \begin{bmatrix} \frac{V_{CC}}{2} & 0 \\ 0 & -\frac{V_{CC}}{2} \end{bmatrix}\right)U_m \tag{E.5}$$

Again we can ignore the terms proportional to identity $\mathbb{1}$. Hence we get:

$$H^m = U_m^{\dagger}\left(\frac{1}{4E}\begin{bmatrix} -\Delta\cos 2\theta + A & \Delta\sin 2\theta \\ \Delta\sin 2\theta & \Delta\cos 2\theta - A \end{bmatrix}\right)U_m \tag{E.6}$$

where $A = 2EV_{CC}$. On substituting U_m in equation E.6, we get:

$$H^m = \frac{1}{4E}\begin{bmatrix} \cos\theta_m & -\sin\theta_m \\ \sin\theta_m & \cos\theta_m \end{bmatrix}\begin{bmatrix} -\Delta\cos 2\theta + A & \Delta\sin 2\theta \\ \Delta\sin 2\theta & \Delta\cos 2\theta - A \end{bmatrix}\begin{bmatrix} \cos\theta_m & \sin\theta_m \\ -\sin\theta_m & \cos\theta_m \end{bmatrix} \tag{E.7}$$

On carrying out the multiplication in equation E.7, the diagonal elements of matrix H^m are found out to be:

$$(H^m)_{1,1} = -(H^m)_{2,2} = \frac{1}{4E}[(A - \Delta\cos 2\theta)\cos 2\theta_m - (\Delta\sin 2\theta)\sin 2\theta_m] \tag{E.8}$$

and the off-diagonal elements are:

$$(H^m)_{1,2} = (H^m)_{2,1} = \frac{1}{4E}[(\Delta \sin 2\theta)\cos 2\theta_m + (A - \Delta\cos 2\theta)\sin 2\theta_m] \tag{E.9}$$

E.2 Three Flavor Case

The hamiltonian in flavor eigenbasis will be:

$$H^{flav} = UHU^\dagger \tag{E.10}$$

$$= \frac{1}{2E} U \begin{bmatrix} m_1^2 & 0 & 0 \\ 0 & m_2^2 & 0 \\ 0 & 0 & m_3^2 \end{bmatrix} U^\dagger \tag{E.11}$$

$$= \frac{1}{2E} U \begin{bmatrix} 0 & 0 & 0 \\ 0 & \Delta_{21} & 0 \\ 0 & 0 & \Delta_{31} \end{bmatrix} U^\dagger \qquad = \frac{1}{2E}(UM^2U^\dagger) \tag{E.12}$$

The time-evolution in flavor eigenbasis, with matter potential added, will be given by:

$$\iota \frac{\partial}{\partial t} |\nu\rangle_{flav} = \widetilde{H} |\nu\rangle_{flav} \tag{E.13}$$

where $\widetilde{H}$ is the matter-modified hamiltonian.

$$\widetilde{H} = H^{flav} + V \tag{E.14}$$

$$= \frac{1}{2E}(UM^2U^\dagger + A) \tag{E.15}$$

Here,

$$A = \begin{bmatrix} A & 0 & 0 \\ 0 & 0 & 0 \\ 0 & 0 & 0 \end{bmatrix} \tag{E.16}$$

Hence, equation E.13 becomes,

$$\iota \frac{\partial}{\partial t} |\nu\rangle_{flav} = \frac{1}{2E}(UM^2U^\dagger + A) |\nu\rangle_{flav} \tag{E.17}$$

It can be checked that

$$U_{13}(\theta_{13}, \delta) = U_\delta U_{13}(\theta_{13}) U_\delta^\dagger \tag{E.18}$$

where

$$U_\delta = \begin{bmatrix} 1 & 0 & 0 \\ 0 & 1 & 0 \\ 0 & 0 & e^{\iota\delta} \end{bmatrix} \tag{E.19}$$

Thus, the PMNS matrix U can be written as,

$$U = U_{23}(\theta_{23})U_\delta U_{13}(\theta_{13})U_\delta^\dagger U_{12}(\theta_{12}) \tag{E.20}$$

Using the fact the elements of the (2,3) sub-matrix A are all zeros, one can write A as,

$$A = U_{23}(\theta_{23})U_\delta A U_\delta^\dagger U_{23}(\theta_{23}) \tag{E.21}$$

Expressing U and A as given in equations E.20 and E.20, equation E.17 can be written as:

$$\iota\frac{\partial}{\partial t}|\nu\rangle_{flav} = \frac{1}{2E}\left[U_A(U_B M^2 U_B^\dagger + A)U_A^\dagger\right]|\nu\rangle_{flav} \tag{E.22}$$

where

$$U_A = U_{23}(\theta_{23})U_\delta; U_B = U_{13}(\theta_{13})U_\delta^\dagger U_{12}(\theta_{12}) \tag{E.23}$$

Therefore,

$$\iota\frac{\partial}{\partial t}U_A^\dagger|\nu\rangle_{flav} = \frac{1}{2E}(U_B M^2 U_B^\dagger + A)U_A^\dagger|\nu\rangle_{flav} \tag{E.24}$$

$$\Rightarrow \iota\frac{\partial}{\partial t}\widetilde{|\nu\rangle}_{flav} = \frac{1}{2E}(U_B M^2 U_B^\dagger + A)\widetilde{|\nu\rangle}_{flav} \tag{E.25}$$

$$\Rightarrow \iota\frac{\partial}{\partial t}\widetilde{|\nu\rangle}_{flav} = \frac{1}{2E}(M^2_{matt})\widetilde{|\nu\rangle}_{flav}; \tag{E.26}$$

where

$$\widetilde{|\nu\rangle}_{flav} = U_A^\dagger|\nu\rangle_{flav} \tag{E.27}$$

$$M^2_{matt} = U_B M^2 U_B^\dagger + A \tag{E.28}$$

$$= U_B \begin{bmatrix} 0 & 0 & 0 \\ 0 & \Delta_{21} & 0 \\ 0 & 0 & \Delta_{31} \end{bmatrix} U_B^\dagger + \begin{bmatrix} A & 0 & 0 \\ 0 & 0 & 0 \\ 0 & 0 & 0 \end{bmatrix} \tag{E.29}$$

We know that $\Delta_{31} \approx O(10^{-3}eV^2)$ and $\Delta_{21} \approx O(10^{-5}eV^2)$. Therefore, Δ_{21}-dependent part can be considered as a perturbation and can be ignored for **OMSD approximation**.

E.2.1 OMSD approximation

$$M^2_{matt} = \underbrace{U_B \begin{bmatrix} 0 & 0 & 0 \\ 0 & 0 & 0 \\ 0 & 0 & \Delta_{31} \end{bmatrix} U_B^\dagger + \begin{bmatrix} A & 0 & 0 \\ 0 & 0 & 0 \\ 0 & 0 & 0 \end{bmatrix}}_{M_0} + \underbrace{U_B \begin{bmatrix} 0 & 0 & 0 \\ 0 & \Delta_{21} & 0 \\ 0 & 0 & 0 \end{bmatrix} U_B^\dagger}_{M_1} \tag{E.30}$$

Here M_0 is the dominant term and M_1 represents the perturbation in M^2_{matt}.

It can be checked that $U_\delta^\dagger$ commutes with$U_{12}(\theta_{12})$ and hence U_B can be written as $U_{13}(\theta_{13})U_{12}(\theta_{12})U_\delta^\dagger$. Hence calculating M_0 we get

$$M_0 = \begin{bmatrix} A + \Delta_{31} sin^2\theta_{13} & 0 & \Delta_{31} sin\theta_{13} cos\theta_{13} \\ 0 & 0 & 0 \\ \Delta_{31} sin\theta_{13} cos\theta_{13} & 0 & \Delta_{31} cos^2\theta_{13} \end{bmatrix} \tag{E.31}$$

Because of the symmetric nature of M_0, it can be made diagonal in a fixed basis. Let that basis be $|\nu\rangle^m$. Also let the matter-modified flavor eigen-basis ($\widetilde{|\nu\rangle}_{flav}$) be connected to $|\nu\rangle^m$ by the unitary matrix U_B^m. Hence

$$\widetilde{|\nu\rangle}_{flav} = U_B^m |\nu\rangle^m \tag{E.32}$$

$$\Rightarrow |\nu\rangle_{flav} = U_A U_B^m |\nu\rangle^m \tag{E.33}$$

From equation E.26 we get:

$$\iota \frac{\partial}{\partial t} \widetilde{|\nu\rangle}_{flav} = \frac{1}{2E}(M_0 + M_1)\widetilde{|\nu\rangle}_{flav} \tag{E.34}$$

$$\Rightarrow \iota \frac{\partial}{\partial t} U_B^m |\nu\rangle^m = \frac{1}{2E}(M_0 + M_1) U_B^m |\nu\rangle^m \tag{E.35}$$

$$\Rightarrow \iota \frac{\partial}{\partial t} |\nu\rangle^m = \frac{1}{2E} U_B^{m\dagger}(M_0 + M_1) U_B^m |\nu\rangle^m \tag{E.36}$$

Ignoring the non-diagonal perturbing term $U_B^{m\dagger}(M_1)U_B^m$, we are only left with the dominant diagonal term $U_B^{m\dagger}(M_0)U_B^m$. Take U_B^m as $U_{13}(\theta_{13}^m)$, we have

$$U_B^{m\dagger}(M_0)U_B^m = \begin{bmatrix} \lambda_1 & 0 & 0 \\ 0 & \lambda_2 & 0 \\ 0 & 0 & \lambda_3 \end{bmatrix} \tag{E.37}$$

$$= \begin{bmatrix} \frac{1}{2}(\Delta_{31} + A - \Delta_{31}^m) & 0 & 0 \\ 0 & 0 & 0 \\ 0 & 0 & \frac{1}{2}(\Delta_{31} + A + \Delta_{31}^m) \end{bmatrix} \tag{E.38}$$

where

$$\Delta_{31}^{m} = \sqrt{(\Delta_{31} cos2\theta_{13} - A)^2 + (\Delta_{31} sin2\theta_{13})^2} = \lambda_3 - \lambda_1 \tag{E.39}$$

We can also define

$$\Delta_{21}^{m} = \lambda_2 - \lambda_1 = \frac{1}{2}(\Delta_{31}^{m} - \Delta_{31} - A) \tag{E.40}$$

and

$$\Delta_{23}^{m} = \lambda_2 - \lambda_3 = \frac{1}{2}(-\Delta_{31}^{m} - \Delta_{31} - A) \tag{E.41}$$

Equating the off-diagonal term to zero gives

$$\theta_{13}^{m} = \frac{1}{2} tan^{-1}\left(\frac{\Delta_{31} sin2\theta_{13}}{\Delta_{31} cos2\theta_{13} - A}\right) \tag{E.42}$$

Hence, the matter modified PMNS matrix is given by

$$U^{OMSD} = U_A U_B^{m} \tag{E.43}$$

$$= \begin{bmatrix} U_{e1}^{m} & U_{e2}^{m} & U_{e3}^{m} \\ U_{\mu 1}^{m} & U_{\mu 2}^{m} & U_{\mu 3}^{m} \\ U_{\tau 1}^{m} & U_{\tau 2}^{m} & U_{\tau 3}^{m} \end{bmatrix}^{OMSD} \tag{E.44}$$

$$= U_{23}(\theta_{23}) U_{\delta} U_{13}(\theta_{13}^{m}) \tag{E.45}$$

$$= \begin{bmatrix} 1 & 0 & 0 \\ 0 & c_{23} & s_{23} \\ 0 & -s_{23} & c_{23} \end{bmatrix} \begin{bmatrix} 1 & 0 & 0 \\ 0 & 1 & 0 \\ 0 & 0 & e_{\iota\delta} \end{bmatrix} \begin{bmatrix} c_{13}^{m} & 0 & s_{13}^{m} \\ 0 & 1 & 0 \\ -s_{13} & 0 & c_{13}^{m} \end{bmatrix} \tag{E.46}$$

$$= \begin{bmatrix} c_{13}^{m} & 0 & s_{13}^{m} \\ -s_{23} s_{13}^{m} e^{\iota\delta} & c_{23} & s_{23} c_{13}^{m} e^{\iota\delta} \\ -c_{23} s_{13}^{m} e^{\iota\delta} & -s_{23} & c_{23} c_{13}^{m} e^{\iota\delta} \end{bmatrix} \tag{E.47}$$

Using mass eigenvalues from equation E.38 and elements of PMNS matrix from equation E.47, the probability expressions can be given as (in natural units):

$$P_{ee} = 1 - \sin^2 2\theta_{13}^{m} \sin^2\left[\frac{1.27(\Delta_{31}^{m})L}{E}\right] \tag{E.48}$$

$$\begin{aligned} P_{\mu\mu} = 1 &- \cos^2 2\theta_{13}^{m} sin^2 2\theta_{23} \sin^2\left[\frac{1.27(\Delta_{31} + A + \Delta_{31}^{m})L}{2E}\right] \\ &- \sin^2 2\theta_{13}^{m} sin^2 2\theta_{23} \sin^2\left[\frac{1.27(\Delta_{31} + A - \Delta_{31}^{m})L}{2E}\right] \\ &- \sin^4 \theta_{23} \sin^2 2\theta_{13} \sin^2\left[\frac{1.27\Delta_{31}^{m} L}{E}\right] \end{aligned} \tag{E.49}$$

$$P_{\mu e} = \sin^2\theta_{13}\sin^2\theta_{23}\sin^2\left[\frac{1.27\Delta^m_{31}L}{E}\right] \quad \textit{and so on...} \tag{E.50}$$

E.2.2 Without OMSD approximation

In the OMSD approximation, the δ_{CP}-dependence is lost from the probability expressions.Hence, to obtain δ_{CP} information we have to obtain expression without OMSD approximation. Moreover, for certain values of L and E, the phase in the leading term can diminish the leading term to the extent at which α cannot be ignored. Hence we need to include Δ_{21} in the calculations.

The Δ_{21}-perturbation in the hamiltonian in equation E.30 is

$$U_B^{m\dagger}M_1U_B^m = \begin{bmatrix} \Delta_{21}sin^2\theta_{12}cos^2\theta & \Delta_{21}sin\theta_{12}cos\theta_{12}cos\theta & -\Delta_{21}sin^2\theta_{12}cos\theta sin\theta \\ \Delta_{21}sin\theta_{12}cos\theta_{12}cos\theta & \Delta_{21}cos^2\theta_{12} & -\Delta_{21}sin\theta_{12}cos\theta_{12}sin\theta \\ \Delta_{21}sin^2\theta_{12}cos\theta sin\theta & \Delta_{21}sin\theta_{12}cos\theta_{12}sin\theta & \Delta_{21}sin^2\theta_{12}sin^2\theta \end{bmatrix} \tag{E.51}$$

To first order in Δ_{21}, the matter-modified squared-mass eigenvalues are

$$\Lambda_1 = \frac{1}{2}(\Delta_{31} + A - \Delta^m_{31}) + \Delta_{21}sin^2\theta_{12}cos^2\theta \tag{E.52}$$

$$\Lambda_2 = \Delta_{21}cos^2\theta_{12} \tag{E.53}$$

$$\Lambda_3 = \frac{1}{2}(\Delta_{31} + A + \Delta^m_{31}) + \Delta_{21}sin^2\theta_{12}sin^2\theta \tag{E.54}$$

and the eigenvectors of M_0 are

$$|\nu^m_1\rangle = \begin{bmatrix} cos\theta^m_{13} \\ 0 \\ -sin\theta^m_{13} \end{bmatrix} \textit{ corresponding to } \lambda_1 \tag{E.55}$$

$$|\nu^m_1\rangle = \begin{bmatrix} 0 \\ 1 \\ 0 \end{bmatrix} \textit{ corresponding to } \lambda_2 \tag{E.56}$$

$$|\nu^m_1\rangle = \begin{bmatrix} sin\theta^m_{13} \\ 0 \\ cos\theta^m_{13} \end{bmatrix} \textit{ corresponding to } \lambda_3 \tag{E.57}$$

To obtain the matter-modified PMNS matrix without OMSD approximation, we need to know what is U_B^m to first order in Δ_{21}. It is the eigenvectors of M_0 with order-Δ_{21} correction, expressed as columns of U_B^m.

Using first-order perturbation theory, calculating corrections in $|\nu\rangle^m$:

$$
\begin{aligned}
&\textit{Correction in } |\nu_1^m\rangle : \\
&= \frac{\nu_2^m|M_1|\nu_1^m}{\lambda_1-\lambda_2}|\nu_2^m\rangle + \frac{\nu_3^m|M_1|\nu_1^m}{\lambda_1-\lambda_3}|\nu_3^m\rangle \\
&= \begin{bmatrix}0 & 1 & 0\end{bmatrix} M_1 \begin{bmatrix} cos\theta_{13}^m \\ 0 \\ -sin\theta_{13}^m \end{bmatrix} \frac{|\nu_2^m\rangle}{-\Delta_{21}^m} + \begin{bmatrix} sin\theta_{13}^m & 0 & cos\theta_{13}^m \end{bmatrix} M_1 \begin{bmatrix} cos\theta_{13}^m \\ 0 \\ -sin\theta_{13}^m \end{bmatrix} \frac{|\nu_3^m\rangle}{-\Delta_{31}^m} \\
&= (\frac{-\Delta_{21}}{2\Delta_{21}^m} sin2\theta_{12} cos\widetilde{\theta}) \begin{bmatrix} 0 \\ 1 \\ 0 \end{bmatrix} + (\frac{\Delta_{21}}{2\Delta_{31}^m} sin^2\theta_{12} sin2\widetilde{\theta}) \begin{bmatrix} sin\theta_{13}^m \\ 0 \\ cos\theta_{13}^m \end{bmatrix} \\
&\Rightarrow |\nu_1^m\rangle^{O(\Delta_{21})} = \begin{bmatrix} cos\theta_{13}^m + \frac{\Delta_{21}}{2\Delta_{31}^m} sin^2\theta_{12} sin2\widetilde{\theta} sin\theta_{13}^m \\ \frac{-\Delta_{21}}{2\Delta_{31}^m} sin2\theta_{12} cos\widetilde{\theta} \\ -sin\theta_{13}^m + \frac{\Delta_{21}}{2\Delta_{31}^m} sin^2\theta_{12} sin2\widetilde{\theta} cos\theta_{13}^m \end{bmatrix}
\end{aligned} \tag{E.58}
$$

Here $\widetilde{\theta} = \theta_{13} - 2\theta_{13}^m$.

Similarly Correction in $|\nu_2^m\rangle$:

$$
\Rightarrow |\nu_2^m\rangle^{O(\Delta_{21})} = \begin{bmatrix} \frac{\Delta_{21}}{2\Delta_{21}^m} sin2\theta_{12} cos\widetilde{\theta} cos\theta_{13}^m + \frac{\Delta_{21}}{2\Delta_{32}^m} sin2\theta_{12} sin\widetilde{\theta} sin\theta_{13}^m \\ 1 \\ \frac{-\Delta_{21}}{2\Delta_{21}^m} sin2\theta_{12} cos\widetilde{\theta} sin\theta_{13}^m + \frac{\Delta_{21}}{2\Delta_{32}^m} sin2\theta_{12} sin\widetilde{\theta} cos\theta_{13}^m \end{bmatrix} \tag{E.59}
$$

Similarly Correction in $|\nu_3^m\rangle$:

$$
\Rightarrow |\nu_3^m\rangle^{O(\Delta_{21})} = \begin{bmatrix} sin\theta_{13}^m - \frac{\Delta_{21}}{2\Delta_{31}^m} sin^2\theta_{12} sin2\widetilde{\theta} cos\theta_{13}^m \\ \frac{-\Delta_{21}}{2\Delta_{32}^m} sin2\theta_{12} sin\widetilde{\theta} \\ cos\theta_{13}^m + \frac{\Delta_{21}}{2\Delta_{31}^m} sin^2\theta_{12} sin2\widetilde{\theta} sin\theta_{13}^m \end{bmatrix} \tag{E.60}
$$

Hence matrix U_B^m is:

$$
U_B^m = \begin{bmatrix} |\nu_1^m\rangle^{O(\Delta_{21})} & |\nu_2^m\rangle^{O(\Delta_{21})} & |\nu_3^m\rangle^{O(\Delta_{21})} \end{bmatrix} \tag{E.61}
$$

And,

$$U^m = \begin{bmatrix} U^m_{e1} & U^m_{e2} & U^m_{e3} \\ U^m_{\mu 1} & U^m_{\mu 2} & U^m_{\mu 3} \\ U^m_{\tau 1} & U^m_{\tau 2} & U^m_{\tau 3} \end{bmatrix} = U_A U^m_B = U_{23}(\theta_{23}) U_\delta U^m_B \tag{E.62}$$

Hence the elements of matter-modified PMNS matrix up to first orer in Δ_{21} are:

- $U^m_{e1} = cos\theta^m_{13} + ysin^2\theta_{12} sin2\widetilde{\theta} sin\theta^m_{13}$
- $U^m_{e2} = xsin2\theta_{12} cos\widetilde{\theta} sin\theta^m_{13} + zsin2\theta_{12} sin\widetilde{\theta} cos\theta^m_{13}$
- $U^m_{e3} = sin\theta^m_{13} - ysin^2\theta_{12} sin2\widetilde{\theta} cos\theta^m_{13}$
- $U^m_{\mu 1} = -sin\theta^m_{13} sin\theta_{23} e^{\iota\delta} - xsin2\theta_{12} cos\widetilde{\theta} cos\theta_{23} + ysin^2\theta_{12} sin2\widetilde{\theta} cos\theta^m_{13} sin\theta_{23} e^{\iota\delta}$
- $U^m_{\mu 2} = cos\theta_{23} - xsin2\theta_{12} cos\widetilde{\theta} sin\theta^m_{13} sin\theta_{23} e^{\iota\delta} + zsin2\theta_{12} sin\widetilde{\theta} cos\theta^m_{13} sin\theta_{23} e^{\iota\delta}$
- $U^m_{\mu 3} = cos\theta^m_{13} sin\theta_{23} e^{\iota\delta} - zsin2\theta_{12} sin\widetilde{\theta} cos\theta_{23} + ysin^2\theta_{12} sin2\widetilde{\theta} sin\theta^m_{13} sin\theta_{23} e^{\iota\delta}$
- $U^m_{\tau 1} = -sin\theta^m_{13} cos\theta_{23} e^{\iota\delta} + xsin2\theta_{12} cos\widetilde{\theta} sin\theta_{23} + ysin^2\theta_{12} sin2\widetilde{\theta} cos\theta^m_{13} cos\theta_{23} e^{\iota\delta}$
- $U^m_{\tau 2} = -sin\theta_{23} - xsin2\theta_{12} cos\widetilde{\theta} sin\theta^m_{13} cos\theta_{23} e^{\iota\delta} + zsin2\theta_{12} sin\widetilde{\theta} cos\theta^m_{13} cos\theta_{23} e^{\iota\delta}$
- $U^m_{\tau 3} = cos\theta^m_{13} cos\theta_{23} e^{\iota\delta} + zsin2\theta_{12} sin\widetilde{\theta} sin\theta_{23} + ysin^2\theta_{12} sin2\widetilde{\theta} sin\theta^m_{13} cos\theta_{23} e^{\iota\delta}$

In all the above expressions we have:

- $x = \frac{\Delta_{21}}{2\Delta^m_{21}}$
- $y = \frac{\Delta_{21}}{2\Delta^m_{31}}$ and
- $z = \frac{\Delta_{21}}{2\Delta^m_{23}}$

To obtain any probability expression for matter-modified case we now just need to use the formulas derived in **Appendix B** and **Appendix C**, with the vacuum parameters replaced by matter-modified parameters.

Bibliography

[A+94] J. N. Abdurashitov et al., *Results from SAGE*, Phys. Lett. **B328** (1994), 234–248.

[A+04] I. Ambats et al., *Nova proposal to build a 30-kiloton off-axis detector to study neutrino oscillations in the fermilab numi beamline*.

[A+05] E. Aliu et al., *Evidence for muon neutrino oscillation in an accelerator-based experiment*, Phys. Rev. Lett. **94** (2005), 081802.

[A+11] K. Abe et al., *The T2K Experiment*, Nucl. Instrum. Meth. **A659** (2011), 106–135.

[A+16] L. Aliaga et al., *Neutrino Flux Predictions for the NuMI Beam*, Phys. Rev. **D94** (2016), no. 9, 092005, [Addendum: Phys. Rev.D95,no.3,039903(2017)].

[ACR07] Sanjib Kumar Agarwalla, Sandhya Choubey, and Amitava Raychaudhuri, *Neutrino mass hierarchy and theta(13) with a magic baseline beta-beam experiment*, Nucl. Phys. **B771** (2007), 1–27.

[AJL+04] Evgeny K. Akhmedov, Robert Johansson, Manfred Lindner, Tommy Ohlsson, and Thomas Schwetz, *Series expansions for three flavor neutrino oscillation probabilities in matter*, JHEP **04** (2004), 078.

[ARS05] Sanjib Kumar Agarwalla, Amitava Raychaudhuri, and Abhijit Samanta, *Exploration prospects of a long baseline beta beam neutrino experiment with an iron calorimeter detector*, Phys. Lett. **B629** (2005), 33–40.

[B+06] G. Belli et al., *RPC: From high energy physics to positron emission tomography*, J. Phys. Conf. Ser. **41** (2006), 555–560.

[B+14] M. Bogomilov et al., *Neutrino Factory*, Phys. Rev. ST Accel. Beams **17** (2014), no. 12, 121002.

[Bah99] John N. Bahcall, *Standard solar models*, Nucl. Phys. Proc. Suppl. **77** (1999), 64–72, [,64(1998)].

[BBP98] John N. Bahcall, Sarbani Basu, and M. H. Pinsonneault, *How uncertain are solar neutrino predictions?*, Phys. Lett. **B433** (1998), 1–8.

[Bel04] Alain Bellerive, *Review of solar neutrino experiments*, Int. J. Mod. Phys. **A19** (2004), 1167–1179.

[BLM04] Jacques Bouchez, Mats Lindroos, and Mauro Mezzetto, *Beta beams: Present design and expected performances*, AIP Conf. Proc. **721** (2004), no. 1, 37–47.

[Caz04] Antoine Cazes, *Etude du faisceau CNGS et identification des muons dans l'expérience OPERA. Optimisation de la ligne de faisceau du projet SPL-Fréjus*, Theses, Université Pierre et Marie Curie - Paris VI, December 2004.

[CC06] Jean Eric Campagne and Antoine Cazes, *The theta(13) and delta(cp) sensitivities of the spl-frejus project revisited*, Eur. Phys. J. **C45** (2006), 643–657.

[CLP13] Pilar Coloma, Tracey Li, and Silvia Pascoli, *Long Baseline Super-Beam Experiments in Europe within LAGUNA*, J. Phys. Conf. Ser. **408** (2013), 012036.

[CMMS06] J. E. Campagne, M. Maltoni, M. Mezzetto, and T. Schwetz, *Physics potential of the cern-memphys neutrino oscillation project*.

[Cri11] Michel Cribier, *Reactor monitoring with neutrinos*, Nucl. Phys. Proc. Suppl. **221** (2011), 57–61.

[D$^+$18] Andrea Dell'Acqua et al., *Future Opportunities in Accelerator-based Neutrino Physics*, European Neutrino "Town" meeting and ESPP 2019 discussion Geneva, Switzerland, October 22-24, 2018, 2018.

[DA81] A. M. Dziewonski and D. L. Anderson, *Preliminary reference earth model*, Phys. Earth Planet. Interiors **25** (1981), 297–356.

[Dav94] R. Davis, *A review of the Homestake solar neutrino experiment*, Prog. Part. Nucl. Phys. **32** (1994), 13–32.

[DGG+62] G. Danby, J. M. Gaillard, Konstantin A. Goulianos, L. M. Lederman, Nari B. Mistry, M. Schwartz, and J. Steinberger, *Observation of High-Energy Neutrino Reactions and the Existence of Two Kinds of Neutrinos*, Phys. Rev. Lett. **9** (1962), 36–44.

[DHH68] Raymond Davis, Jr., Don S. Harmer, and Kenneth C. Hoffman, *Search for neutrinos from the sun*, Phys. Rev. Lett. **20** (1968), 1205–1209.

[DPRS19] Andrea Donini, Sergio Palomares-Ruiz, and Jordi Salvado, *Neutrino tomography of Earth*, Nature Phys. **15** (2019), no. 1, 37–40.

[DV99] Shashikant R. Dugad and Francesco Vissani, *Proposal to look for an up / down asymmetry in atmospheric neutrinos beyond multi-GeV region with existing experimental data*, Phys. Lett. **B469** (1999), 171–178.

[F+98] Y. Fukuda et al., *Evidence for oscillation of atmospheric neutrinos*, Phys. Rev. Lett. **81** (1998), 1562–1567.

[Fec06] M. Fechner, *Détermination des performances attendues sur la recherche de l'oscillation $\nu_\mu \to \nu_e$ dans l'experiénce t2k depuis l'étude des données recueilles dans l'éxperience k2k*, Ph.D. thesis, Université Paris VI, 2006.

[Fre17] Ben Freemire, *Accelerator R&D; at Fermilab's FAST/IOTA for Future High Intensity Proton Accelerators*, PoS **NuFact2017** (2017), 089.

[G+00] M. Guler et al., *OPERA: An appearance experiment to search for nu/mu ↔ nu/tau oscillations in the CNGS beam. Experimental proposal*.

[Gal12] Vyacheslav Galymov, *Neutrino flux predictions for the T2K long baseline neutrino oscillation experiment*, Ph.D. thesis, York U., Canada, 2012.

[Gav01] V. N. Gavrin, *Solar neutrino results from SAGE*, Nucl. Phys. Proc. Suppl. **91** (2001), 36–43, [,36(2001)].

[GG06] F. Gerigk and R. Garoby, *Operational flexibility of the SPL as proton driver for neutrino and other applications*, High intensity, high brightness hadron beams. Proceedings, 39th ICFA Advanced Beam Dynamics Workshop, HB2006, Tsukuba, Japan, May 29-June 2, 2006, 2006, pp. 150–152.

[GGM08] M. C. Gonzalez-Garcia and Michele Maltoni, *Phenomenology with Massive Neutrinos*, Phys. Rept. **460** (2008), 1–129.

[Gos17] Srubabati Goswami, *The Status of INO*, J. Phys. Conf. Ser. **888** (2017), no. 1, 012025.

[H+96] W. Hampel et al., *GALLEX solar neutrino observations: Results for GALLEX III.*, Phys. Lett. **B388** (1996), 384–396.

[HLS+05] P. Huber, M. Lindner, T. Schwetz, M. Rolinec, and W. Winter, *GLoBES – General Long Baseline Experiment Simulator*, Nucl. Phys. Proc. Suppl. **143** (2005), 565–565.

[HLSW09] P Huber, M Lindner, T Schwetz, and W Winter, *First hint for cp violation in neutrino oscillations from upcoming superbeam and reactor experiments*.

[JP19] J-PARC, *J-parc neutrino experimental facility*, https://j-parc.jp/Neutrino/en/index.html , 2019.

[K+01] K. Kodama et al., *Observation of tau neutrino interactions*, Phys. Lett. **B504** (2001), 218–224.

[Kat08] *Neutrino 2008*, 2008.

[Kik09] Tatsuya Kikawa, *Measurement of Neutrino Interactions and Three Flavor Neutrino Oscillations in the T2K Experiment*, Ph.D. thesis, Kyoto U. (main), 2014-09.

[Kle02] Joshua R. Klein, *Solar neutrino results from the Sudbury Neutrino Observatory*, Int. J. Mod. Phys. **A17** (2002), 3378–3392, [,470(2001)].

[Kop07] Sacha E. Kopp, *Accelerator-based neutrino beams*, Phys. Rept. **439** (2007), 101–159.

[Kot79] R. Bostrom; J. J. Lord; P. Kotzer, *Accelerator Neutrinos - New Aid to Earthquake Protections*.

[M+06] D. G. Michael et al., *Observation of muon neutrino disappearance with the MINOS detectors and the NuMI neutrino beam*, Phys. Rev. Lett. **97** (2006), 191801.

[McC19] Allen McCloud, *Earth's radial density distribution (or profile)*, https://urlzs.com/YUiL , 2019.

[Mes] Mark D. Messier, *Evidence for neutrino mass from observations of atmospheric neutrinos with super-kamiokande*, UMI-99-23965.

[Mez03] Mauro Mezzetto, *Physics potential of the spl super beam*, J. Phys. **G29** (2003), 1781–1784.

[Min08] Hisakazu Minakata, *Long Baseline Neutrino Experiments with Two-Detector Setup*, Int. J. Mod. Phys. **A23** (2008), 3388–3394.

[MP16] Hisakazu Minakata and Stephen J Parke, *Simple and Compact Expressions for Neutrino Oscillation Probabilities in Matter*, JHEP **01** (2016), 180.

[Nez75] F. Nezrick, *Neutrino-Horn Focussing System*, IEEE Transactions on Nuclear Science **NS-22, No. 3 24 TM-0617** (June 1975).

[NP16] Tsuyoshi Nakaya and Robert K. Plunkett, *Neutrino Oscillations with the MINOS, MINOS+, T2K, and NOvA Experiments*, New J. Phys. **18** (2016), no. 1, 015009.

[Oku82] Lev B. Okun, *Leptons and Quarks*, North-Holland, Amsterdam, Netherlands, 1982.

[Orm09] Christopher David Orme, *Phenomenology of long baseline neutrino oscillation beta beam experiments and their related technologies*, Ph.D. thesis, Durham University, 2009.

[Pon57] B. Pontecorvo, *Mesonium and anti-mesonium*, Sov. Phys. JETP **6** (1957), 429, [Zh. Eksp. Teor. Fiz.33,549(1957)].

[Pra13] S. Prakash, *A comparative study of long-baseline super-beam neutrino experiments*, Ph.D. thesis, Indian Institute of Technology, Bombay, India, 2013.

[PY02] E. A. Paschos and J. Y. Yu, *Neutrino interactions in oscillation experiments*, Phys. Rev. **D65** (2002), 033002.

[RC97] F. Reines and C. Cowan, *The Reines-Cowan experiments: Detecting the Poltergeist*, Los Alamos Sci. **25** (1997), 4–27.

[Rei96] F. Reines, *The Detection of Pauli's Neutrino*, NATO Sci. Ser. B **352** (1996), 401–419.

[Ric00] Burton Richter, *Conventional beams or neutrino factories: The Next generation of accelerator based neutrino experiments*.

[Sch60] M. Schwartz, *Feasibility of using high-energy neutrinos to study the weak interactions*, Phys. Rev. Lett. **4** (1960), 306–307.

[Ske02] P. Skensved, *Results from SNO*, AIP Conf. Proc. **624** (2002), no. 1, 306–315.

[Smi03] A. Yu. Smirnov, *The MSW effect and solar neutrinos*, Neutrino telescopes. Proceedings, 10th International Workshop, Venice, Italy, March 11-14, 2003. Vol. 1+2, 2003, pp. 23–43.

[Smy01] M. B. Smy, *Solar neutrino results from Super-Kamiokande*, 36th Rencontres de Moriond on Electroweak Interactions and Unified Theories Les Arcs, France, March 10-17, 2001, 2001.

[Spu18] Maurizio Spurio, *Probes of Multimessenger Astrophysics*, Astron. Astrophys. Lib. **9783319968544** (2018), pp.1–591.

[STIE15] Amitabh Sinha (The Indian Express), *The ghost particle*, https://indianexpress.com/article/technology/science/the-ghost-particle , 2015.

[Str19] Matt Strassler, *Of particular significance*, https://profmattstrassler.com/, 2019.

[Suz06] Y. Suzuki, *Atmospheric and accelerator neutrinos*, Int. J. Mod. Phys. **A21** (2006), 1844–1854, [,267(2006)].

[T$^+$18] M. Tanabashi et al., *Review of Particle Physics*, Phys. Rev. **D98** (2018), no. 3, 030001.

[TW09] Jian Tang and Walter Winter, *Physics with near detectors at a neutrino factory*, Phys. Rev. **D80** (2009), 053001.

[Vig98] D. Vignaud, *Final results of the GALLEX solar neutrino experiment*, High-energy physics. Proceedings, 29th International Conference, ICHEP'98, Vancouver, Canada, July 23-29, 1998. Vol. 1, 2, 1998, pp. 601–605.

[Vih14] Sampsa Vihonen, *Simulations of CERN to Pyhasalmi Neutrino Experiments with GLoBES*, Master's thesis, Jyvaskyla U., 2014.

[Win10] W. Winter, *Lectures on neutrino phenomenology*, Nucl. Phys. Proc. Suppl. **203-204** (2010), 45–81.

[Wol78] L. Wolfenstein, *Neutrino Oscillations in Matter*, Phys. Rev. **D17** (1978), 2369–2374, [,294(1977)].

[You97] Kenneth K. Young, *First results from the Super-Kamiokande experiment*.

[YW04] T. Yang and S. Woijcicki, *Study of physics sensitivity of ν_{mu} disappearance in a totally active version of nova detector*.